Significant differences between the high temperature electrical conductivity of “natural” and synthetic olivine rocks, with and without iron, using Impedance Spectroscopy.

By: Robert Farla

MSc report submitted to the department of Earth Sciences, Utrecht University, 03-08-2006

Significant differences between the high temperature electrical conductivity of "natural" and synthetic olivine rocks, with and without iron, using Impedance Spectroscopy.

By Robert Farla

Abstract

The electrical conduction properties of olivine, the most abundant mineral in the Earth's mantle, are beneficial to scientists studying deformation processes involving diffusive mass transfer, and deep geo-thermometry inferred from magneto-telluric methods. To date, studies have only concentrated on dry 'natural' iron-bearing olivine and synthetic, polycrystalline, iron-free olivine (forsterite). This study will largely be focused on dry iron-bearing (Fe10%) synthetic olivine, to properly determine the magnitude of electrical conduction in upper mantle olivine in addition to better define the charge-transport mechanisms, which are seen in impure natural iron-bearing olivine. Using advanced sol-gel synthesis techniques of pure, fine-grained, iron-bearing olivine material with 10% fayalite / 90% forsterite composition and impedance spectroscopy, the effects of controlled atmosphere (redox conditions) on conductivity, at temperatures between 800°C and 1200°C, are further investigated. Experiments show that the conductivity of the iron-bearing material is similar in magnitude to the pure magnesium-olivine and for different grain sizes, with apparent activation energies at around 200 kJ/mole (800-1200) °C. This is a significant difference to the reported conductivities of "natural" olivine which show a spread in conductivity for two orders of magnitude. "Natural" (probably oxidized) olivine requires a mechanism involving Fe^{2+} to Fe^{3+} oxidation (small polaron formation) and magnesium vacancies, to explain the excess conduction and a 1/6 relation with the oxygen fugacity. Impedance spectroscopy and quantitative modelling of the defect population in our iron-bearing material shows no presence of the contribution of small polarons within the olivine stability field but is found to become one of the major charge carriers upon oxidation under normal atmospheric conditions. Instead under reducing conditions electrons and magnesium vacancies are the major charge carriers. Furthermore, evidence for reduced conduction via grain boundaries is found with higher oxygen fugacity. The apparent activation energy in the grain boundaries is at around 320 kJ/mol. There the most likely major charge carriers are iron and magnesium interstitials. Lastly, no apparent relation of the conductivity with increasing grain size was found. Most likely the conduction path of least resistance is through the bulk, or grain interiors.

Title page displays the furnace used.

TABLE OF CONTENTS

1. Introduction

The upper mantle is mainly composed of the mineral olivine or better yet, 90% forsterite and 10% fayalite and some amounts of pyroxene and spinel. The temperature distribution in this zone in the Earth is frequently studied by geophysicists. Specifically magneto-telluric methods are used to determine the temperatures at that depth from conduction measurements. The conduction, or its reciprocal resistance, of olivine can be determined at different temperatures and oxygen fugacities in the laboratory. The oxygen fugacity is a measure of how reduced the atmosphere or surroundings are. It is known that most igneous rocks are formed in reducing conditions in the Earth. The range of oxygen fugacity also determines the stability of the mineral in question, in this case olivine. The stability field of olivine also varies with temperature. For example, at 1200°C the stability field of olivine with 10% fayalite is in the oxygen fugacity range of 1E-9 Pa to 1 Pa (Du Frane *et al.*, 2005). This study will determine the conductivities of synthetic forsterite and synthetic olivine with 10% fayalite at different temperatures in order to give accurate and reliable conduction-temperature data. Further goals are to seek out the true role of the charge carriers in olivine and their identity. For this the defect chemistry of olivine becomes invaluable knowledge. In addition, an Arrhenius type relation can be created from a log-conductivity versus the reciprocal of temperature plot from which the total activation energy can be deduced. The activation energy is the amount of energy required for charged species to hop to the next (empty) position in the crystal lattice. Because we are using polycrystalline samples, not only can the conduction mechanism in the grain interior (i.e. through the grains) be identified, but also the nature of conduction in the grain boundaries. The corresponding aim is to determine whether conduction through grain boundaries is slower or faster than conduction through the grain interior material at different oxygen fugacity and temperatures. But most importantly, this study attempts to challenge the use of natural olivine material versus synthetic material because natural olivine rock is strictly impure and is often crushed and re-sintered to a compact sample with 'new' grain boundaries. This study is also highly relevant to understanding the nature and temperature distribution in shear zones in the upper mantle. The synthetic samples have a grain size of 1 micron and higher typical of grains found in shear zones.

In the crustal region in the Earth there exist weak zones along which seismic activity occurs caused by the build up of stress and its sudden release. These weak zones or faults are sometimes connected to shear zones running deep into the upper mantle that have a characteristically small grain size up to a few micrometres. In addition, the majority of these shear zones are highly conductive in relation to the surrounding rocks as discovered by magneto-telluric studies. Both a reduction of grain size and the presence of fluids such as CO, CO_2, H_2O, and other fluids play a large role in this. Furthermore, many shear zones into the upper mantle region have been determined to be composed of mainly the mineral olivine and some pyroxene and maybe trace amounts of spinel. Olivine, however, has two end-members. The iron (Fe) rich end-member called Fayalite and the Magnesium (Mg) end-member called Forsterite. A solid solution range occurs between the two. It has been proven in the laboratory that the stability of olivine depends on many thermodynamic degrees of freedom. These are pressure, temperature, composition, oxygen fugacity, water activity, silica activity and iron activity. Now it is

possible to control these parameters, but only to a certain extent due to apparatus limitations or the nature of the material used for sensors. For example, it is possible to create a closed system to metal and silicon components or to control all parameters and vary the oxygen fugacity.

Fugacity is a state function of matter at fixed temperature. The fugacity, which has units of pressure (Pa or bar), represents the tendency of a fluid to escape or expand isothermally. At low temperatures gases approximate the ideal gas law. However, for this experiment the temperature range will be from 800°C to 1200°C. There are two ways to reduce the oxygen fugacity. One is via diluting the atmosphere using a gas mixture that creates a reducing environment (eg CO/CO_2) or two, via actively taking away the oxygen using a H_2 gas (very reducing!). This investigation will primarily be conducted using CO/CO_2 as a means to reduce the oxygen fugacity. The other option is less favourable because the reaction of O_2 and H_2 gas creates water and will affect the conductivity results. However, also the CO/CO_2 gas mixture must be used with caution because below a certain temperature and oxygen fugacity carbon will precipitate. The mathematics of rewriting the general fugacity equation for a CO/CO_2 gas mixture is further explained in the background section.

In this study the electrical conductivity of dry polycrystalline synthetic olivine is measured at different temperatures and oxygen fugacity and the process of diffusion identified. This investigation will therefore give a better understanding of the temperature distribution in the upper mantle and in shear zones. Previous studies have carried out similar experiments on the conductivity of synthetic forsterite (ten Grotenhuis *et al.*, 2004; Hinze *et al.*, 1980). That has been much easier because the oxygen fugacity component was thought not to affect the results of the experiment and thus was ignored. However, in this study the synthetic olivine will contain 10% iron as well. Iron can change its oxidation state from 2+ to 3+ when in contact with an oxygen rich environment. When that happens an electron is lost from one of the iron orbitals causing an increase in conductivity due to free electrons moving about in the conduction band. So in order to avoid that happening, i.e. oxidising all the iron in the sample, we need to control the oxygen fugacity in the atmosphere.

In addition to carrying out experiments on synthetic iron-bearing olivine with varying oxygen fugacity's at a constant temperature, two more are conducted. One, where the oxygen fugacity is fixed and temperature is varied and two, a forsterite control experiment where the temperature is held constant and the oxygen fugacity is varied. In the method section the experiments are summarised in table 4.

The aim of the experiments is to check whether the impedance, or resistance to conduction, is the same as in previous studies. But also to check whether the apparent activation energy, as well as the type of process that allows electrical conduction to occur are comparable to other experimental results. Electrical conduction either occurs via the movement of electrons or ions. However, this may not be entirely true as holes (e.g. electron holes or vacancies in the crystal lattice) can equally behave as conductors. The impedance is similar to the resistance but applies to an AC current instead of a DC one. For an AC current there is an additional component in the imaginary plane. Impedance is a complex quantity that includes the regular ohmic resistance (Z') but also a capacitive reactance (Z'', the imaginary component) or the resistance at 90 degrees out of phase. This extra component exists because of a phase shift in the current versus time compared

to the voltage versus time causing the sample, through which the current flows, to act as a capacitor. The physics behind circuits and electrical conduction via an AC current is further explained in the background section. The electrical conduction for a mineral like olivine is controlled by defect diffusion and thus relates to the diffusion of charge carrying species (interstitials and vacancies) by the Nernst-Einstein equation. Thus the conductivity in olivine is dependent on the defect population and the mobility of these defects in the crystal lattice. Noticeably, the net flow of diffusion species is zero. This is caused by the alternating current applied. A direct current does cause a net flow of diffusing species into one direction. Electrical impedance experiments therefore do not concern mass transport, but the charge is instead passed on from one neighbouring species to the next, which are the most mobile and in highest concentration.

The final two experiments performed will be an investigation on the oxidation and grain size relationship with conductivity. Controlled oxidation of one of the iron-bearing samples should provide good insights into the actual conductivity increase that one might expect from the release of electrons from Fe^{2+} to Fe^{3+}, i.e. and significant increase in small polaron concentrations. The conductivity on grain size experiments will be carried out with various samples of different grain sizes obtained through the re-sintering of the samples at very high temperature for different time spans. This should provide extra insights in determining the role of the grain boundaries versus grain interior conduction.

1.1. Background

1.1.1. Oxygen fugacity

Fugacity, as has been explained in the introduction, is a state function of matter at a fixed temperature. Or in other words, it is a property of the system that only depends on the current state of the system but not on how the system got to that state. One might actually view the fugacity as a partial pressure. This is because it is a strong function of the mole fraction of a component, such as oxygen, in the gas phase and the total pressure of the gas phase.

The fugacity is linked to the chemical potential of the system. The fugacity of a component can be used to account for the difference between the chemical potential of interest μ(P,T) and the chemical potential of the pure substance at T, 1 bar. So we can write:

$$f_i = \exp\left(\frac{\mu(T,P) - \mu\left(T, 1 \text{ bar, pure}\right)}{RT}\right) \tag{1}$$

Where f_i is the fugacity of component i in a mixture, μ is the chemical potential, R is the gas constant, T is the temperature and P is the pressure. Having T and P fixed, there are only two variables, $\mu(P,T)$ and f_i and so for example a high fugacity of oxygen means a high chemical potential of oxygen which in turn indicates an "oxidised" system. For a general equation of fugacity we have:

$$f = \phi P \tag{2}$$

Where ϕ is the fugacity coefficient. One can think of fugacity simply as a measure of how much the chemical potential of the component in the gas deviates from the chemical potential of some reference, namely, the standard state.

However, the fugacity does slightly deviate from the concept of partial pressure or total pressure. From the general equation, we see that *f* deviates from *P*. This goes back to the fact that the rate of change of the chemical potential of a pure gas (i) with respect to changes in *P* (at a given *T*) equals the volume of the gas, *V*. Or for an ideal gas:

$$V = \frac{RT}{P}; \quad d\mu = VdP \tag{3}$$

Which then becomes:

$$d\mu = RT\left(\frac{dP}{P}\right) \tag{4}$$

Integrating:

$$\mu(P) = \mu(1bar) + RT\ln P \tag{5}$$

However, we are dealing with a non-ideal gas so *V* has a different value from *RT/P*. So *RTlnP*, must, in fact, become $RTln(f_i)$. Fugacity coefficients are tabulated or available as output from computer models but are in reality derived from experiments. So fugacity is not a corrected pressure and only has meaning when related to a chemical potential.

In this experiment we are dealing with the fO_2, or the oxygen fugacity. It is important to note that a high fO_2 (oxidising conditions) is still much lower than the fO_2 = *x(i) P* = 0.21x (bar). Or fO_2 = 0.21 bar (21000 Pa) of the present atmosphere (ideal gas behaviour assumed). Instead an fO_2 of 10^{-5} Pa or higher is already considered oxidising depending on the rock/mineral material in question.

For a given temperature, the general differential equation for the fugacity is:

$$d\ln\frac{f}{f_0} = \frac{dG}{RT} = \frac{VdP}{RT} \tag{6}$$

where *G* is the Gibbs free energy, *R* is the gas constant, *V* is the fluids volume and f_0 is the reference fugacity which is generally taken as that of an ideal gas at 1 bar. This equation can easily be derived from a chemical reaction of interest. In this case we will be looking at the reaction between carbon dioxide and carbon monoxide.

$$CO_2 \rightleftharpoons CO + 1/2\,O_2 \tag{7}$$

From this reaction an equilibrium constant can be written as

$$K = \frac{(fCO)(fO_2)^{1/2}}{(fCO_2)} = e^{-\Delta G/RT} \tag{8}$$

We are assuming a constant pressure and thus the equilibrium constant is a function of temperature. We will also assume ideal gas behaviour at this point allowing us to rewrite equation (8) as

$$\frac{pCO}{pCO_2} = (pO_2)^{-1/2}\, e^{-\Delta G/RT} \tag{9}$$

Yet another assumption will be that these gases are the only ones present which is valid because this will be a controlled experiment. So the total pressure will be

$$P_{CO_2} + P_{CO} + P_{O_2} = 1 \ \text{bar} \tag{10}$$

At this point we will substitute pO_2 for fO_2 in equation (9) and we have the equation

$$\frac{p\mathrm{CO}}{p\mathrm{CO}_2} = \left(fO_2\right)^{-1/2} e^{-\Delta G/RT} \tag{11}$$

This will allow the calculation of the CO/CO_2 concentrations we need at a given oxygen fugacity and temperature assuming ideal gas behaviour. Note that ΔG also changes with temperature. The Gibbs free energy of the components at given temperatures are tabulated in the JANAF tables or from the NASA Glenn database, the preferred and up to date source used in this study. It is important that the input gases (CO and CO_2) are well mixed and allowed to flow into the furnace stepwise allowing the gases to reach equilibrium establishing an oxygen fugacity. Adding a CO/CO_2 mixture will create reducing conditions which is one of the objectives of the experiment.

There are, however, limits to the oxygen fugacity range. It cannot go below 10^{-8} Pa because of several reasons. One, lower fO_2 might cause increased iron loss to the Pt electrodes. Two, carbon will precipitate at low fO_2 from the CO/CO_2 gas mixture. Three, the olivine (forsterite – fayalite) stability field is very narrow and does not allow a greater range for fO_2 values. The fO_2 range used in previous studies is between 10^{-8} and 1 Pa (Schock and Duba, 1985; Constable and Duba, 2002) but varies at different temperatures slightly. The same range will be used in this investigation. In real (igneous) rocks fO_2 values often do not increase above 10^{-11} bar but depends on many factors including the temperature, pressure and mineral composition as stated in the introduction. A comparison with these rocks is therefore impossible.

1.1.2. Impedance spectroscopy

Movable charges in a material define conductivity. In other words we are dealing with the movement of ions, electrons, or even holes and vacancies in a material. This investigation will make use of an AC current from which extra, valuable, information can be taken. In addition, the electrical charges remain in place whereas a DC current transports them from one location to another. An AC current can be described as a sinusoid wave with a phase shift due to the delay in response from the current to the voltage. This changes the traditional Ohm's law equation of resistance is the voltage over the current to

$$Z = \frac{E_t}{I_t} = \frac{E_0 \sin(\omega t)}{I_0 \sin(\omega t + \phi)} = Z_0 \frac{\sin(\omega t)}{\sin(\omega t + \phi)} \tag{12}$$

Where Z is the impedance, E is the voltage, I is the current, ω is the angular frequency, t is time and φ is the phase shift. With the current plotted against the voltage a "Lissajous curve" can be plotted. This used to be the conventional way of measuring the impedance.

The impedance can be expressed as a complex function. So equation (13) can also be expressed with the imaginary number j ($=\sqrt{-1}$).

$$Z(\omega) = \frac{E_t}{I_t} = \frac{E_0 \exp(j\omega t)}{I_0 \exp(j\omega t + \phi)} = Z_0 \exp\left(j\phi\right) = Z_0\left(\cos\phi + j\sin\phi\right) \tag{13}$$

Bearing in mind Eulers relationship $\exp\left(j\phi\right) = \cos\phi + j\sin\phi$. So here we have two expressions of the impedance represented in terms of phase shift. If the phase shift is 90°,

the system or sample behaves as a capacitor. The system or sample behaves as a resistor when there is no phase shift.

However, the impedance can also be expressed as a resistance and a capacitance. In the real plane you have the resistance, as with a DC current (Z'), but in the imaginary plane you have the capacitive resistance (Z''). In other words $Z' = R$ and $Z'' = 1/\omega C$ where C is the capacitance. The complex impedance then becomes

$$Z^* = Z' - jZ'' \tag{14}$$

Note that with an increase in frequency, the capacitor's impedance decreases.

The magnitude of the impedance is $|Z| = \sqrt{(Z')^2 + (Z'')^2}$.

The capacitance can be described as an electric charge stored over an electric potential or as the electric flux over the voltage.

$$C = \frac{Q}{V} = \frac{\theta}{E} \tag{15}$$

Figure 1 shows the basic setup of a capacitor. The conductors must have an equal but opposite charge Q. The SI unit of a capacitor is the Farad (F). Often results are written in μF. There is yet another way capacitance can be written (a more practical way) which is

$$C = \varepsilon_0 \varepsilon_r \frac{A}{d} \tag{16}$$

Where ε_0 is the permittivity of free space (Fm^{-1}), ε_r is the dielectric constant, A is the area of each plate electrode (m^2) and d is the separation between the electrodes (m). The capacitance reflects that electrons cannot pass through a capacitor, yet an AC current can, the higher the frequency, the better (see above).

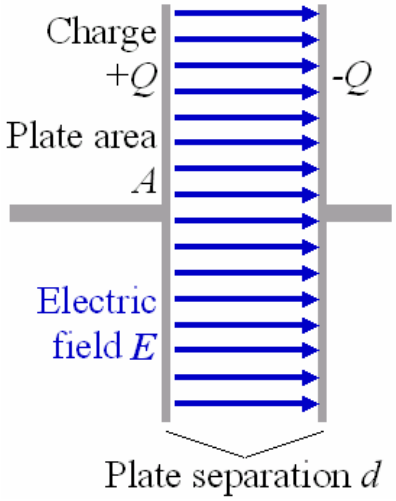

Figure 1. A capacitor. When electric charge accumulates on the plates, an electric field is created in the region between the plates that is proportional to the amount of accumulated charge. This electric field creates a potential difference $V = E \cdot d$ between the plates of this simple parallel-plate capacitor.

It is often said that a DC current is 'blocked' by a capacitor. Yet this is not really true. The voltage across the capacitor cannot exceed the voltage of the source. So at a certain moment the voltage across the capacitor is constant ($dV = 0$) and the current through the capacitor is zero as shown in the relation: $I = \frac{dQ}{dt} = C\frac{dV}{dt}$. The capacitor

current (of AC type) is non-zero at all times during a cycle because the voltage and the current are out of phase by a quarter cycle. Technically an AC current can therefore pass through a capacitor but no actual electrons cross between the plates. It is important to note that an ideal capacitor does not dissipate power but stores energy due to the potential difference build up between the two plates. So in conclusion, the experimental setup will resemble a capacitor. The olivine sample is the insulator and the platinum electrodes on either side act as conductors.

However, there is more to it than simply measuring the impedance. The computer attached to the electric interface will automatically plot the measured impedance on a Z' versus Z'' graph called a Nyquist plot. On this plot one or more arcs will show up. Each arc represents a conduction process with a different relaxation time In this case it would be related to diffusion of magnesium, iron, and possibly silica interstitials or vacancies. In addition, the diffusing species can be electrons. The difference between ionic and electronic diffusion can be seen on an Arrhenius plot from a sharp change in slopes. A gradual change indicates a mixed conduction region. In the Nyquist plot, the arc closer to the origin is the higher frequency arc.

The Bode plot is another plot that the computer can produce from the impedance data. It is log (Z) versus ω and φ versus ω. This plot, unlike the Nyquist plot, does show frequency information.

The impedance arcs obtained in a Nyquist (or impedance) plot are often depressed semicircles. This means that the origin of the circle lies below the real axis. The CPE (constant phase element) is a component in the electric circuit which explains this depression. The CPE is a non-intuitive circuit element that was discovered (or invented) while looking at the response of real world systems. These depressed semi-circles are commonly explained by a property of the system being non-homogeneous or that there is some distribution of the value of some physical property in the system. The CPE's impedance is given by

$$1/Z = Y = Q(j\omega)^n \tag{17}$$

Where Q has units of S s^n. Q has the numerical value of the admittance ($1/|Z|$) at ω = 1 rad/s. This equation shows that the phase angle of the CPE impedance is independent of the frequency and has a value of -(90*n) degrees. Hence constant phase element. When we have n = 1, the equation becomes the same as the equation for the impedance of a capacitor where Q = C. When n is close to 1, the CPE resembles a capacitor, but the phase angle is not 90°, but constant and somewhat less than 90° at all frequencies. See Figure 2 how a CPE explains a depression in the impedance arc.

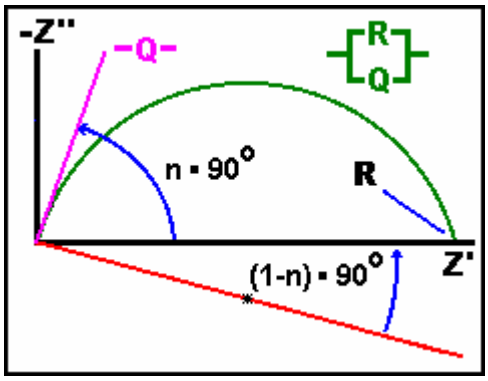

Figure 2. The Nyquist (Complex Impedance Plane) plot of a CPE is a simple one. For a solitary CPE (symbolized here by Q), it is just a straight line which makes an angle of (n*90°) with the x-axis as shown in pink in the Figure. The plot for a resistor (symbolized by R) in parallel with a CPE is shown in green. In this case the center of the semicircle is depressed by an angle of (1-n)*90°. From http://www.consultrsr.com/resources/eis/cpe1.htm.

There are several theories that go on to try to explain what causes a CPE to exist. These include surface roughness of the electrode in contact with the sample, a distribution of reaction rates, varying thickness or composition of a coating and non-uniform current distribution along the radius of the electrode. The electrode roughness relates to the fractal dimension (D) of a surface which is between 2 and 3 dimensions because it is not 100% flat. It has been shown by Mulder *et al.* (1990) that for these electrodes, the interfacial impedance is changed by an exponent, n = 1/(D-1). For a smooth surface D = 2 and n =1 to a highly contorted surface where D = 3 and n = 0.5. Usually an electrode surface (metallic or solid) gives a CPE with a value n between n = 0.9 and n = 1. Another reason for a depressed impedance arc is that there could be inhomogeneous reaction rates taking place on a surface. Carbon electrodes are particularly affected by this but also metal electrodes can show a distribution of active sites with varying activation energies on the surface. Varying thickness or composition of a coating can also affect the conductivity through it. A thicker coating may decrease conductivity approximating a CPE. Lastly, a non-uniform current distribution along the electrode surface could also yield a CPE. Jorcin *et al.* (2004) looked at the varying n value along the radius of an electrode and discovered that in the centre the n value was largest (n = 1) indicating true capacitance, but near the edges the n value for the CPE was 0.83. Therefore 'edge effects' are not to be ignored. However, in this study a precaution has been taken to avoid this scattering effect and the interference of electric fluxes around the sample with the fluxes through the sample. A guard ring does just the trick. This ring is typically zeroed or earthed so that a point of zero potential exists between the edge of the electrode and the guard ring positioned around the electrode. This way all conduction is attributed to electric fluxes going straight through the sample to the other electrode and not around the sample. In a recent study the 2D and 3D components contributing to CPE behaviour was investigated. For a 2D distribution an AZ91 Mg alloy was used and for a mixed contribution an aluminium electrode. For the 2D distribution it has been found that the origin of CPE behaviour was the distribution of high frequency resistance associated with the geometry of the disk electrode; whereas the capacitance was independent of position (Jorcin *et al.*, 2006).

In the past the CPE was still unknown and another way was used to approach the depressed impedance arc which was done using the ZARC element. The semicircle was modelled directly as a system with a distribution of time constants. The term ZARC is derived from the (depressed) arc that is produced in the impedance plane, Z' vs Z''.

Normally with just one arc in the Nyquist plot a simple circuit can be drawn as shown in Figure 3. However with more than one arc the circuit will need to be expanded. The trick is to keep the circuit as simple as possible without too many unnecessary circuit elements. This is the biggest problem with impedance spectroscopy. It provides only an indirect characterisation of a given system. The consequence of this inferential character is that many models can provide fits that fall within the apparent confidence limits of the data (Orazem *et al.*, 1994). Therefore ideally impedance spectroscopy should not be used as a 'stand – alone' technique. In this study the best and most intuitive approach is taken to provide an appropriate model to the system and not solely targeted to provide the best possible fit to the data.

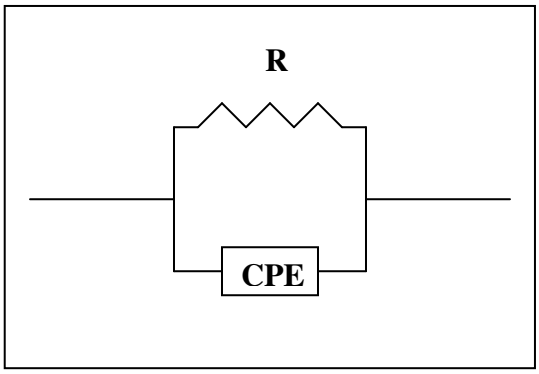

Figure 3. A simple circuit which yields one depressed arc in an impedance plot.

1.1.3. Defect chemistry of olivine in relation to conductivity

Olivine, like other crystalline magmatic minerals, contains an amount of defects that increases as the mineral experiences higher temperatures. These defects contribute to the diffusion mechanisms that can take place within the crystals. Possible diffusion carriers can be Mg^{2+}, Fe^{2+} O^{2-}, or even Si^{4+} interstitial ions or vacancies. The most common vacancies are of course magnesium and iron vacancies as the two ions can hop from an M1 site to an M2 site although recent ab initio studies have shown that atoms preferably hop from one M1 site to another M1 site instead to an M2 site (Brodholt, 1997). In addition, the diffusing species can be electrons or electron holes as well. Olivine is a semi-conductor at high temperatures (1000°C - 1400°C) like silicon and has a certain population of electrons in the conduction band at these temperatures. The electron density of a typical olivine crystal would be $\rho_{electron}$ = 3.25 g/cc[1]. Still because electrons move relatively easier through the crystal lattice in the conduction band than large ions, associated with higher activation energies, one can assume that at lower temperatures electrons are the dominating diffusing species. However, it may be tricky to distinguish between pure electron movement due to an electric current and ions/vacancies because it may be that some electrons behave like polarons when moving through the

[1] http://webmineral.com/data/Olivine.shtml

crystal lattice (e.g. Mihály and Martin, 1996). Polarons are defined as a charge moving through a crystal lattice and due to its polarization effect it can shorten and lengthen the bonds between atoms nearby thus slowing it down.

The defect diffusion processes depend a lot on the composition of the olivine in question. For example, an iron rich olivine is more likely to demonstrate electronic diffusion under relatively oxidizing conditions and high temperatures as opposed to forsterite in which the Mg^{2+} will generally not lose an electron under oxidizing conditions. Past research has shown various reactions that can take place for forsterite and olivine to fayalite (see Table 3 at the end of this section). Some assumptions will have to be made. For example electrons and electron holes created as a result of changes in point defect concentration can become charge carriers in the conduction and valence bands respectively. The other assumption deals with the fact that only two phases are present, olivine and oxygen gas. It is possible to use CO/CO_2 gas mixes to obtain reducing conditions but the current temperature and the olivine and carbon stability fields limit the range of oxygen fugacity experimental work can be done in (see Figure 4).

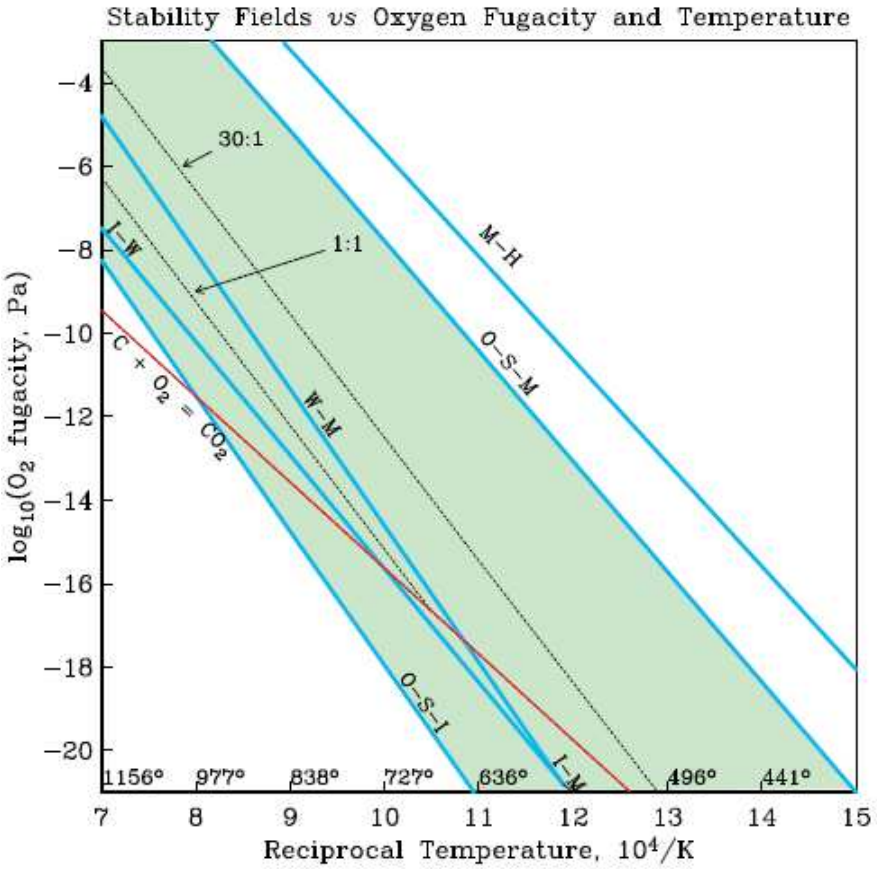

Figure 4. Stability fields of olivine versus temperature and oxygen fugacity. M = magnetite, H =hematite, O=olivine, S = silicon, W = wüstite, I = iron. Gas mix ratios are indicated as CO_2:CO. The shaded area is the region where olivine is stable. After Constable and Duba (1990), Constable (2005).

In a simple system the conductivity is related to the concentration of the charged species by multiplying the concentration of the species by its mobility (or drift velocity per applied field E) and its charge of the mobile species. The same is done to other

species and as a whole the sum of them is the total conductivity where different conduction mechanisms are acting in parallel. See below:

$$\sigma = \sum_i \sigma_i = \sum_i c_i q_i \mu_i \tag{18}$$

Where c is the concentration, q is the charge and μ is the mobility of species *i*. The concentrations of defects, such as Frenkel and Schottky defects or vacancies, are thermally induced so the number of defects and thus conductivity increases with increasing temperature. The relationship is a Boltzmann relation; e.g. for Schottky defects or vacancies we have:

$$c_s = N\, exp\left(-\frac{E_v}{kT}\right) \tag{19}$$

The defect chemistry of olivine deals with the mobility or diffusion of defects through the crystal lattice and grain boundaries in a polycrystalline sample. Table 3 for instance shows the possible defect reaction that can take place. Or see Figure 5 for a visual approach to the defect nomenclature used. The diffusion of defects is given as the flux of particles J_N crossing an unit area in unit time under the influence of a concentration gradient, ∇ N. This is Fick's first law:

$$J_N = -D\nabla N \tag{20}$$

Where D is the diffusivity which are found to vary with temperature as a thermally activated Boltzmann process:

$$D = D_0\, exp\left(-\frac{E_d}{kT}\right) \tag{21}$$

where E_d is another activation energy for diffusion. Using the Nernst-Einstein equation we can relate diffusivities to mobilities of defects:

$$kT\mu = qD \tag{22}$$

So the mobility $\mu = qD/kT$. The conductivity of, for example, Schottky defects becomes:

$$\begin{aligned} \sigma &= c_s \cdot q \cdot \mu \\ &= N\, exp\left(-\frac{E_v}{kT}\right) \cdot q \cdot \frac{qD}{kT} \\ &= \frac{Nq^2 D_0}{kT} exp\left(-\frac{E_v}{kT}\right) exp\left(-\frac{E_d}{kT}\right) \end{aligned} \tag{23}$$

The exponential terms dominate so to a first approximation conductivity is given by:

$$\sigma = \sigma_0 \, exp\left(-\frac{E_a}{kT}\right) \tag{24}$$

Where E_a is the total activation energy of the mixed conduction processes going on associated with defect concentration and mobility.

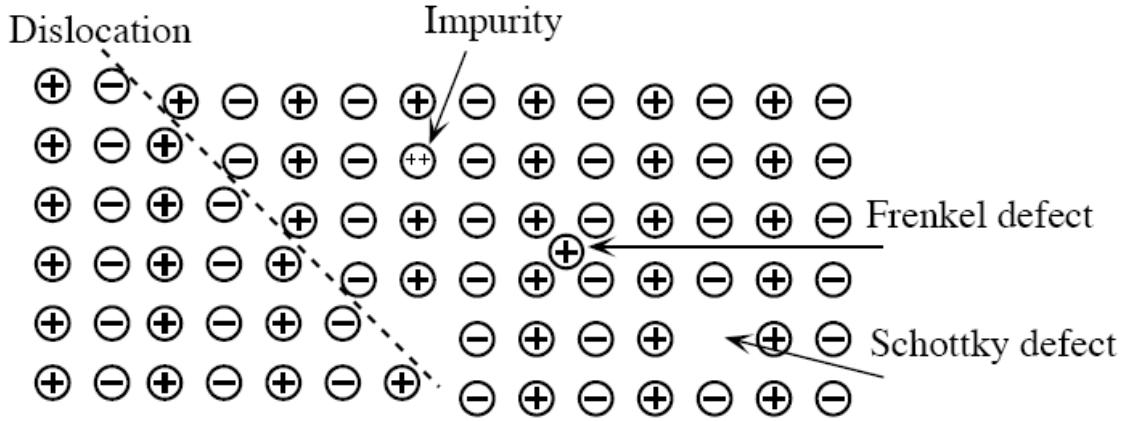

Figure 5. Defects in crystals. From Constable (2005).

1.1.4. Obtaining an adequate quantitative model

One of the more exhaustive models is from Hirsch and Shankland (1993) where various conservation laws were applied like mass conservation, charge neutrality condition and lattice-site conservation. For mass conservation it means that the specimen can only interact and exchange oxygen atoms with an external gas like a CO/CO_2 mixture. This constrains the ratio of the Mg to Fe atoms. Other chemical reactions that can take place constrain the ratio of the concentrations of Mg and Fe atoms to Si atoms as 2. The charge neutrality condition has been enhanced, as earlier models (eg Stocker 1978b) did not allow a complete charge neutrality condition. The formula for this condition can be seen in Table 2 (at the end of this section) along with the other conservation laws incorporated into the model. The lattice site conservation law simple states that the sum of the site fractions of all the occupied and vacant magnesium sites must be unity to conserve site stoichiometry. The defect model predicts that at a temperature of 1200C and olivine containing 10% fayalite, the dominant charge carriers are magnesium vacancies V''_{Mg}, electrons e^- and small polarons of iron in magnesium sites $Fe^{\bullet}_{Mg}$. The reaction describing the formation of small polarons is shown as:

$$8Fe^{\times}_{Mg} + 2O_2 \longleftrightarrow 2V''_{Mg} + V''''_{Si} + 4O^{\times}_{O} + 8Fe^{\bullet}_{Mg} \qquad (\mathrm{I})$$

See Table 1 for explanation of defect notation and the nomenclature of the various species involved. This reaction shows how normal, reduced iron in its lattice site becomes oxidised upon contact with oxygen in gas phase. This causes the release of an

electron as according to the redox mechanisms. This free electron is taken up by either a magnesium or silicon vacancy that has formed due to the release of the oxidised iron (or small polaron) from the crystal lattice. In fact, the reaction states that 8 iron atoms (in magnesium sites) have to be oxidised to create two magnesium vacancies and one silicon vacancy. The oxygen atoms have taken position in the crystal lattice in a neutral state to preserve charge balance. The small polarons are then free to move as charge carriers through the crystal lattice.

In contrast to previous studies, this study will show it is questionable to what extent reaction (I) takes place to form small polarons ($Fe_{Mg}^{\bullet}$) as one of the dominant charge carriers in synthetic olivine. Table 3 shows some of the possible reactions that could potentially take place. Each reaction is associated with a certain equilibrium constant. The exponential relationship with the oxygen fugacity and this equilibrium constant is of a certain order of magnitude for each reaction. For example, a reaction involving the generation of electrons from oxygen interstitials or the formation of holes and free electrons yields an fO_2 dependence of –1/6. Reaction (I) above predicts a +1/6 slope dependence of fO_2 for small polarons and magnesium vacancies (Stocker and Smyth, 1977). For pure forsterite fO_2 is theoretically independent, i.e. the charge carrier concentrations remain unaffected at every oxygen partial pressure but as Hirsch and Shankland (1993) have shown in their quantitative model, is that with as little as 0.01% Fe present, the system of charge carrier concentrations is affected (at higher fO_2). Anyhow, it would theoretically appear that magnesium vacancies, electrons, and small polarons are the effective charge carriers.

Now that we have identified the possible charge carriers in olivine containing 10% fayalite, it is essential to understand the link between the concentrations of charged species to the overall conductivity measured. Already knowing the link between the conductivity and the mobility and concentration of a defect, as described earlier, we can now write:

$$\sigma = \sigma_{Fe} + \sigma_{e} + \sigma_{Mg} \tag{25}$$

$$\sigma = \left[Fe_{Mg}^{\bullet}\right]\mu_{Fe}e + c_{e}\mu_{e}e + 2\left[V_{Mg}^{\bullet}\right]\mu_{Mg}e \tag{26}$$

Here we are assuming that small polarons (localised holes on Fe), electrons, and magnesium vacancies are the dominant charge carriers. However, finding the two important components, the concentration and the mobility of each species is not a trivial task. Even though the model by Hirsch and Shankland (1993) serves as a guideline, their results cannot be used directly. This is because certain constants have to be incorporated into the final model such as the activation energies of the small polarons and magnesium vacancies. In addition, from experimental results we see an arrhenius type behaviour very often and would be the starting place for finding a relationship between the concentration dependence of the species on the oxygen fugacity and constraining unknown constants which will later on need a physical meaning if the model is to be verified.

Constable and Duba (1990) empirically modelled the conductivity as function of the oxygen fugacity as:

$$\sigma = \sigma_0 + \sigma_1 \left(fO_2 \right)^C \qquad (27)$$

Where σ_0 is a fitting parameter. This was later adopted by Constable and Roberts (1997) with the introduction of an extra arrhenius relationship for σ_1 to account for the activation energy for the dominant charge carriers involved. c is the exponential dependence constant derived from the chemical reaction in question and equilibrium constant. It equals 1/6 for reaction (1) and –1/6 for the electron contribution (see Hirsch and Shankland 1993).

The mobility of a particular species in olivine is even more speculative. Finding the mobility of an electron can at least be somewhat constrained at around 0.14 $m^2V^{-1}s^{-1}$ which is for silicon and is assumed not to vary greatly for olivine[2]. For other species like magnesium vacancies the only way to obtain a value is from previous experimental work. The mobility of a dominant charged species is also calculated from an Arrhenius type relationship using the activation energy of mobility for each species. This value, again, must come from previous experimental work, which is very hard to find.

As mentioned before, when modelling the data the activation energy is required for each defect species, which is able to carry a charge. With these experiments it is possible to obtain an activation energy by executing experiments at different temperatures. By selecting the data at a specific oxygen fugacity, the only variable is the temperature. In a plot of the log conductivity versus 1/T, a straight slope is obtained. This type of plot is also called an arrhenius plot. From the slope an activation energy can be obtained. The activation energy obtained could be, for a temperature range between 800°C and 1200°C, related to mixed conduction of electrons and magnesium (and iron) vacancies. If so, it would be incorrect to use this value for say, for instance, magnesium vacancies. The activation energy is a lower limit because electrons, with hardly any activation energy, lower the total activation energy. Therefore, the activation energy for magnesium ions/vacancies is best obtained from electrical experiments carried out at much higher temperature (1200°C-1400°C) or from creep experiments on the same olivine material.

It is also important to know the approximate electron concentration. Even though some quantitative models like the one by Hirsch and Shankland (1993) show the electron concentration as a function of fO_2 at a specific temperature of 1200°C, the absolute concentration of electrons may vary in the real world. The best way to obtain reasonable values for the electron concentration at different temperatures is to know the approximate bandgap of forsterite with 10% fayalite. There have only been two (or few more) studies where this was determined as well as the bandgap of forsterite. One is by Shankland (1968) and the other is by Morin et al (1977). In these papers it is suggested that the (thermal) band gap of forsterite with 10% fayalite is at or around 6.4 eV. Assuming the effective electron mass is around 0.26 (as it is for Silicon[3]), then the concentration of electrons can be calculated using a modified Fermi function for semi-conductors. The

[2] http://www.ioffe.rssi.ru/SVA/NSM/Semicond/Si/electric.html
[3] http://www.ioffe.rssi.ru/SVA/NSM/Semicond/Si/bandstr.html

conduction electron population for a semiconductor is calculated by multiplying the density of conduction electron states r(E) times the Fermi function f(E) of the form

$$f(E) = \frac{1}{e^{(E-E_f)/kT} + 1} \tag{28}$$

The number of conduction electrons as a function of energy is then given by:

$$N(E)dE = \rho(E)f(E)dE = \frac{8\sqrt{2}\pi m^{3/2}}{h^3}\sqrt{E - E_{gap}}\,\frac{1}{e^{(E-E_F)/kT} + 1}dE \tag{29}$$

This can be simplified by noting that for the energies of the conduction band, $E-E_F >> kT$, so the 1 in the denominator of the Fermi function becomes insignificant. I.e., the tail of the function, which extends into the conduction band, is so far out that it can be approximated by the Boltzmann function. Using the fact that

$$E_F = E_{gap}/2 \tag{30}$$

The population density can then be written:

$$N(E)dE = \frac{8\sqrt{2}\pi m^{3/2}}{h^3}\sqrt{E - E_{gap}}\,e^{-(E-E_{gap})/2}dE \tag{31}$$

The total number of electrons in the conduction band, N_{cb}, can then be obtained by integrating the above function from the bottom of the conduction band upward. For all practical purposes, the upper limit of the integral can be taken to be infinity since by the time we reach the top of the conduction band, the integrand will be essentially zero. The resulting relation is:

$$N_{cb} = \int_{E_{gap}}^{\infty} N(E)dE = \frac{2^{5/2}(m\pi kT)^{3/2}}{h^3}e^{-E_{gap}/2kT} \tag{32}$$

Where N_{cb} is the population of conducting electrons in electrons/m^3, m is the effective mass of electrons, E_{gap} is the energy (band) gap, h is Plank's constant, k is boltzmann's constant and T is the temperature (Simpson, 1987). For pure forsterite the bandgap is in the order of 8.4 to 9 eV (Shankland, 1968 and Kitaura *et al.*, 2001). It's evident that the presence of iron greatly lowers the bandgap, which is no surprise as iron has, for example, multiple oxidation states.

The method used in this study for modelling a fitting curve to the conduction data is similar to that of Constable and Roberts (1997). However, due to the nature of the material Constable and Roberts used (i.e. natural olivine versus synthetic olivine), the b_{Mg} constant must satisfy a different value. For more detail, see the method and results sections.

Table 1. Defect notation and description thereof (after Kröger and Vink, 1956)

Notation	Description
V_A	Vacancy where atom A is missing
$V_A^{\bullet}$	Vacancy V_A with a net positive charge (more $^{\bullet}$ for higher charge)
$V_A^{\times}$	Neutral vacancy V_A
$V_A^{'}$	Vacancy V_A with a net negative charge (more $^{'}$ for higher charge)
A_A	Atom A residing in its own lattice site (with $^{\bullet}$, $^{\times}$ and $^{'}$ in superscript denoting charge)
A_B	Atom A residing in site position of atom B (with $^{\bullet}$, $^{\times}$ and $^{'}$ in superscript denoting charge)
A_I or I_A	Atom A residing in an interstitial site (with $^{\bullet}$, $^{\times}$ and $^{'}$ in superscript denoting charge)
Common species in this paper	
$V_{Mg}^{''}$	Magnesium vacancy
$V_{Si}^{''''}$	Silicon vacancy
$Fe_{Mg}^{\bullet}$	Small polaron (electron hole on iron or Fe^{3+} on the Mg site)
e^{-}	Electron
$h^{\bullet}$	Electron hole
$O_I^{''}$	Oxygen interstitial

Table 2. Conservation laws after Hirsch and Shankland (1993)

Mass conservation	$Y\times\left(\left\{Mg_{Mg}^{X}\right\}+\left\{Mg_{I}^{\bullet\bullet}\right\}\right)=(1-Y)\times\left(\left\{Fe_{Mg}^{X}\right\}+\left\{Fe_{Mg}^{\bullet}\right\}+\left\{Fe_{I}^{\bullet\bullet}\right\}+\left\{Fe_{I}^{\bullet\bullet\bullet}\right\}\right)$ $2\times\left(\left\{Si_{Si}^{X}\right\}+\left\{Si_{I}^{\bullet\bullet\bullet\bullet}\right\}\right)=\left\{Mg_{Mg}^{X}\right\}+\left\{Mg_{I}^{\bullet\bullet}\right\}+\left\{Fe_{Mg}^{X}\right\}+\left\{Fe_{Mg}^{\bullet}\right\}+\left\{Fe_{I}^{\bullet\bullet}\right\}+\left\{Fe_{I}^{\bullet\bullet\bullet}\right\}$
Charge neutrality condition	$2\left\{Mg_{I}^{\bullet\bullet}\right\}+2\left\{Fe_{I}^{\bullet\bullet}\right\}+3\left\{Fe_{I}^{\bullet\bullet\bullet}\right\}+\left\{Fe_{Mg}^{\bullet}\right\}+4\left\{Si_{I}^{\bullet\bullet\bullet\bullet}\right\}+\left\{h^{\bullet}\right\}+2\left\{V_{O}^{\bullet\bullet}\right\}$ $-2\left\{V_{Mg}^{''}\right\}-2\left\{O_{I}^{''}\right\}-4\left\{V_{Si}^{''''}\right\}-\left\{e^{'}\right\}=0$
Lattice-site conservation	$1=\left\{V_{Mg}^{''}\right\}+\left\{Mg_{Mg}^{X}\right\}+\left\{Fe_{Mg}^{X}\right\}+\left\{Fe_{Mg}^{\bullet}\right\}$ $1=\left\{V_{O}^{X}\right\}+\left\{O_{O}^{X}\right\}$ $1=\left\{V_{Si}^{''''}\right\}+\left\{Si_{Si}^{X}\right\}$

Table 3. Most probable defect reaction mechanisms (after Smyth and Stocker, 1975, Stocker, 1978 and Schock et al., 1989)

Intrinsic reactions		
Frenkel defects	Movement of ions from normally occupied sites to normally vacant sites. E.g. $\text{nil} \longleftrightarrow Mg_I^{\bullet\bullet} + V_{Mg}^{''}$	
Schottky defects	One formula unit of Mg_2SiO_4 moves from normally occupied sites to an external or internal surface, creating new lattice sites and leaving vacancies of all three kinds. E.g. $\text{nil} \longleftrightarrow 2V_{Mg}^{''} + V_{Si}^{''''} + 4V_O^{\bullet\bullet}$	
Electronic disorder	Electrons are promoted across the band gap from the valence band to the conduction band: $\text{nil} \longleftrightarrow e' + h^{\bullet}$	
Interesting extrinsic reactions		
Incorporation of SiO_2	$2SiO_2 \longleftrightarrow 4O_O^{\times} + Si_{Si}^{\times} + Si_I^{\bullet\bullet\bullet\bullet} + 2V_{Mg}^{''}$	New Mg sites remain vacant
Incorporation of MgO	$4MgO \longleftrightarrow 4O_O^{\times} + 2Mg_{Mg}^{\times} + 2Mg_I^{\bullet\bullet} + V_{Si}^{''''}$	New Mg interstitials
Oxygen excess region	Vacancies: $2O_2 \longleftrightarrow 4O_O^{\times} + 2V_{Mg}^{''} + V_{Si}^{''''} + 8h^{\bullet}$ Interstitials: $2O_2 \longleftrightarrow 4O_I^{''} + 8h^{\bullet}$	
Oxygen deficient region	Vacancies: $4O_O^{\times} \longleftrightarrow 2O_2 + 4V_O^{\bullet\bullet} + 8e'$ Interstitials: $4O_O^{\times} + 2Mg_{Mg}^{\times} + Si_{Si}^{\times} \longleftrightarrow 2O_2 + 2Mg_I^{\bullet\bullet} + Si_I^{\bullet\bullet\bullet\bullet} + 8e'$	
Ionisation reactions	Oxygen: $V_O^{\times} \longleftrightarrow V_O^{\bullet} + e'$ (and again). Iron on magnesium sites: $Fe_{Mg}^{\times} \longleftrightarrow Fe_{Mg}^{\bullet} + e'$ Interstitial iron: $Fe_I^{\bullet\bullet} \longleftrightarrow Fe_I^{\bullet\bullet\bullet} + e'$	
Iron oxidation by adsorption of O	$8Fe_{Mg}^{\times} + 2O_2 \longleftrightarrow 2V_{Mg}^{''} + V_{Si}^{''''} + 4O_O^{\times} + 8Fe_{Mg}^{\bullet}$	

2. Method

Due to the wide variety of experiments, qualitative and quantitative modelling the method is divided into two sections. One section is directly related to the experimental procedure and the other is related to modelling the data. For the latter most background information on the matter can be found in the introduction. The sections are then further subdivided accordingly.

2.1. Conductivity experiments

2.1.1. Sample preparation

The olivine samples were created via a solgel synthesis method as described by McDonnell *et al*. (2002). Two kinds of synthetic olivine were made, one with 100% magnesium dubbed Fo_{100} (from forsterite) and various samples of 90% forsterite 10% fayalite composition (ie 10% Fe) which are dubbed as Fo_{90} or in tables as Fe0#, where # is sample number. Note that in preventing MgO to form, the samples contain excess Si instead, which exists as pyroxene. However there is no more than 5% pyroxene present in all samples and is not considered to affect the overall electrical conductivity processes going on. The samples are small discs, around 12 mm in diameter and 1 – 1.5 mm thick. A hard ceramic of the samples was formed after being fired for 40 minutes at 1400 C for Fo and for 40 minutes at 1250 C for Fe under a controlled reducing atmosphere.

As can be seen in Figure 6, the samples have a foam texture with a narrow grain size distribution. The average grain size is 1.1 ± 0.4 μm as determined from the orientation contrast scanning electron microscope (SEM) images. The grain boundaries are free of precipitates and impurities while the grain size distribution is roughly the same everywhere. The porosity of the samples is about 13%. To produce different grain sizes, the Fe samples were sintered at 1300 C or 1350 C at different times. This caused further porosity reduction. Ten Grotenhuis *et al.* (2004) used a similar method to obtain these synthetic olivine samples. They discovered that there is no significant effect of porosity variations on the electrical conductivity by hot isostatically press (HIP) a sample in an Ar gas pressure vessel in a gold jacket at 900 C with 0.2 wt% water present. The result was a porosity decrease without changing the average grain size. After the impedance measurements the samples were checked on grain size using the SEM to ensure that grain growth was limited.

The Fo sample was given special treatment. The top and bottom region of the disc was painted using porous platinum paint to allow maximum gas contact with the sample in a reducing atmosphere to verify that the electrical conductivity of the sample is really independent of the oxygen fugacity within the olivine stability field. Ordinarily, the top and bottom electrode would form a solid contact with the sample, preventing gas to get in between and interact with the sample. See Figure 7 for the setup. However, due to reproducibly problems of data at every new higher temperature the method was discontinued for the Fe samples. See for more information in the appendix.

The thickness of the samples was measured before and after experiments using a micrometer.

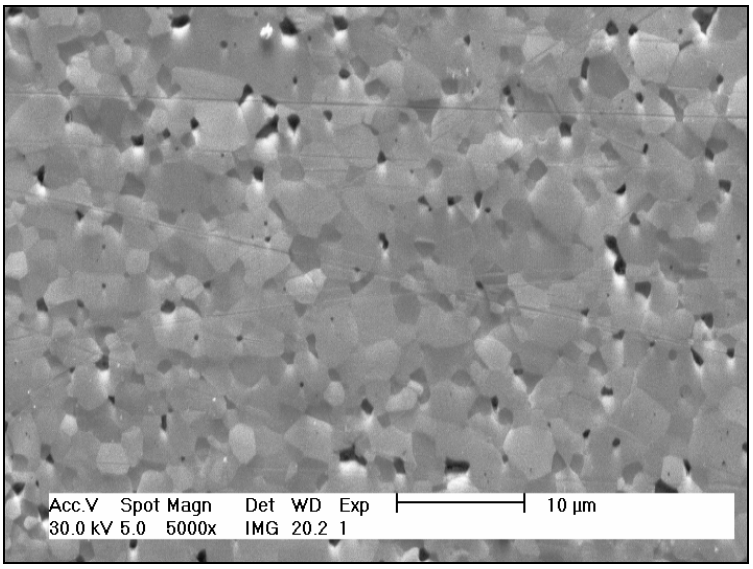

Figure 6. Forsterite sample SEM image showing a foam texture, with an average 1.1 micron grain size and about 13% porosity (black holes).

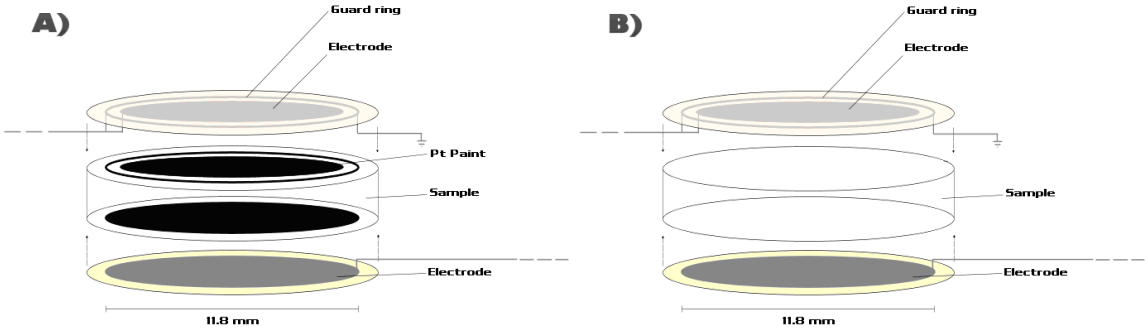

Figure 7. Sample setup for forsterite with the Pt paint (A) and for Fo_{90} samples without Pt paint (B).

2.1.2. Impedance measurements

The electrical impedance measurements were taken with a Solartron 1260A impedance analyser with the ability to measure tiny conductivities with the addition of the Solartron 1296A dielectric interface. The exact impedance range is then 10^{14} Ohm and lower capacitance determination is down to 10^{-12} F both measured with an accuracy of 2%. The capacitance of the system is 10^{-12} F. Figure 8 shows the experimental setup which resides in a vertically mounted controlled atmosphere furnace. The electrodes are made of 0.5 mm thick Pt plates which are pressed onto the sample by the weight of the column made of alumina. The wires coming from the electrodes and guard ring and shielding go through separate holes in the two alumina tubes. These tubes are painted with Pt paint and earthed to avoid additional signals from the AC power supply.

The method used was with 2 electrodes only. The guard ring made sure that fluxes around the sample were eliminated and that the conductivity (or resistance)

measured is only going straight through the sample. One Type-S Pt / Pt-10%Rh thermocouple resides below the sample and the other above the sample. An additional thermocouple from the oxygen sensor is present in close proximity to the sample as well. For all experiments, upon initial heating to the set temperature, the sample is left to equilibrate for 2 hours before commencing measuring the impedance. After each change in temperature, the standard equilibration time is 45 minutes. This is the same for each change in oxygen fugacity. The data was collected during one or more cycles, depending on the time available, to check the reproducibility of the data. In some cases the same experiment was carried out the next day to see if a full cooling and heating cycle had any effect on the impedance measurements. A control experiment on Fo was carried out to see if the oxygen fugacity has any effect on the conductivity of the sample, while for Fe the atmosphere had to be reduced to an oxygen fugacity range at which olivine is stable using a CO / CO_2 gas mix. H_2 was not used because that would introduce the risk of unwanted water vapour despite an increase in reducing conditions. The oxygen fugacity was first predicted using calculations for the reaction in equilibrium: $CO_2 \longleftrightarrow CO + 1/2O_2$. The updated thermodynamic properties for each species at different temperatures were obtained from NASA[4]. The calculations give the ratio of CO_2 versus CO at each fO_2. By inserting the desired fO2 value into the calculation one can therefore see what amount CO needs to be added to achieve the target fO2. The initial CO_2:CO ratio used, while heating the furnace, was 1:5 in order to remain as short as possible outside the carbon stability field but reducing enough so that the olivine sample does not oxidise. After initial equilibration of 2 hours, measurements were taken at 45 minute intervals and the oxygen fugacity, while calculated, was in reality read from a computer which in turn gave readings from the oxygen sensor up to high accuracy. The oxygen sensor was coupled to a thermocouple which reads to an accuracy of 0.2°C and two other thermocouples, one below and one above the sample, read to an accuracy of 0.2°C.

Once the apparatus is readied for impedance measurements, the data obtained is corrected for the geometry of the sample. Only the real impedance is used because it is equivalent to the resistance of the sample. This is taken where the impedance arc touches the x-axis. The geometrical correction, the area divided by the thickness of the sample, is multiplied by the real impedance. The reciprocal is equivalent to the conductivity.

[4] MS Excel thermovader plugin by Stuart Scott and Paul Fennell (2004) from the NASA Glenn thermodynamic database (http://cea.grc.nasa.gov/about).

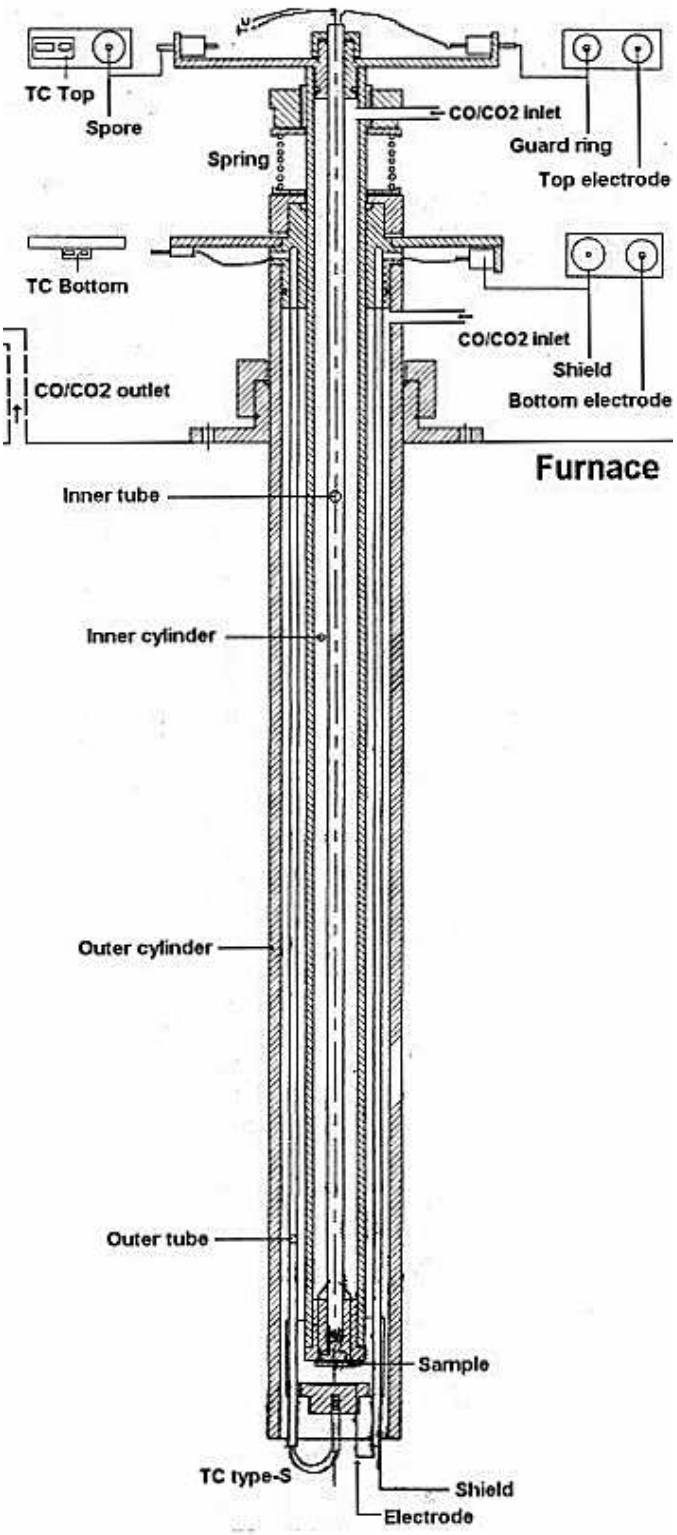

Figure 8. Gas mixing furnace for making electrical conductivity measurements at room pressure and high temperature. The mixture of CO and CO_2 is controlled by separate mass flow controllers for each gas.

2.1.2.1. Experiments on Fo_{100}

Electrical measurements on the Fo_{100} sample were taken in the temperature range of 800 C to 1200 C in the frequency range of 10^{-1} Hz to 10^{6} Hz with 8 measurements per decade at each temperature with an AC level of 0.5 V and a 10 second integration time. The first set of measurements was taken under normal atmospheric pressure and composition. While the atmospheric pressure was kept the same, the second set of experiments was done under controlled oxygen fugacity using a gas mix of CO and CO_2. The account of the exact sequence of events and problems encountered can be read in the appendix.

2.1.2.2. Experiments on Fo_{90}

Impedance measurements on the Fo_{90} samples were taken in the temperature range of 1000 C to 1200 C and between oxygen fugacity values of 1E-8 Pa to 1E-2 Pa, well within the stability field of olivine at those temperatures. The same frequency range and number of measurements per decade was adopted with an AC level of 0.5 V and a 10 second integration time as was used for experiments on Fo_{100}. There was one exception when a prolonged measurement was taken down to a frequency of 10^{-3} Hz in order to confirm the presence of a third impedance arc. Again measurements were carried out in cycles to confirm the reproducibility of the data. Grain size was varied by sintering the other samples for 5 hours and 16 hours at 1350 C in a platinum jacket in a bucket. Because all Fo_{90} samples come from the same sol-gel substance and were heat treated the same, they are of the same composition and initial average grain size of 1 micron. To make sure that all samples yield the same order of magnitude resistance before sintering, conductivity experiments were done on each sample at 1100°C and compared. Because the samples are of different thickness, a geometric correction is applied.

Table 4 shows an overview of all the experiments conducted and Table 5 shows the properties of each sample used.

Table 4. Overview of all the experiments performed.

	Temperature range/ set T (°C)	Oxygen fugacity range/ set fO2 (Pa)	Grain size (µm)	Frequency range/ points per decade
Fo01	800C-1200	21,000	1.1 +/- 0.4	1Mhz – 0.1 Hz/ 8
Fo02	1100	1E-8 – 1E-2	1.0 +/- 0.4	1Mhz – 0.1 Hz/ 8
Fe01a	1000	1E-8 – 1E-2	1.0 +/- 0.4	1Mhz – 0.1 Hz/ 8
Fe01b	1050	1E-8 – 1E-2	1.0 +/- 0.4	1Mhz – 0.1 Hz/ 8
Fe01c	1100	1E-8 – 1E-2	1.0 +/- 0.4	1Mhz – 0.1 Hz/ 8
Fe01d	1200	1E-8 – 1E-2	1.0 +/- 0.4	1Mhz – 0.1 Hz/ 8
Fe01total	1000-1200	1E-8 – 1E-2	1.0 +/- 0.4	1Mhz – 0.1 Hz/ 8
Fe02a	1000	1E-8 – 1E-2	2.6 +/- 0.7	1Mhz – 0.1 Hz/ 8
Fe02b	1100	1E-8 – 1E-2	2.6 +/- 0.7	1Mhz – 0.1 Hz/ 8
Fe02c	1200	1E-8 – 1E-2	2.6 +/- 0.7	1Mhz – 0.1 Hz/ 8
Fe02total	1000-1200	1E-8 – 1E-2	2.6 +/- 0.7	1Mhz – 0.1 Hz/ 8
Fe03a	1000	1E-8 – 1E-2	3.2 +/- 1.1	1Mhz – 0.1 Hz/ 8
Fe03b	1100	1E-8 – 1E-2	3.2 +/- 1.1	1Mhz – 0.1 Hz/ 8
Fe03c	1200	1E-8 – 1E-2	3.2 +/- 1.1	1Mhz – 0.1 Hz/ 8
Fe03total	1000-1200	1E-8 – 1E-2	3.2 +/- 1.1	1Mhz – 0.1 Hz/ 8
Fe01-oxi	1100	1E-8 – 1E-2	1.1 +/- 0.6	1Mhz – 0.001 Hz/ 8

Table 5. Overview of the properties of each sample.

Sample	A/l, m	Sintering time / temperature	Av. grainsize, µm	Porosity, %
Fo01	0.0350	0	1.1 +/- 0.4	13%
Fe01	0.0367	0	1.0 +/- 0.4	13%
Fe02	0.0336	5h / 1350°C	2.6 +/- 0.7	5.2%
Fe03	0.0507	16h / 1350°C	3.2 +/- 1.1	4.8%
Fe01-oxi	0.0367	0	1.1 +/- 0.6	10.6%

2.2. Modelling the data

Using controlled atmospheric conditions with a gas mix of CO / CO_2, when every variable except the oxygen fugacity is kept constant, the data shows a relationship with the oxygen fugacity and resistance which is in turn coupled to the species and concentration of charge carriers in the material. Numerous quantitative models have been proposed in the early 90's (Constable and Duba, 1990, Hirsch and Shankland, 1993 and Schock *et al.*, 1989) which model the concentration of various defect species in olivine under different oxygen fugacities. These models, however, only apply to single crystals. In other words, the grain boundary effect is not incorporated and hence will not be modelled in this study.

The model used in this study is a modified approach adopted by Constable and Duba (1990) and Constable and Roberts (1997). Most details have already been stated in the introduction / background sections but the actual equations used to obtain the conduction contribution of the various charge carriers are shown here.

As has been described earlier, in order to obtain the conduction contribution of each charge carrier, one will need to know the concentration of that carrier, its mobility and the effective charge it carries (which can be approximated to be the charge of an electron) as shown in this model for this reaction:

$$8Fe_{Mg}^{\times} + 2O_2 \longleftrightarrow 2V_{Mg}^{''} + V_{Si}^{''''} + 4O_O^{\times} + 8Fe_{Mg}^{\bullet}$$

$$\Vert$$

$$\vee$$

$$\sigma = \left[Fe_{Mg}^{\bullet}\right]\mu_{Fe}e + c_e\mu_e e + 2\left[V_{Mg}^{\bullet}\right]\mu_{Mg}e$$

The mobility of magnesium vacancies and small polarons can be approximated with an Arrhenius relationship, i.e. as thermally activated processes. The same can be said of the constants b_{Fe} and b_{Mg} (Constable and Roberts, 1997) which appear in the equation for the concentration of charged species shown below. The corresponding activation energies for the mobility of the charged species appear to be estimated by Constable and Roberts (1997). This study will adopt the same values. The activation energies in the equation for the concentration of the charged species are not adopted but the value obtained from recent creep experiments, on synthetic forsterite with 10% fayalite which yielded an activation energy of 270 +/- 50 kJ/mol, is adopted (Slotemaker and de Bresser, work in progress). The reason being is that with creep experiments there is only ionic displacement (not electronic) thus this activation energy belongs to magnesium ions. Similar but somewhat higher activation energies at temperatures of 1200 – 1400°C were obtained for forsterite where ionic conduction is thought to completely dominate over electronic conduction (see Table 6 for values and references in results section 3.6). Experiments on Fe0# are carried out between 1000°C and 1200°C. The numerical model is shown below (see Table 7 in the discussion section for corresponding values for each parameter):

Mobility: Concentrations:

$$\mu_{Fe} = c_{Fe}\, exp\left(-\frac{A_h}{RT}\right) \qquad \left[Fe_{Mg}^{\bullet}\right] = b_{Fe}(T) + a_{Fe} \cdot exp\left(-\frac{E_h}{RT}\right) \cdot \left(f_{O_2}\right)^{1/6}$$

$$\mu_{mg} = c_{Mg}\, exp\left(-\frac{A_{Mg}}{RT}\right) \qquad \left[V_{Mg}^{''}\right] = b_{Mg}(T) + a_{Mg} \cdot exp\left(-\frac{E_{Mg}}{RT}\right) \cdot \left(f_{O_2}\right)^{1/6}$$

where A_x and E_x are in J/mol.

For electrons the mobility is referenced to be around 0.14 m^2/Vs (see Table 7). Its concentration is calculated from the electron effective mass in Si and the temperature using the modified Fermi function as described in the background section. The relation of the electron concentration against the oxygen fugacity is –1/6 (Hirsch and Shankland, 1993 and Constable and Roberts, 1997).

3. Results

3.1. Test run

The first measurements were done on an iron free synthetic olivine sample under normal atmospheric conditions and at various temperatures. 800°C was taken as a starting temperature because any lower and the resistance of the sample would be too high and our goal is to quantify the behaviour of olivine under mantle conditions. To verify if there would be a possibility of a leaky capacitor in the system, at room temperature for both samples; the forsterite and the iron bearing sample, conductivity measurements were done under these conditions. As Figure 9 shows the sample behaves as a near-perfect capacitor with a phase angle near 90˚.

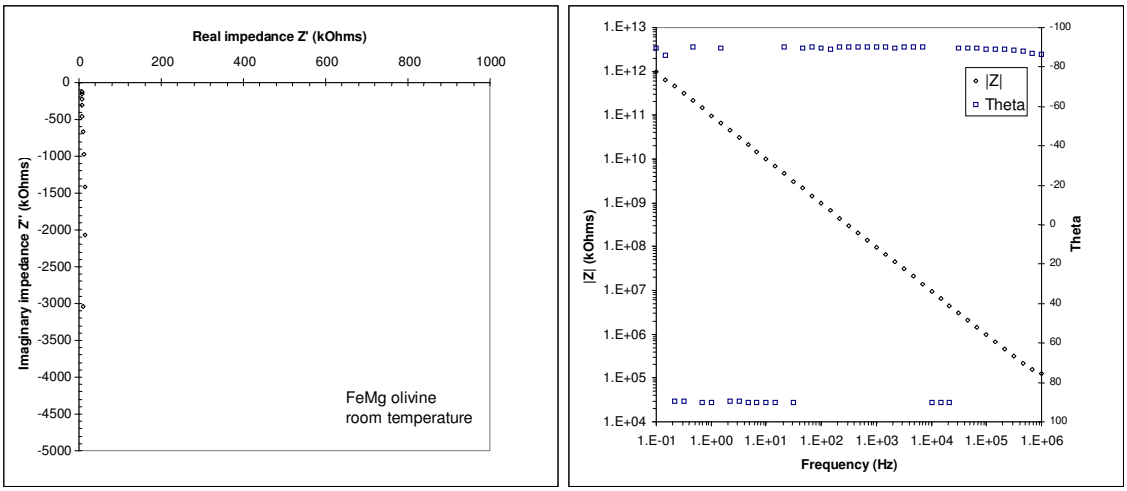

Figure 9. Impedance (Nyquist) plot and merged log-log, linear-log bode plots showing an approximate ideal capacitor indicating no presence of a leaky capacitor. This plot was produced from the Fe01 olivine sample at room temperature.

3.2. Fo_{100} control experiments (forsterite)

At elevated temperatures, however, the typical impedance plots produced show a distinct arc, often depressed to sometimes high degrees like 50°. But more frequently the angle of depression is more in the order of 5°- 10° especially at temperatures below 1100°C. Note that these figures are not 1:1 because in most cases the arc would become very indistinct. Figure 10 is such an impedance plot of a forsterite sample at 900°C where the angle of depression is low and a clear arc is seen. At higher temperatures the main arc becomes smaller and at lower frequencies one could argue that there is a second arc present and a beginning of a third, but the scatter is great. The scatter is probably an effect of the electrodes seen often with the two electrode technique (Roberts and Tyburczy, 1991 and ten Grotenhuis, 2004). Each arc has a different relaxation time, τ. These arcs can be seen in the impedance plot of forsterite at 1200°C in Figure 11.

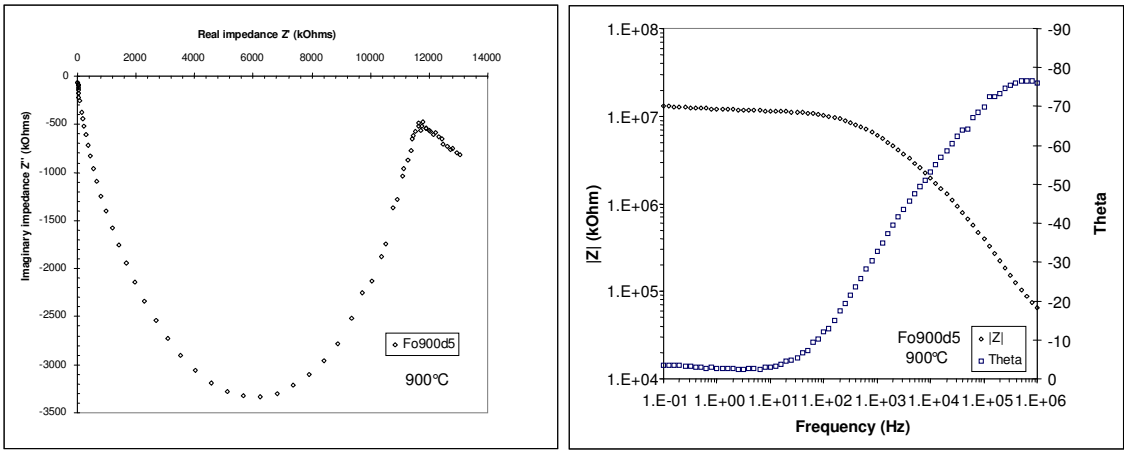

Figure 10. Impedance and merged log-log, linear-log bode plots of forsterite (Fo01) at 900°C.

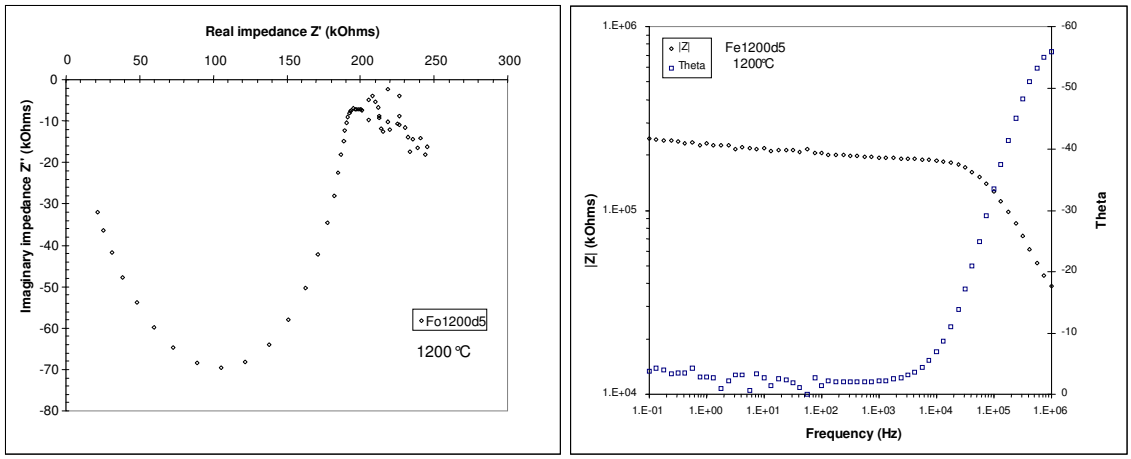

Figure 11. Impedance and merged log-log, linear-log bode plots of forsterite (Fo01) at 1200°C.

After enough data was collected at different temperatures, the forsterite sample was left at a constant temperature of 1100°C and the oxygen fugacity was changed. Figure 12 shows that at different oxygen fugacity the conductivity through the sample remains within 0.1 order of magnitude and when compared to conductivity measurements taken under normal atmospheric conditions, there is virtually no change.

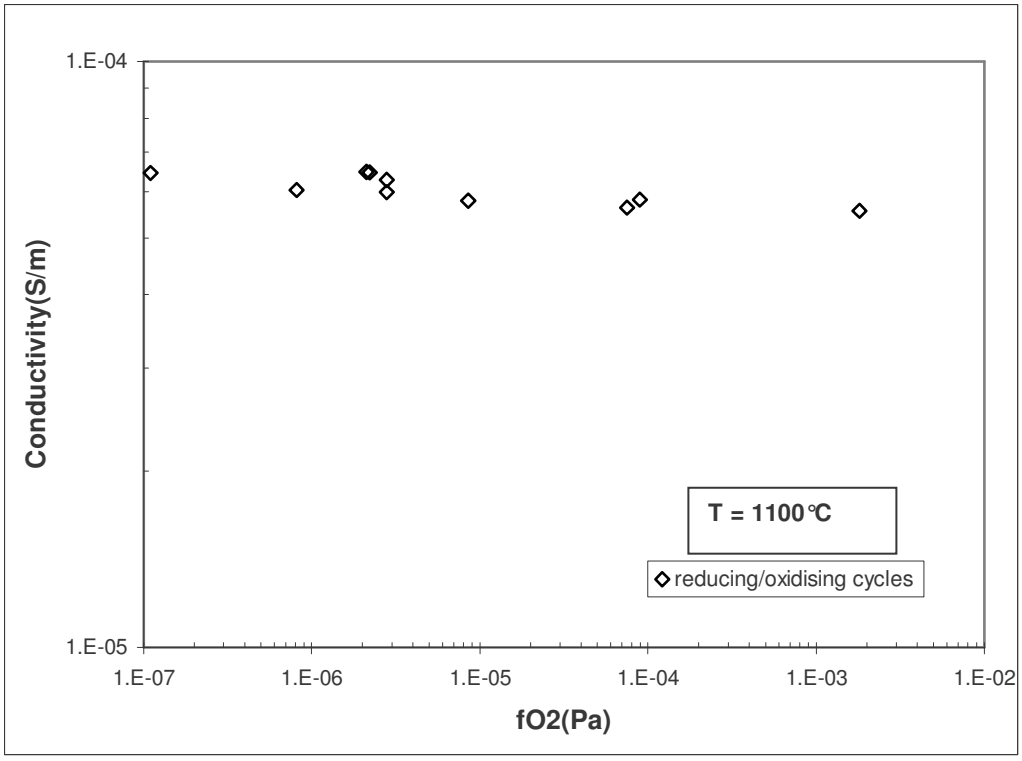

Figure 12. Conductivity versus oxygen fugacity log-log plot showing the effect of reducing conditions on the conductivity through forsterite (Fo01). Note the y-axis is only one order of magnitude.

Despite the fact that the data lies in the range of a mere (5E-5 to 6E-5) S/m there can be a small negative slope distinguished. More oxidising conditions seem to indicate higher resistance. If this falls within the margin of error of measurement is unsure, however, it must be noted that there were former problems with reproducing same results. See more about this in the appendix.

Figure 13 shows two Arrhenius plots with the grain interior conductivity plotted against 1000/T. As for Figure 12, the grain interior conductivity values in Figure 13 were taken at the lower frequency end of the impedance arc where the phase shift is closest to zero on the real axis in the impedance plot, thus omitting the imaginary component of the impedance. A geometric correction, taking into account the contact surface area and the thickness of the sample, was applied to the values (A/l). As can be seen, heating and cooling cycles reproduce almost perfectly. An activation energy was obtained from the slope which equals about 191 kJ/mol.

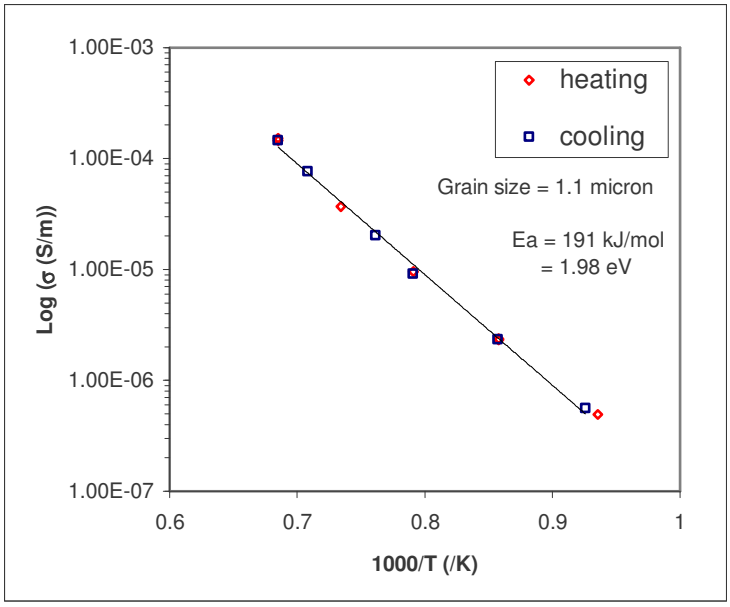

Figure 13. Arrhenius log-linear plot showing the conductivity data for forsterite (Fo01) at during different heating and cooling cycles. Temperature range is between 800°C and 1200°C. A slight curvature upwards can be seen.

3.3. Fo_{90} (Fe01) experiments (average grain size: 1 micron)

Unlike Figure 10 and Figure 11, conductivity measurements on iron bearing olivine at 1100°C and at different oxygen fugacity show a distinct second arc and a beginning of a third (see Figure 16). This arc increases in size, but shifts to the right (ie higher resistivity) at higher oxygen fugacity. As with all results the arcs are depressed as seen in Figure 14. At low oxygen fugacity the second arc is almost indiscernible. In addition, at higher temperatures the second arc is also much less well developed. The overall conductivity at 1100°C is much higher too, but not much higher as compared to the forsterite sample at 1100°C (with a difference of 50kOhm) (see Figure 15).

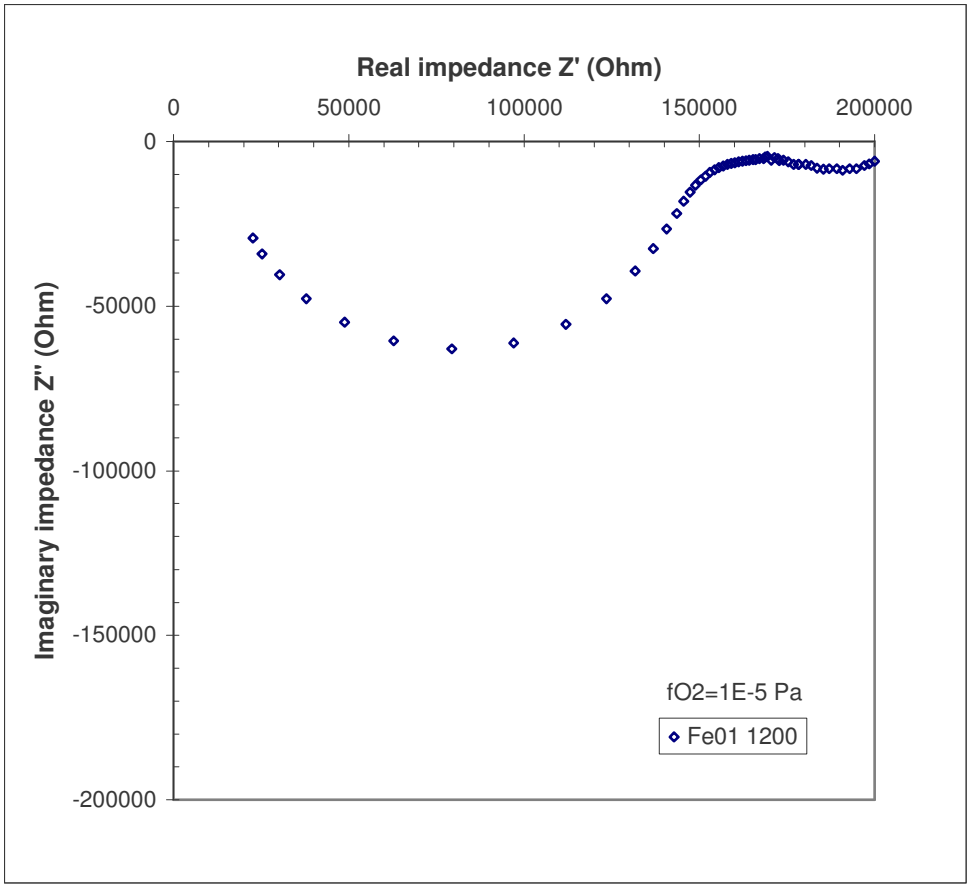

Figure 14. A 1:1 representation of the depressed arcs obtained. This is Fe01 at 1200°C and *f*O2 of 1E-5 Pa.

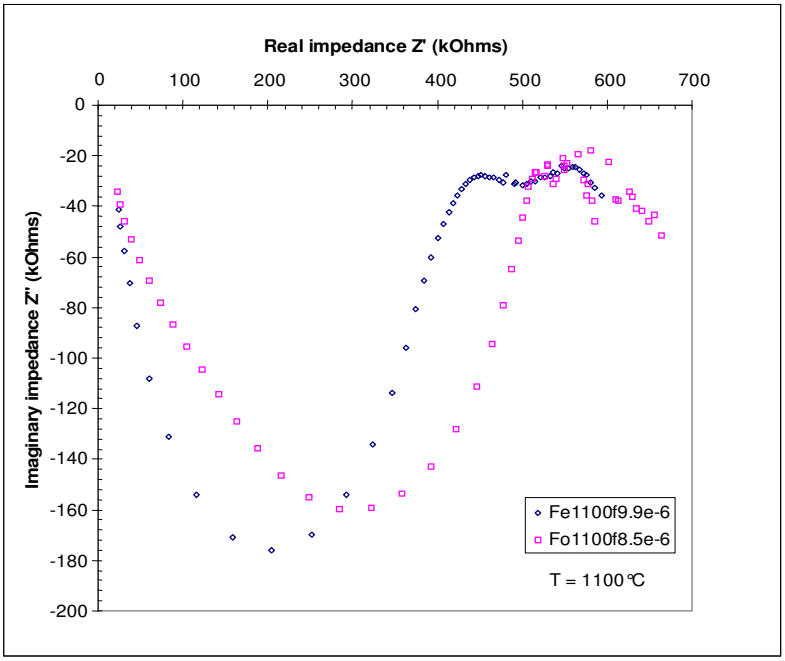

Figure 15. Impedance plot at 1100°C and at an oxygen fugacity of roughly 9e-6 Pa showing the conductivities of forsterite (Fo01) and Fe01 olivine.

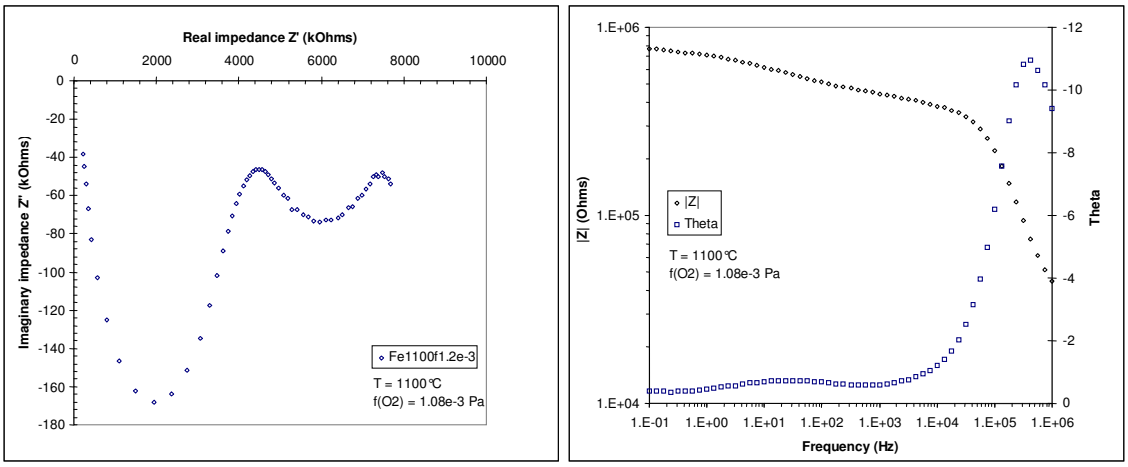

Figure 16. Impedance and merged log-log, linear-log bode plots of Fe01 olivine at 1100°C and oxygen fugacity of 1.2e-3 Pa. Note that the phase angle theta is even initially not very high. Also note the distinct second arc in the impedance plot.

Figure 17 is similar to Figure 12 where the conductivity measured is plotted against various oxygen fugacities. Double measurements at one oxygen fugacity means that a reduced atmosphere has been relatively more oxidised and subsequently been brought back to the same reducing conditions thus showing that data is reproducible. Data has been plotted from measurements taken at 1100°C and at 1200°C. For comparison with forsterite, that data is also shown. In addition, for the Fe01 olivine sample, It was possible to obtain conductivity data of the second arc as seen in Figure 16 and that data has been plotted as well as a function of fO_2. At first sight, it is readily apparent that there is little response of the olivine samples to different oxygen fugacity. All slopes are even slightly negative, especially the data obtained at from the second arcs. In the plot is also shown a slope of 1/6. Many authors have obtained this slope from measurements on natural iron bearing olivine within the olivine stability field (Du Frane *et al.* (2005), Schock *et al.* (1989), Wanamaker and Duba (1993), Constable and Duba (1990), Sato (1986)). It is clear that current data does not support this.

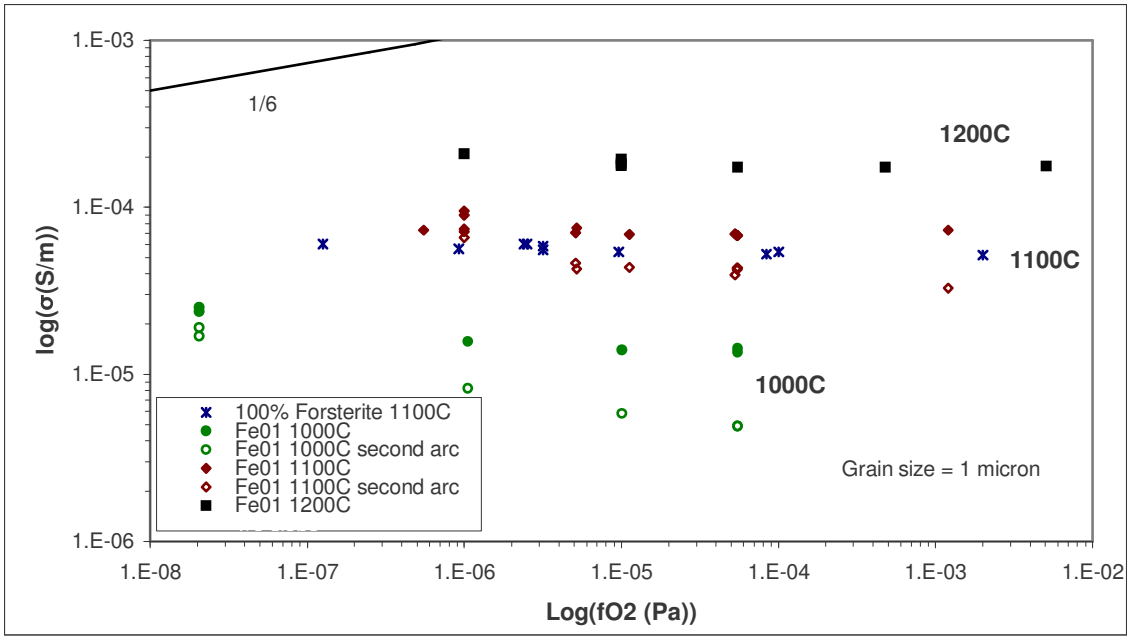

Figure 17. Conductivity versus oxygen fugacity log-log plot. Shown is data from Fo_{90} olivine (Fe01) at 1000°C, 1100°C and at 1200°C and data from the forsterite. Note how the slope of the data indicated as the second impedance arc is steeper than for the first arc. The slope 1/6 is a typical slope many authors obtain for natural occurring iron bearing olivine (Du Frane et al. (2005), Schock et al. (1989), Wanamaker and Duba (1993), Constable and Duba (1990), Sato (1986)).

The next figure (Figure 18) shows an Arrhenius plot similar to Figure 13, but for the iron bearing olivine sample. Despite the fact that there are fewer data points, the slope obtained isn't unreasonably different than the one obtained from the forsterite data. The activation energy that can be calculated from the slope is about 200 kJ/mol. Figure 19 shows that at very low frequency (1E-3 Hz) a third arc is formed.

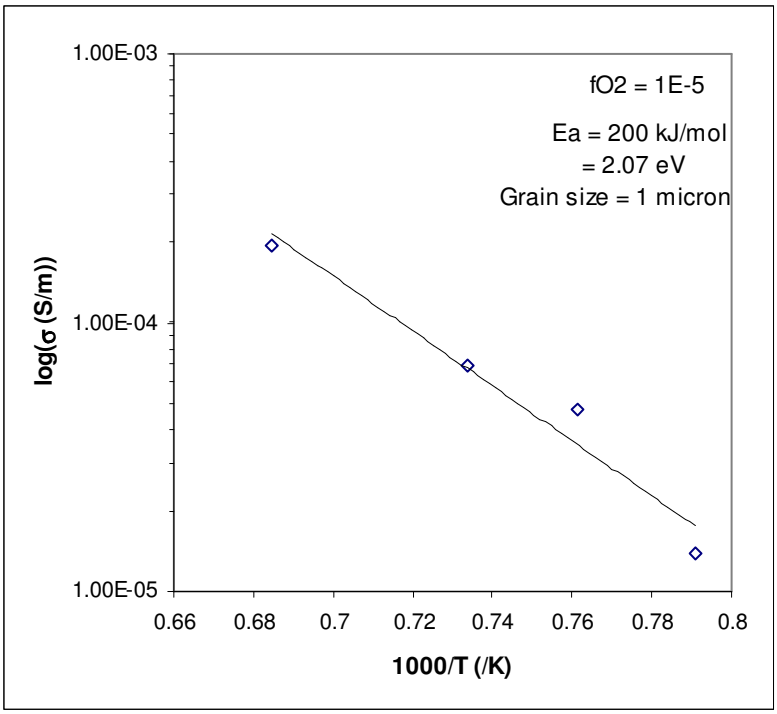

Figure 18. Log-linear Arrhenius plot of the conductivity*T versus the reciprocal of the temperature for Fo_{90} olivine between 1000°C and 1200°C and at $f(O_2)$ of 1 x 10^{-5} Pa. The activation energy obtained is around 200 kJ/mol.

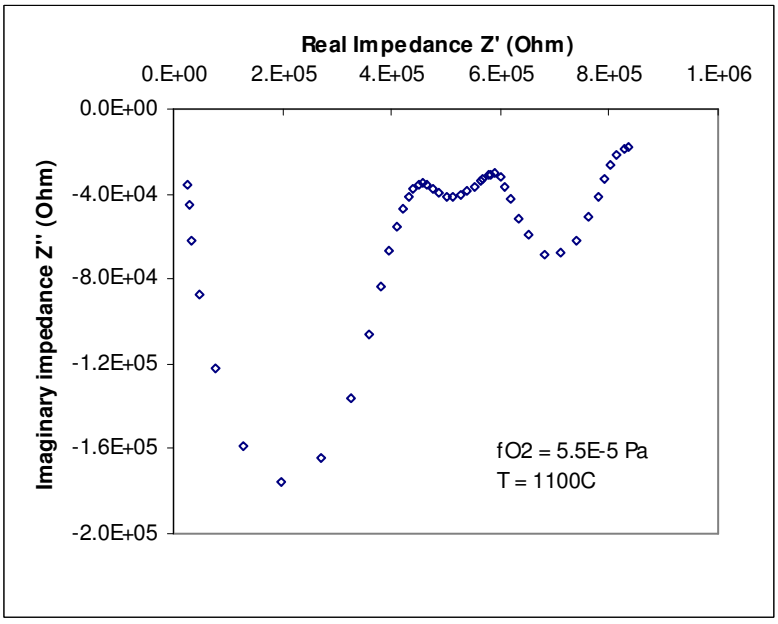

Figure 19. Nyquist plot of the Fe01 sample at 1100˚C and at an oxygen fugacity of 5.5E-5 Pa. The frequency range is from 1MHz to 0.001 Hz. Three distinct arcs are shown each one with a different relaxation time.

3.4. Fo_{90} (Fe02) experiments (average grain size: 2.6 micron)

Electrical impedance measurements were performed on synthetic iron-bearing olivine that had re-sintered for 5 hours at 1350°C. The temperature range is 1000°C - 1200°C. Similar to experiments performed on Fe01, the slopes in Figure 20 are almost horizontal instead of 1/6 as shown in natural material. The apparent activation energy obtained is 185 kJ/mol.

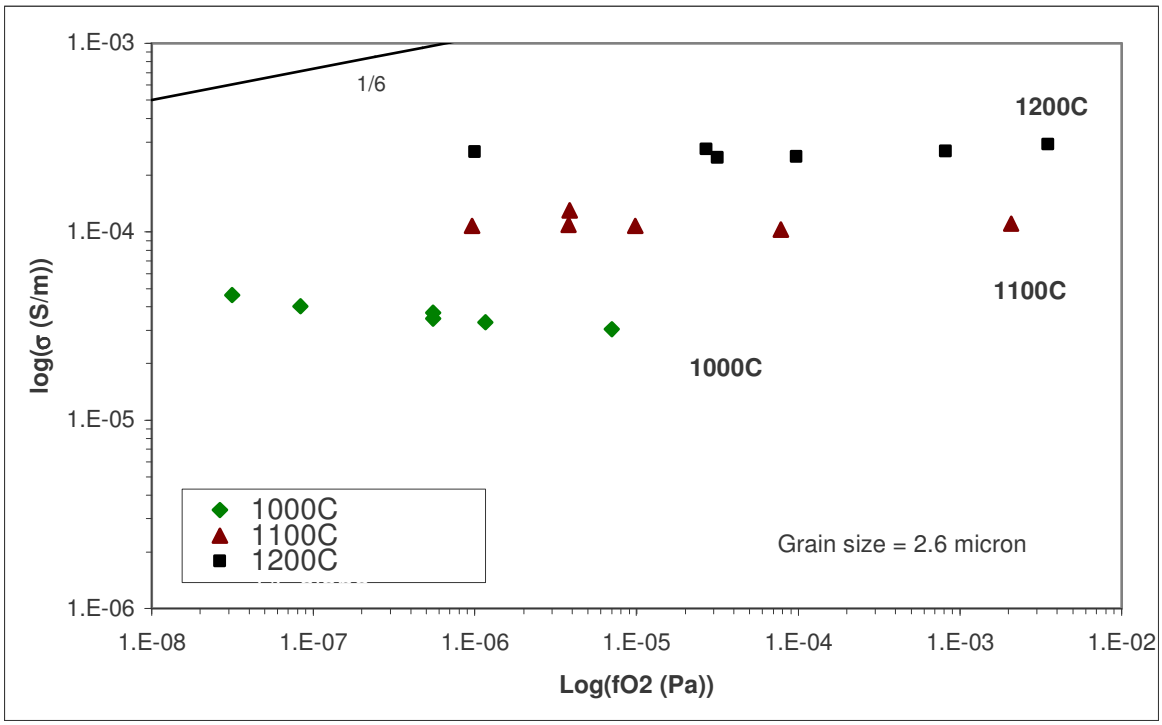

Figure 20. Conductivity versus oxygen fugacity log-log plot. Shown is data from Fe02 olivine at 1000°C, 1100°C and at 1200°. Note again how the slope of the data indicated as the second impedance arc is steeper than for the first arc. The slope 1/6 is a typical slope many authors obtain for natural occurring iron bearing olivine.

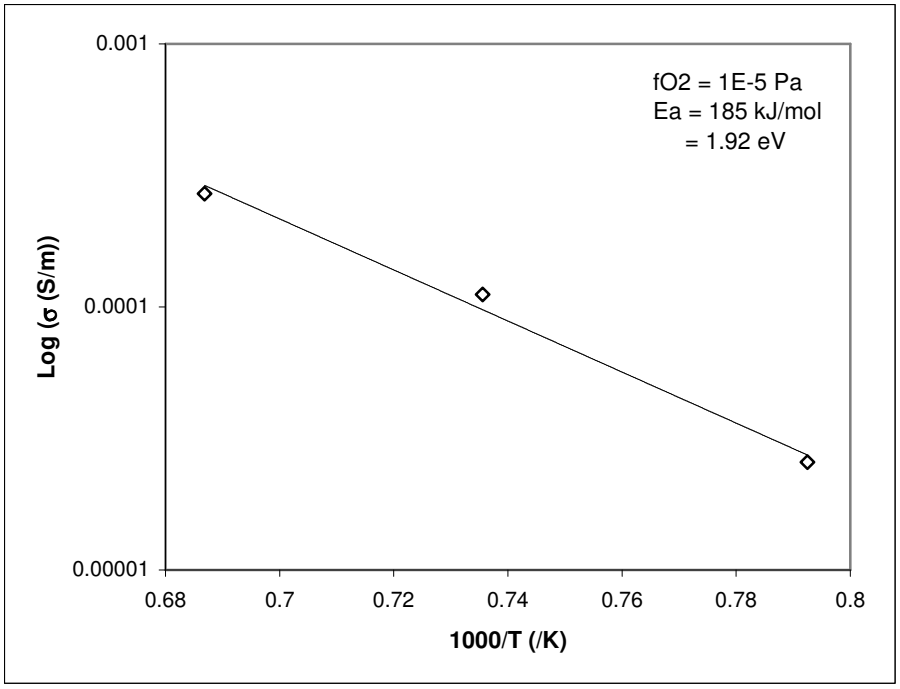

Figure 21. Log-linear Arrhenius plot of the conductivity*T versus the reciprocal of the temperature for Fe02 olivine between 1000°C and 1200°C and at f(O_2) of 5.5 x 10^{-5} Pa. The activation energy obtained is around 175 kJ/mol.

3.5. Fo_{90} (Fe03) experiments (average grain size: 3.2 micron)

The next sample, Fe03, was sintered at 1350°C in a Pt jacket for 16 hours. Electrical impedance experiments were carried out thereafter between 1000°C and 1200°C. Due to unexpected interference at low frequencies the second arc could not be properly identified. However, the first arc was fully formed. The conductivities obtained at the various temperatures under different oxygen fugacities can be seen in Figure 22. When comparing this figure to Figure 17, it is apparent that the conductivities at each temperature are almost the same or the same within the range of error. This would suggest no grain size dependency. See the section on grain size dependence for more details. Figure 23 shows an Arrhenius plot for Fe03. The activation energy obtained from the slope is around 207 kJ/mol which is very close to what was obtained for Fe01.

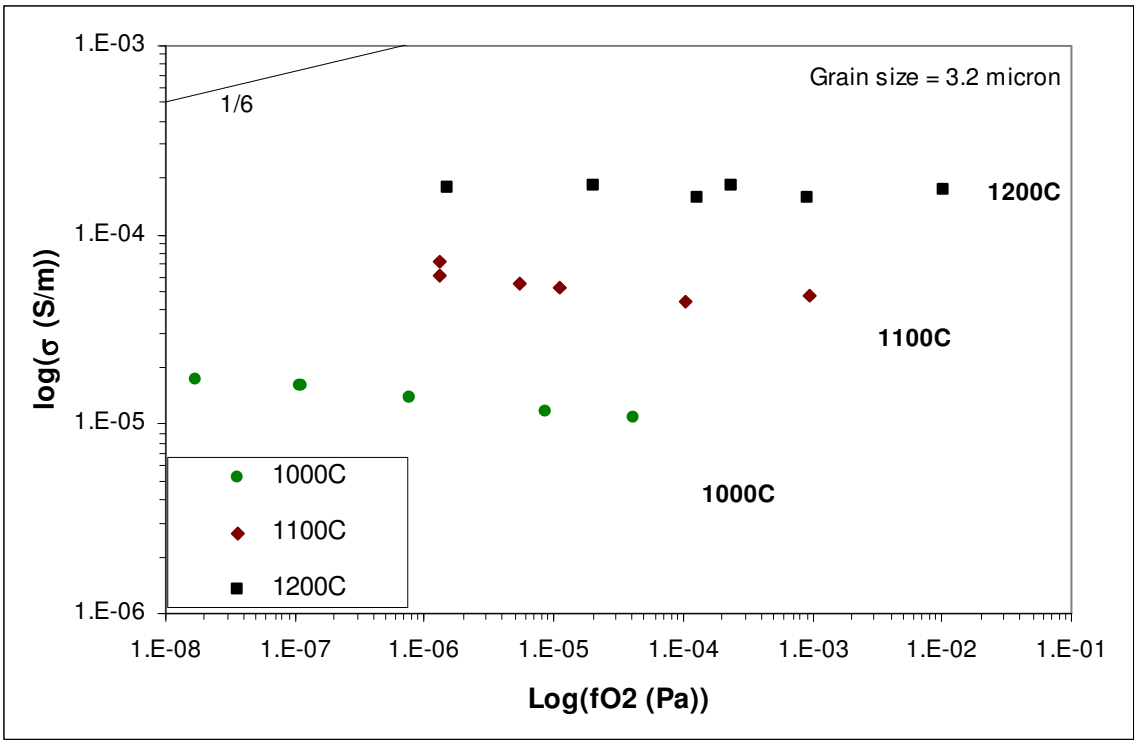

Figure 22. Conductivity data at different fO2 and temperatures.

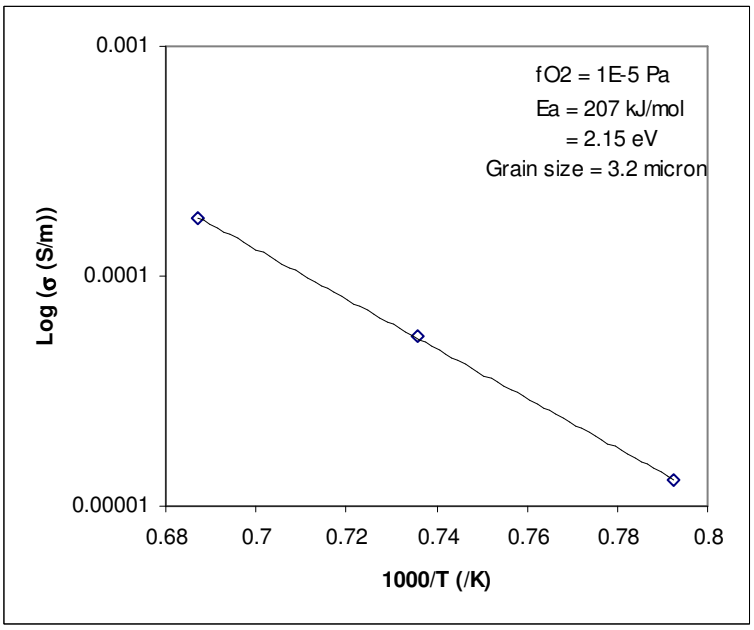

Figure 23. Log-linear Arrhenius plot of the conductivity*T versus the reciprocal of the temperature for Fe03 olivine between 1000°C and 1200°C and at f(O_2) of 1 x 10^{-5} Pa. The activation energy obtained is around 207 kJ/mol.

3.6. Summary

Figure 24 is a compilation plot to give a better overview of the conductivities obtained for the various samples at one specific temperature of 1100°C. As can clearly be seen, most data plots in one area on a line including the forsterite data indicating that forsterite is not necessarily less conductive than forsterite with 10% Fe because all the iron is in reduced form. Table 6 shows an overview of all the samples and used and their respective properties like grain size and associated apparent activation energy obtained.

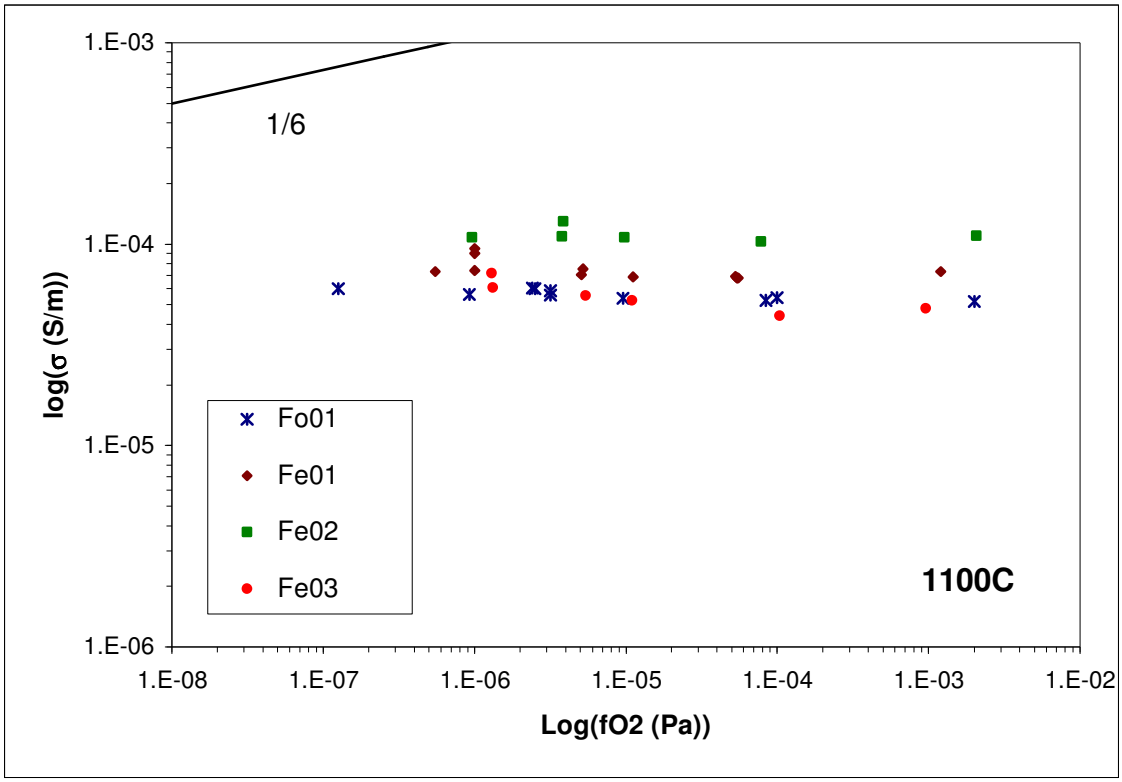

Figure 24. This chart sums up the conductivity data from all samples at 1100°C. Note how most data clusters one line and that conductivity of forsterite is not specifically less than that of forsterite with 10% fayalite. The conductivity data for Fe02 lies somewhat higher than the rest.

Table 6. Summary of the apparent activation energies obtained for the various samples for bulk and grain boundary conduction.

Sample	Average grain size	Activation energy	
	µm	*kJ/mol*	*eV*
Fo01	1.1 +/- 0.4	191	1.98
Fe01	1.0 +/- 0.4	200	2.07
Fe01 Grain boundaries	1.0 +/- 0.4	324	3.36
Fe02	2.6 +/- 0.7	185	1.92
Fe03	3.2 +/- 1.1	207	2.15

3.7. Oxidation experiment on Fe01 (Fe01-oxi)

Figure 25 shows what would happen if olivine we brought outside its stability field. It is apparent that beyond the olivine stability field the data points lie on a slope of

1/6. The last set of data points at fO_2 = 21 000 Pa were taken at t = 0 to t = 44 minutes, where t = 0 is immediately after the flow of CO and CO_2 gases was stopped and ordinary air was introduced. The steady increase in conductivity with time indicates that eventually the conductivity will approach the 1/6 slope. Later, when the sample was examined, it was confirmed that the inside was not yet fully oxidised as compared to the outside of the sample. This can also be seen in Figure 41 in the appendix. The red conductivity data point was taken after the CO/CO_2 gases were re-introduced after about 1 hour. Whether the oxidised sample has undergone permanent change will be discussed later.

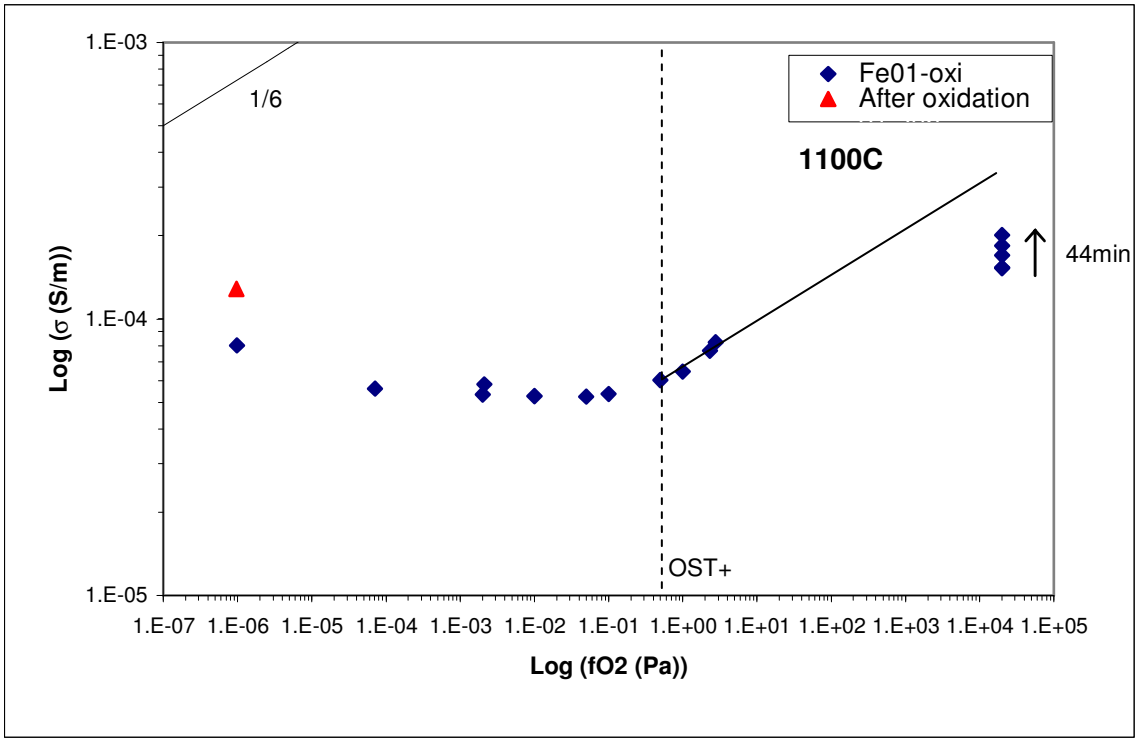

Figure 25. Conductivity data plotted as a function of the oxygen fugacity in a log-log plot. OST+ indicates the upper boundary of the olivine stability field.

4. Discussion

4.1. Problems with repeatability of results

Normally any mention of experiments that have gone wrong are not reported. However, in this case it is appropriate to briefly mention some of the biggest obstacles.

Initial experiments on Fo01, with Pt paint, did not go smoothly. The problem was noticed when increasing the temperature from 1100 C to 1200 C and back again. The data would not be reproducible within the wanted error margin. It is suspected that the platinum paint would reconfigure its coverage on the sample thus altering the total surface contact area. The idea of adding platinum paint and inserting a platinum coil on the forsterite sample between the paint and electrode therefore proved to be less than worth it. The idea was to grand ample access for the reducing atmosphere to the sample between the electrodes. But in practice the platinum paint made it difficult to yield reproducible results. Every other day the absolute electrical conductivity values would decrease over the selected frequency range. This was going to be especially problematic when the time would come to measure the electrical conductivity at different oxygen fugacities and constant temperature. To tackle the problem, the temperature of the furnace was raised to 1400°C for 15 minutes to allow the platinum paint to sinter once and for all. This seemed to have been successful. The following conductivity measurements at various temperatures were all reproducible during heating and cooling cycles and at different days within reasonable margin of error (see Figure 13). See appendix for a detailed account of the problems with the Pt paint.

Later, during experimentation on the iron bearing olivine, it happened more than once where the guard ring short-circuited with the top electrode even though this was checked beforehand. This appeared to cause an increase in conductivity by over an order of magnitude. Experiments were therefore mostly repeated to check for this possible problem.

4.2. Data comparison

It is apparent that the impedance data for 10% iron containing olivine (Fe0#) shows no real changes over an oxygen fugacity range of more than three orders of magnitude. What is even more apparent is that the conductivities calculated for forsterite at different f(O2) and at 1100C (corrected for contact surface area due to Pt paint) plot within 0.2 order of magnitude close to the data of Fe01 at 1100C (Figure 24). This would indicate that the conduction process in forsterite is likely to be very similar as in Fe0# olivine. However, unlike the forsterite data seems to indicate in the larger amount of noise at low frequency, the impedance measurements of Fe01 produce a complete second arc at higher f(O2) and lower temperature. The apparent activation energies obtained for the various olivine samples are quite close to each other at around 200 kJ/mol. This can be seen in Table 6.

When comparing the impedance results of this study for forsterite and Fe0# olivine (which are relatively of the same magnitude) it is striking that these absolute conductivity values do not compare with values obtained by other studies. For Fe01 olivine with a grain size of 1μm and porosity of 13%, the absolute conductivity values calculated are roughly at 1E-4 S/m at 1100C. An extensive and study by Du Frane *et al.*

(2005) obtains data in the range of 1E-3 S/m to 5E-3 S/m at 1100C for single crystal San Carlos olivine ($Fo_{89.1}$). Constable and Duba (2002) obtained conductivity values in the range of 3E-4 S/m to 1E-3 S/m at 1100C for a lherzolite (65% olivine). For more comparison, also at different temperatures, see Figure 35. So generally speaking the conductivities obtained in this study for synthetic olivine seem to be lower than for single crystal / polycrystalline natural samples. Once explanation is that due to the presence of more phases in polycrystalline samples or due to the altered impure chemistry of single crystals containing more defects, natural materials contain more charge carriers than synthetic olivine samples. More on this will be discussed in section 4.3.3.

4.3. Current data and model

4.3.1. Circuit modelling

Figure 26 shows a bricklayer model for electrical transport through a polycrystalline medium such as olivine. The two pathways shown are the end members. It is apparent that path 2 is the longer route. Unless the grain interiors are more resistive relative to grain boundaries, most conduction is expected to go through the grain interiors.

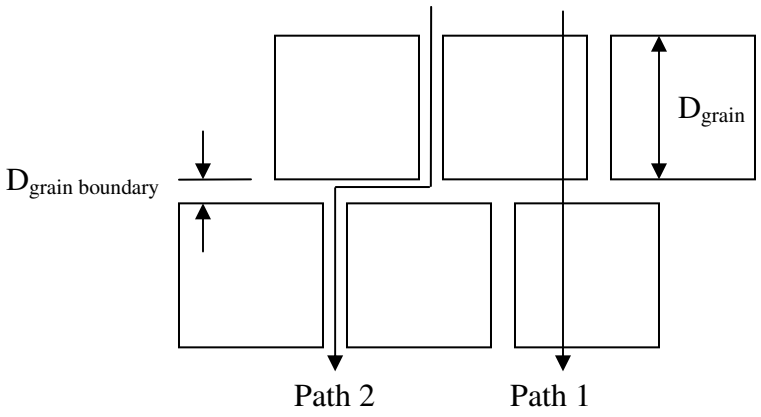

Figure 26. Bricklayer model for electrical transport through a polycrystalline olivine sample. The two pathways shown are end-members with one path fully going through the grain boundaries and another going straight through the grain interiors.

The first arc in an the impedance plot corresponds to the first component of a CPE in parallel to a resistor. Three such components form three arcs as seen in Figure 27. Figure 28 shows how the data is fitted using this model. In effect, the grain interior, grain boundary and electrode effect conduction pathways act in serial as can be seen in Figure 28. If the arc for the grain boundaries becomes small or may not even appear, it means virtually all conduction will take place through the grain interiors and grain boundaries equally. When grain boundary conduction is less than that of grain interior conduction then two arcs are shown and sometimes even three if an electrode effect is present too. If grain boundary conduction would be modelled in parallel to grain interiors then, if grain interiors were highly resistive, conduction would be dominated through grain boundaries in one arc only. However, if grain boundaries are highly resistive then grain interior

conduction would prevail together in series with some grain boundary crossing as shown by path 1 in Figure 26. This would predict at least one arc and up to three with grain boundaries acting very resistive and an electrode effect. This is clearly the case in as seen in Figure 28. Other measurements as shown as in Figure 15 and Figure 16 show at least two arcs and a beginning of a third.

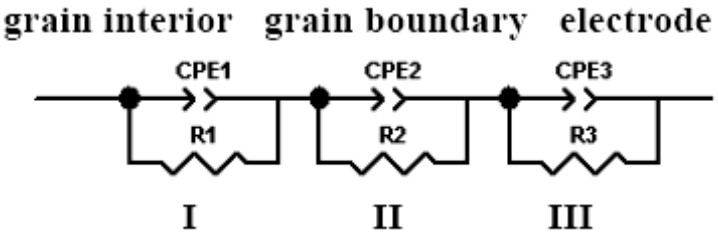

Figure 27. Circuit model for grain interior and grain boundary conduction acting in series (path 1 in Figure 26).

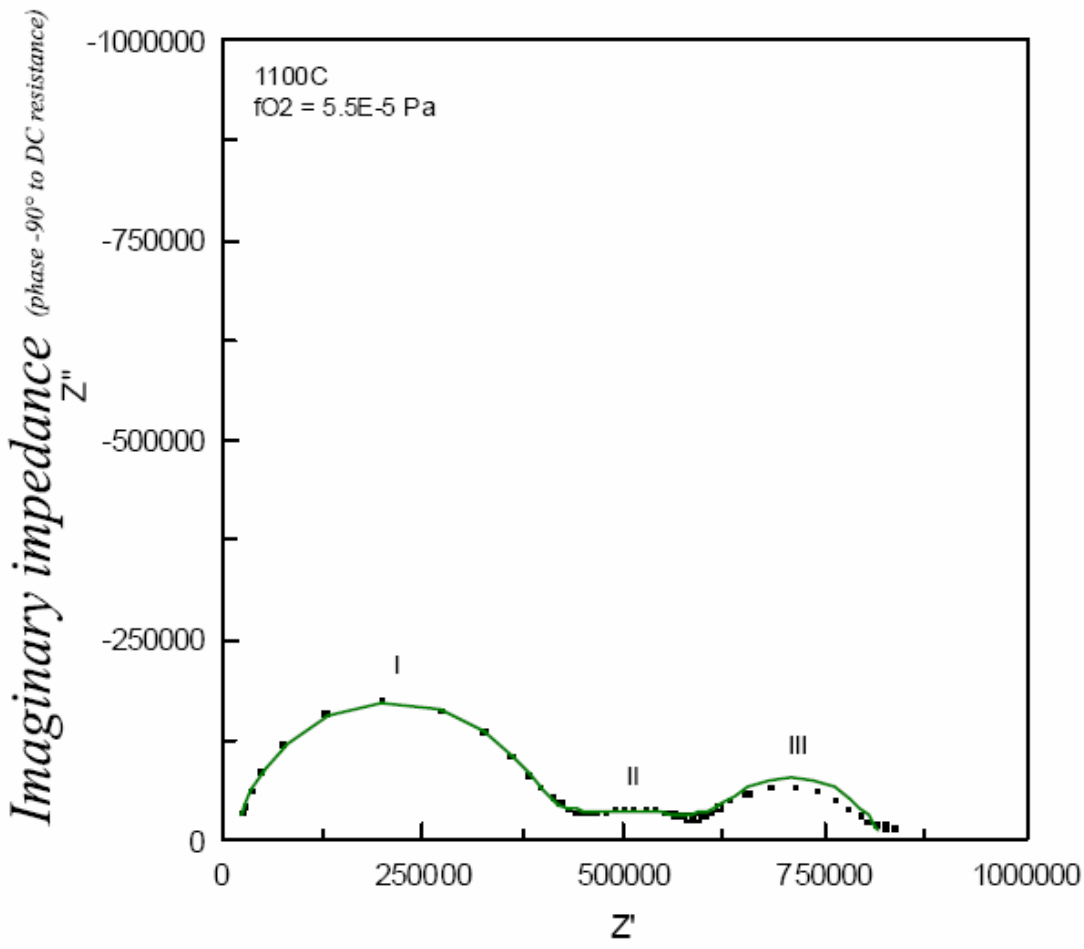

Figure 28. Modelled data from Figure 19 to circuit shown in Figure 27 using Z-view software. Ratio is 1:1.

Authors such as Roberts and Tyburczy (1991, 1993) attributed the first arc to grain interiors, because they thought the grain boundaries are in actuality blocking the current because of impurities and phase / defect aggregation. The reason why in this study the second arc attributed to grain boundaries and not the first arc is not only because of Figure 28 but also because consistently it can be seen that at higher fO2, the second arc becomes more and more resistive to electrical flow. This would be difficult to explain for grain interiors but not for grain boundaries where presumably oxygen atoms or interstitials may be blocking the passing of charge carriers as the oxygen pressure is increased or decreased mobility of iron and magnesium interstitials at higher fO2 at the grain boundaries.

The last (often poorly developed) arc represents the electrodes where the conversion of ionic to electronic conduction acts as a blocking effect to conduction. The rough 3D contact between sample and electrode may also play a part though it is assumed that the platinum becomes soft enough at these temperatures to create a full contact.

The scatter of data at high real impedance (low frequency) in Figure 11 and Figure 15 can be due to two causes. One, the irregular heated platinum paint for Fo01 between the sample surface and the spiral and electrode is affecting the lower frequency region. Reruns show that the general arc remains the same but the scatter in the low frequency region evolves. This may mean that the heated platinum paint has started to creep. Two, it may mean that there is unknown interference from other electrical applicances such as the furnace. Although this interference is expected only at certain frequencies. Or third, the interference is from improper grounding (of the guard ring and shield). For certain experiments the interference was completely gone, especially for Fe01, but returned with experimentation on Fe03. In between the apparatus was repaired for gas leaks so something might have changed again.

4.3.2. Modelled data

With all the data obtained from the experiments, the model, as explained in the background and method sections, can be fitted to the data. Table 7 shows the various parameters used and their source. Even though the temperature, concentration of electrons, and the constant b_{Mg} are the variables, only the temperature and the constant are the controllable variables because the concentration of electrons is calculated from the bandgap of olivine and the temperature using the equations derived in the background section 1.1.4.

The mobility of an electron is more of an estimate value taken from silicon, because no source could be found where the mobility of an electron is quoted forsterite with 10% fayalite. The same applies for the effective mass of an electron. The value used really applies to silicon. The normal electron mass could not be used because that is defined for an electron moving in a vacuum and not through a crystal structure of olivine. The average activation energy for magnesium vacancies is taken from recent and ongoing creep experiments carried out on the same synthetic material. With creep experiments one can be sure that the electronic component is not contributing to the activation energy. However, since creep involves the diffusion of mass it must be assumed that the same activation energy for magnesium vacancies applies to diffusion of magnesium (and the small percentage of iron) ions. The activation energy for the magnesium mobility is taken

from Constable and Roberts (1997) and yields a good diffusivity value via the Nernst-Einstein relationship (see section 4.3.5). The other constants, c_{Mg} and a_{Mg} are also taken from the model by Constable and Roberts (1997) where the latter is modified for this study to provide a better approximation. These constants are pre-exponential components and, like the fitting parameter b_{Mg} could contain other dependencies such as temperature, grain size or buffering by pyroxene (which limits the ability to lower the fO_2 state of the sample beyond the threshold value…ensuring a minimum population of small polarons (Constable and Roberts, 1997)). The fO_2 dependence for electrons is -1/6 as described by e.g. Stocker and Smyth, 1977 and Hirsch and Shankland, 1993.

It must be noted, however, that during the modelling of the data it became readily apparent that the small polaron contribution, $Fe_{Mg}^{\bullet}$ is not significant and therefore not included.

Table 7. Model parameters. Note that the only true adjustable variable is b_{Mg}. All other parameters are constrained at different temperatures.

Parameters	***Value***	***Source***
Ea for Mg (J/mol):	270000	Slotemaker, de Bresser (ongoing research, 2006)
Slope electrons	-1/6	e.g. Hirsch and Shankland (1993)
Ea Mg mobility (J/mol)	105000	Constable and Roberts (1997)
Mobility electron (m^2/Vs)	0.14	http://www.ioffe.rssi.ru/SVA/NSM/Semicond/Si
Charge of an electron, *e* (C)	1.60E-19	/
Gas constant (J/Kmol)	8.314	/
c_{Mg}	2.27E-06	Constable and Roberts (1997)
a_{Mg}	9.40E+33	Modified estimate from Constable and Roberts (1997)
Effective electron mass (for conductivity experiments) (kg)	$0.26m_e$	http://www.ioffe.rssi.ru/SVA/NSM/Semicond/Si/bandstr.html
Bandgap (eV)	6.3 (= better fit)	Shankland (1968), Morin et al (1977)

Table continued on next page.

Variables	
Fe01	
b_{Mg}	4.60E+23
T (K)	1263
N_{cb} (electrons/m^3) (calc. from T and band gap)	9.31E+12
b_{Mg}	8.40E+23
T (K)	1363
N_{cb} (electrons/m^3) (calc. from T and band gap)	9.05E+13
b_{Mg}	4.40E+23
T (K)	1453
N_{cb} (electrons/m^3) (calc. from T and band gap)	5.92E+14
Fe02	
b_{Mg}	1.03E+24
T (K)	1263
N_{cb} (electrons/m^3) (calc. from T and band gap)	9.34E+12
b_{Mg}	1.36E+24
T (K)	1363
N_{cb} (electrons/m^3) (calc. from T and band gap)	9.05E+13
b_{Mg}	1.20E+24
T (K)	1453
N_{cb} (electrons/m^3) (calc. from T and band gap)	5.92E+14
Fe03	
b_{Mg}	3.40E+23
T (K)	1263
N_{cb} (electrons/m^3) (calc. from T and band gap)	9.31E+12
b_{Mg}	5.50E+23
T (K)	1363
N_{cb} (electrons/m^3) (calc. from T and band gap)	9.05E+13
b_{Mg}	4.50E+23
T (K)	1453
N_{cb} (electrons/m^3) (calc. from T and band gap)	5.92E+14

The following subsections show the electrical conductivity plots (Figure 29, Figure 30 and Figure 31) for the various samples. The solid line is the modelled result obtained via solving the equations to a best fit using MS Excel's solver plug-in. Despite some scatter at certain temperatures, the fits are generally very well constrained.

4.3.2.1. Fe01 (Fo_{90})

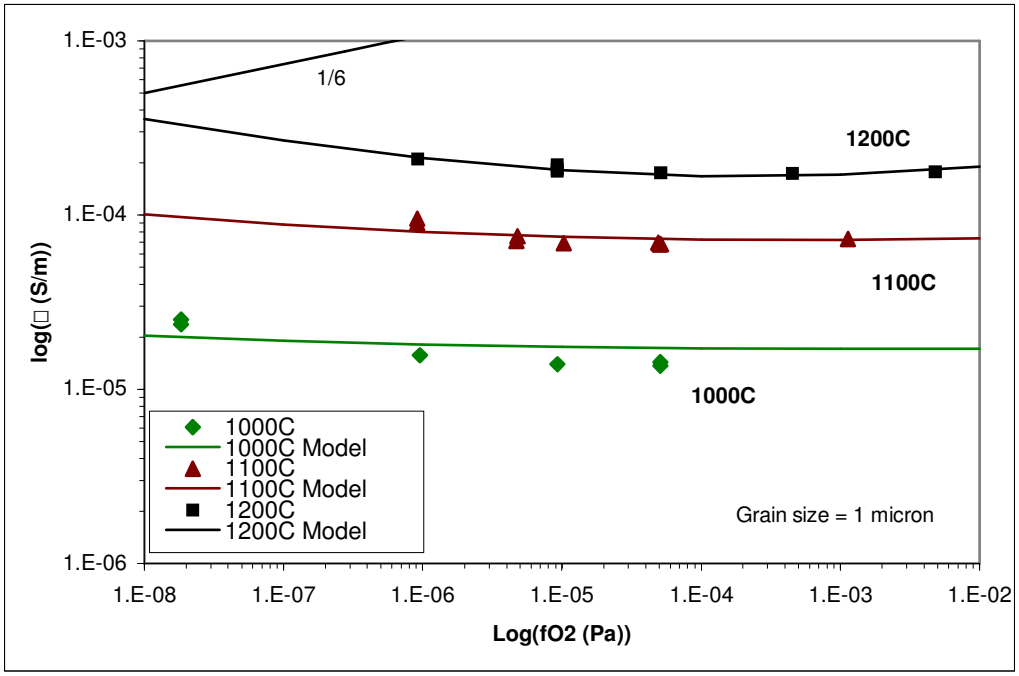

Figure 29. Conductivity data modelled at three different temperatures. The solid lines show the expected trend of the conductivity at different oxygen fugacity. Note the accurate fit for 1200°C and 1100°C. At 1000°C the fit is somewhat less perfect. The entire range in fO2 shown is within the olivine stability field.

4.3.2.2. Fe02 (Fo_{90})

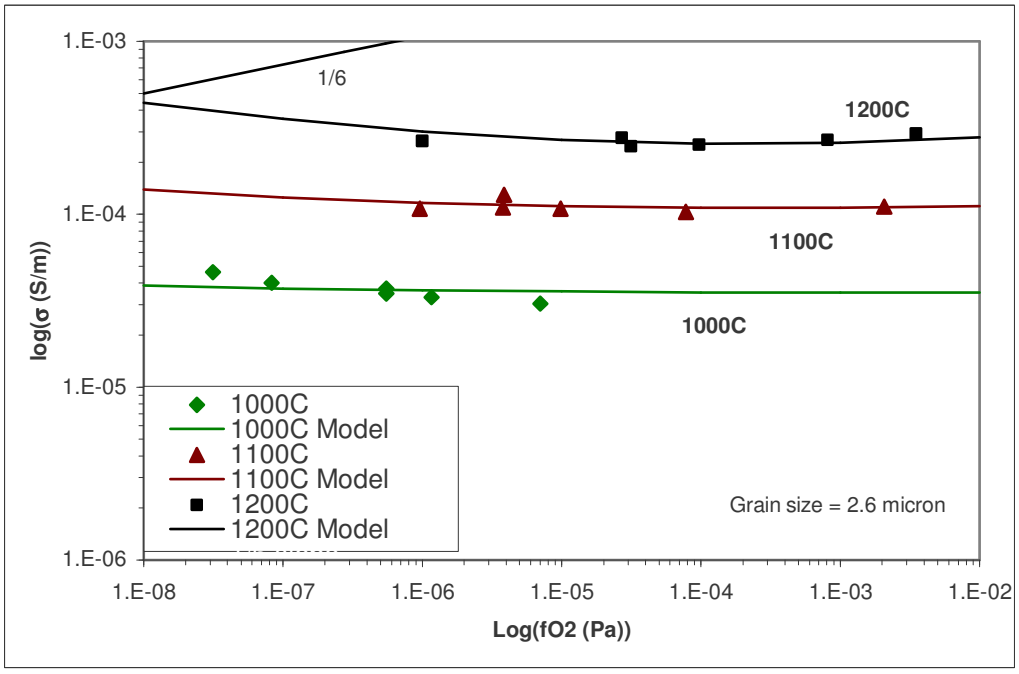

Figure 30. Conductivity data modelled at three different temperatures. The solid lines show the expected trend of the conductivity at different oxygen fugacity. The entire range in fO2 shown is within the olivine stability field.

4.3.2.3. Fe03 (Fo_{90})

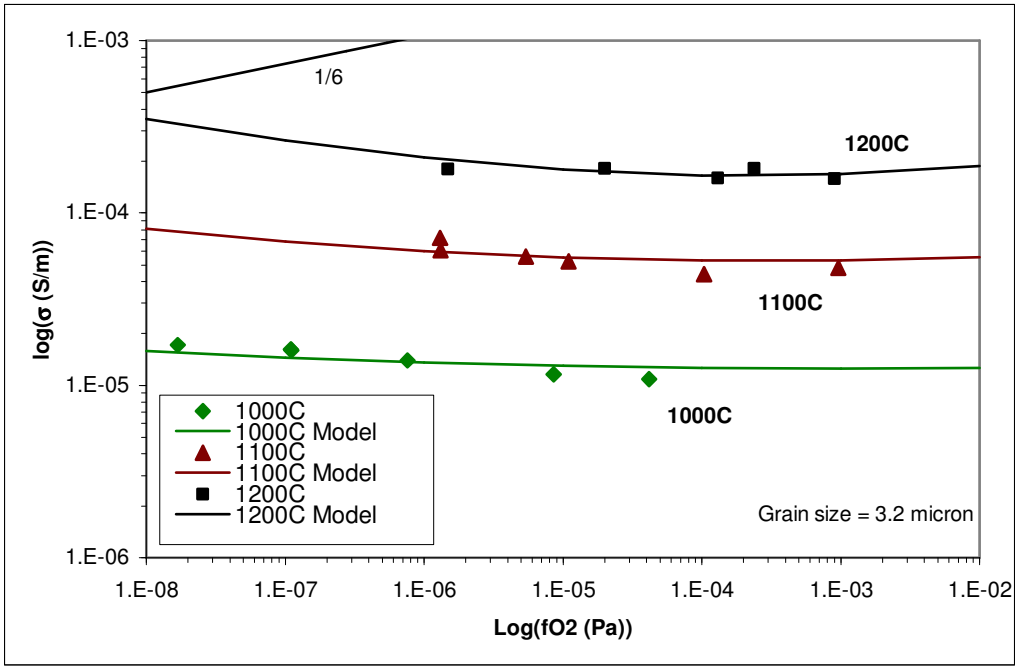

Figure 31. Conductivity data modelled at three different temperatures. The solid lines show the expected trend of the conductivity at different oxygen fugacity. The entire range in fO2 shown is within the olivine stability field.

The model fits the data well, which means that, as predicted, the dominant charge carriers are indeed magnesium vacancies and electrons. The olivine samples, containing (almost) no oxidised iron, therefore do not contain any small polarons to high concentrations and can therefore never contribute as a dominant charge carrier to the overall conductivity. This has major implications for all electrical impedance experiments performed on natural olivine. This is explained in the next sections.

4.3.3. Identifying the charge carriers involved in conduction

4.3.3.1. Grain interior diffusion

As already stated in the previous section, the contribution of $Fe_{Mg}^{\bullet}$ or small polarons, is not included in the final result of the model. It was quickly apparent that $Fe_{Mg}^{\bullet}$ would only add a +1/6 slope, one which is already contributed by Mg vacancies. But that was not the main reason. Inserting the parameters in the equation for $Fe_{Mg}^{\bullet}$ and plotting it as a function of *f*O2 along with the contribution of Mg vacancies showed that the concentration of $Fe_{Mg}^{\bullet}$ was several orders of magnitude less than that of Mg vacancies. Thus the result remained unchanged after deleting the contribution of $Fe_{Mg}^{\bullet}$. However, the most important reason why it was not considered further in the model is that these experiments have been carried out on purpose well within the olivine stability field. This would indicate that the reduced form of iron in the olivine samples stays, for

the greatest part, reduced Fe^{2+}. One would, therefore, not expect $Fe^{\bullet}_{Mg}$ to be a major charge carrier. Eliminating $Fe^{\bullet}_{Mg}$ from the equation leaves Mg vacancies and electrons as the most important, but not the only charge carriers. The contribution of electrons is justified because the conductivity data for Fe01, Fe02 and Fe03 show consistently at different temperatures and low fO_2 a slightly negative slope. Only electrons, which are mobile enough in larger concentrations and contribute with a negative slope of -1/6, can explain this.

Looking in further detail at the diffusion of magnesium vacancies, Brodholt (1997) discovered from ab initio calculations that the magnesium defects on the M1 sites are 0.8eV lower in energy than on the M2 sites. Thus the Mg vacancy hopping mechanism most likely only occurs from M1 sites to other M1 sites. See Figure 32.

Other than magnesium vacancies, small polarons and electrons as charge carriers, other candidates such as Si interstitials are not likely to contribute greatly to the overall conductivity (see Hirsch and Shankland, 1993). Reason being is that Si binds the olivine structure together and is therefore less likely to move in great concentrations. The only other possible candidates are oxygen interstitials or vacancies especially when observing the evolution of the second impedance arc (ie the grain boundaries) at different oxygen fugacity.

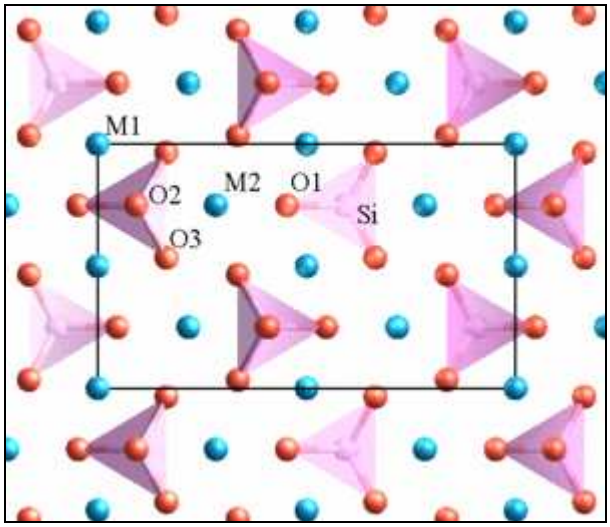

Figure 32. Crystal structure of olivine with the unit cell and the locations of the M1, M2 and the O1, O2, O3 sites. Oxygen is shown in red, silicon in pink and magnesium/iron in blue.

4.3.3.2. Grain boundary diffusion

In previous studies various models have been proposed, which quantitatively describe the concentration of defects (cm^{-3}) at different temperatures and oxygen fugacity but have so far been focused on the diffusion of defects through grain interiors only "to avoid additional uncertainties related to poorly controlled or unknown conditions at grain boundaries in many of the studies of the polycrystalline samples" (Hirsch and Shankland 1993). The first impedance arc (as seen in Figure 15) represents this grain interior or grain interior conduction. However, as seen in Figure 15, Figure 16 and Figure 19, there is a second arc. The point where this arc touches the x-axis (or real impedance or

resistance) can be taken and converted to conductivities. This is represents conduction though the grain boundaries as explained earlier.

Until recently models did not distinguish between the M1, M2 sites and in particular the O1, O2 and O3 sites, which bears a consequence for conduction in grain boundaries. In a study by Walker *et al.* 2003, where oxygen diffusion was quantitatively calculated and in a study by Brodholt (1997), the authors realise that almost all oxygen vacancies are found on the O3 site. This is concluded from the fact that there seems to be a large difference (at least 0.66 eV) between the energy required to form vacancies on the three symmetry-inequivalent oxygen sites (Walker *et al.* 2003). This may limit the effective contribution of oxygen vacancy diffusion and is therefore unlikely to contribute to conduction in high concentrations. For oxygen interstitials it is, however, possible that they are scavenged at reducing conditions thus forming a gradient in oxygen concentration causing further diffusion (of possibly oxygen vacancies) and higher conduction. When looking at the results (as in Figure 17, Figure 20 and Figure 24) increasing oxygen fugacity causes a decrease in conductivity.

Figure 34 is a compilation of the conductivity data obtained for the grain boundaries. The data from the authors, as well as current data show negative slopes. It is interesting to note that different natural materials give different absolute conductivities which seems very unreliable. The synthetic data lies at a lower conductivity than the natural data. Again this might have to do with added small polaron conduction for natural material increasing the overall conductivity. The slopes for natural material are generally also less negative. It is also interesting to see that for 1000˚C the slope is exactly –1/6.

With an increase of oxygen fugacity, the concentration of oxygen vacancies would be expected to drop and the concentration of oxygen interstitials to rise (Walker *et al.,* 2003). If oxygen vacancies are the major charge carriers, then with increasing oxygen fugacity the diffusion of oxygen vacancies would drop and thus the conductivity would drop. This is clearly seen. Furthermore, as seen in Table 8, only oxygen vacancies that have a charge of +2 can contribute such a negative dependence on oxygen fugacity. This at least rules out oxygen interstitials as the dominant charge carriers in the grain boundaries. However, because the slopes vary at different temperatures, there must be at least some sort of mixed conduction with something that contributes a positive relation to the fO_2. This still could be the oxygen interstitials with a low mobility or simply magnesium vacancies.

It is a useful exercise to calculate the diffusivity of oxygen and hence the conductivity via a modified Nernst – Einstein relation and see if oxygen vacancies is a reliable candidate. Using the equation below we can get an estimate of the conductivity from the diffusivity D.

$$\begin{aligned}\sigma &= c_s \cdot q \cdot \mu \\ &= N \exp\left(-\frac{E_v}{kT}\right) \cdot q \cdot \frac{qD}{kT}\end{aligned} \qquad \text{(A)}$$

D can be obtained from Oxygen (self-diffusion) experiments in forsterite. At 1200°C D = 3.16E-16 cm^2/s (Jaoul *et al.,* 1980), D = 2.18E-16 cm^2/s (Reddy *et al.,* 1980) and D = 9.45E-17 cm^2/s (Jaoul and Houlier, 1983) with corresponding activation energies of 320 kJ/mol, 372 kJ/mol and 293 kJ/mol respectively. Not many oxygen diffusion experiments

have been conducted on natural iron-bearing olivine but Houlier *et al.,* 1988 obtained D = 1E-18 m^2/s at 1300°C. We still need some estimation of the concentration of oxygen interstitials and vacancies. For this we turn to the model of Hirsch and Shankland (1993). Even though the model is calculated for grain interiors, the calculated values are for iron-bearing olivine at 1200°C. For oxygen interstitials at around fO_2 = 1E-5 Pa the concentration is 1E18 cm^{-3}. For oxygen vacancies: 1E4 cm^{-3}. Roberts and Tyburczy (1993) faced a similar problem for identifying the charge carriers in the grain boundaries. They ruled out oxygen because oxygen has been shown to diffuse relatively fast in polycrystalline dunite (D ≈ 1E-7 cm^2/s at 1200°C at 1GPa) (Watson, 1986), so higher conductivities would have been expected. However, using equation (A) above a conductivity can be calculated for oxygen interstitials at 1200°C which equals to σ = 1.26E-4 S/m. This is calculated with a concentration of 1E25 /m^3 and Watson's value. If oxygen vacancies can exist in such a concentration than that would explain the negative slopes, but alas. In addition, as we have seen, there is much more research done where much lower and similar D values have been obtained leading only to lower conductivities. This leads to a problem concerning oxygen vacancies as the major conducting species.

Now that we are still at a loss which major charge carries might explain the conductivity in the grain boundaries, we turn to other possible candidates. One other candidate is electrons. Still, the high activation energy associated with grain boundaries (Figure 33) would seem to contradict this and again hints more that we are dealing with oxygen vacancy diffusion. We may be looking at electrons that could be polarised in the grain boundaries and act as polarons. Polarons can contribute to a high activation energy because the electrons have significantly reduced mobility as they distort the lattice bonds around them as they move. In other words a polaron is formed when a moving charge (typically an electron or a hole) in a crystal with some ionic character polarizes (by its electric field) the lattice around it. The resulting lattice polarization acts as a potential well that hinders the movements of the charge, thus decreasing its mobility. Do not, however, confuse polarons with small polarons (e.g. $Fe^{\bullet}_{Mg}$)! They are entirely two different things. However, while electrons may act as polarons within the crystal lattice structure, it is unlikely that they would be slowed down to the same degree in grain boundaries, where there is more space.

Table 8. Variation of point defect concentrations with a_{En} and P_{O2} for various charge neutrality conditions. Calculated from equilibrium constants for several reactions by Stocker and Smyth, 1977. The interesting P_{O2} coefficients are circled in red for the charge neutrality condition of interest.

Range	$[Mg_I^{\cdot\cdot}]$	$[V''_{Mg}]$	$[Si_I^{\cdot\cdot\cdot\cdot}]$	$[V''''_{Si}]$	$[V_O^{\cdot\cdot}]$	$[O_I'']$	$[V_O^X]$	$[V_O^{\cdot}]$	$[Fe'_{Mg}]$	$[Fe_I^{\cdot\cdot}]$	$[Fe_I^{\cdot\cdot\cdot}]$	$[e']$	$[h^{\cdot}]$
$[V''_{Mg}] = [Mg_I^{\cdot\cdot}]$	0; 0	0; 0	4; 0	−4; 0	+1; 0	−1; 0	0; $-\frac{1}{2}$	$+\frac{1}{2}$; $-\frac{1}{4}$	$+\frac{1}{2}$; $+\frac{1}{4}$	0; 0	$+\frac{1}{2}$; $+\frac{1}{4}$	$-\frac{1}{2}$; $-\frac{1}{4}$	$+\frac{1}{2}$; $\frac{1}{4}$
$[e'] = 2[Mg_I^{\cdot\cdot}]$	$-\frac{1}{3}$; $-\frac{1}{6}$	$\frac{1}{3}$; $\frac{1}{6}$	$\frac{10}{3}$; $-\frac{1}{3}$	$-\frac{10}{3}$; $\frac{1}{3}$	$\frac{2}{3}$; $-\frac{1}{6}$	$-\frac{2}{3}$; $\frac{1}{6}$	0; $-\frac{1}{2}$	$\frac{1}{3}$; $-\frac{1}{3}$	$\frac{1}{3}$; $\frac{1}{6}$	$-\frac{1}{3}$; $-\frac{1}{6}$	0; 0	$-\frac{1}{3}$; $-\frac{1}{6}$	$\frac{1}{3}$; $\frac{1}{6}$
$[h^{\cdot}] = 2[V''_{Mg}]$	$-\frac{1}{3}$; $-\frac{1}{6}$	$\frac{1}{3}$; $\frac{1}{6}$	$\frac{10}{3}$; $-\frac{1}{3}$	$-\frac{10}{3}$; $\frac{1}{3}$	$\frac{2}{3}$; $-\frac{1}{6}$	$-\frac{2}{3}$; $\frac{1}{6}$	0; $-\frac{1}{2}$	$\frac{1}{3}$; $-\frac{1}{3}$	$\frac{1}{3}$; $\frac{1}{6}$	$-\frac{1}{3}$; $-\frac{1}{6}$	0; 0	$-\frac{1}{3}$; $-\frac{1}{6}$	$\frac{1}{3}$; $\frac{1}{6}$
$[e'] = 4[Si_I^{\cdot\cdot\cdot\cdot}]$	$-\frac{9}{5}$; $-\frac{1}{10}$	$\frac{9}{5}$; $\frac{1}{10}$	$\frac{2}{5}$; $-\frac{1}{5}$	$-\frac{2}{5}$; $\frac{1}{5}$	$-\frac{4}{5}$; $-\frac{1}{10}$	$\frac{4}{5}$; $\frac{1}{10}$	0; $-\frac{1}{2}$	$-\frac{2}{5}$; $-\frac{3}{10}$	$-\frac{2}{5}$; $\frac{1}{5}$	$-\frac{9}{5}$; $-\frac{1}{10}$	$-\frac{11}{5}$; $\frac{1}{10}$	$\frac{2}{5}$; $-\frac{1}{5}$	$-\frac{2}{5}$; $\frac{1}{5}$
$[h^{\cdot}] = 4[V''''_{Si}]$	$-\frac{9}{5}$; $-\frac{1}{10}$	$\frac{9}{5}$; $\frac{1}{10}$	$\frac{2}{5}$; $-\frac{1}{5}$	$-\frac{2}{5}$; $\frac{1}{5}$	$-\frac{4}{5}$; $-\frac{1}{10}$	$\frac{4}{5}$; $\frac{1}{10}$	0; $-\frac{1}{2}$	$-\frac{2}{5}$; $-\frac{3}{10}$	$-\frac{2}{5}$; $\frac{1}{5}$	$-\frac{9}{5}$; $-\frac{1}{10}$	$-\frac{11}{5}$; $\frac{1}{10}$	$\frac{2}{5}$; $-\frac{1}{5}$	$-\frac{2}{5}$; $\frac{1}{5}$
$[V''_{Mg}] = 2[Si_I^{\cdot\cdot\cdot\cdot}]$	$-\frac{4}{3}$; 0	$\frac{4}{3}$; 0	$\frac{4}{3}$; 0	$-\frac{4}{3}$; 0	$-\frac{1}{3}$; 0	$\frac{1}{3}$; 0	0; $-\frac{1}{2}$	$-\frac{1}{6}$; $-\frac{1}{4}$	$-\frac{1}{6}$; $\frac{1}{4}$	$-\frac{4}{3}$; 0	$-\frac{3}{2}$; $\frac{1}{4}$	$\frac{1}{6}$; $-\frac{1}{4}$	$-\frac{1}{6}$; $\frac{1}{4}$
$[V_O^{\cdot\cdot}] = [V''_{Mg}]$	$-\frac{1}{2}$; 0	$\frac{1}{2}$; 0	3; 0	−3; 0	$\frac{1}{2}$; 0	$-\frac{1}{2}$; 0	0; $-\frac{1}{2}$	$\frac{1}{4}$; $-\frac{1}{4}$	$\frac{1}{4}$; $\frac{1}{4}$	$-\frac{1}{2}$; 0	$-\frac{1}{4}$; $\frac{1}{4}$	$-\frac{1}{4}$; $-\frac{1}{4}$	$\frac{1}{4}$; $\frac{1}{4}$
$[Mg_I^{\cdot\cdot}] = 2[V''''_{Si}]$	$-\frac{4}{3}$; 0	$\frac{4}{3}$; 0	$\frac{4}{3}$; 0	$-\frac{4}{3}$; 0	$-\frac{1}{3}$; 0	$\frac{1}{3}$; 0	0; $-\frac{1}{2}$	$-\frac{1}{6}$; $-\frac{1}{4}$	$-\frac{1}{6}$; $\frac{1}{4}$	$-\frac{4}{3}$; 0	$-\frac{3}{2}$; $\frac{1}{4}$	$\frac{1}{6}$; $-\frac{1}{4}$	$-\frac{1}{6}$; $\frac{1}{4}$
$[Fe'_{Mg}] = 2[V''_{Mg}]$	$-\frac{1}{3}$; $-\frac{1}{6}$	$\frac{1}{3}$; $\frac{1}{6}$	$\frac{10}{3}$; $-\frac{1}{3}$	$-\frac{10}{3}$; $\frac{1}{3}$	$\frac{2}{3}$; $-\frac{1}{6}$	$-\frac{2}{3}$; $\frac{1}{6}$	0; $-\frac{1}{2}$	$\frac{1}{3}$; $-\frac{1}{3}$	$\frac{1}{3}$; $\frac{1}{6}$	$-\frac{1}{3}$; $-\frac{1}{6}$	0; 0	$-\frac{1}{3}$; $-\frac{1}{6}$	$\frac{1}{3}$; $\frac{1}{6}$
$[V_O^{\cdot}] = 2[V''_{Mg}]$	$-\frac{1}{3}$; $\frac{1}{6}$	$\frac{1}{3}$; $-\frac{1}{6}$	$\frac{10}{3}$; $\frac{1}{3}$	$-\frac{10}{3}$; $-\frac{1}{3}$	$\frac{2}{3}$; $\frac{1}{6}$	$-\frac{2}{3}$; $-\frac{1}{6}$	0; $-\frac{1}{2}$	$\frac{1}{3}$; $-\frac{1}{6}$	$\frac{1}{3}$; $\frac{1}{3}$	$-\frac{1}{3}$; $+\frac{1}{6}$	0; $+\frac{1}{2}$	$-\frac{1}{3}$; $-\frac{1}{3}$	$\frac{1}{3}$; $\frac{1}{3}$
$[Fe'_{Mg}] = [e']$	−1; $-\frac{1}{2}$	1; $\frac{1}{2}$	2; −1	−2; +1	0; $-\frac{1}{2}$	0; $\frac{1}{2}$	0; $-\frac{1}{2}$	0; $+\frac{1}{2}$	0; 0	−1; $-\frac{1}{2}$	−1; $-\frac{1}{2}$	0; 0	0; 0
$[Fe_I^{\cdot\cdot}] = [V''_{Mg}]$	0; 0	0; 0	4; 0	−4; 0	+1; 0	−1; 0	0; $-\frac{1}{2}$	$+\frac{1}{2}$; $-\frac{1}{4}$	$+\frac{1}{2}$; $+\frac{1}{4}$	0; 0	$+\frac{1}{2}$; $+\frac{1}{4}$	$-\frac{1}{2}$; $-\frac{1}{4}$	$+\frac{1}{2}$; $\frac{1}{4}$
$3[Fe_I^{\cdot\cdot\cdot}] = 2[V''_{Mg}]$	$-\frac{1}{5}$; $-\frac{1}{10}$	$+\frac{1}{5}$; $\frac{1}{10}$	$\frac{18}{5}$; $-\frac{1}{5}$	$-\frac{18}{5}$; $\frac{1}{5}$	$-\frac{4}{5}$; $-\frac{1}{10}$	$\frac{4}{5}$; $\frac{1}{10}$	0; $-\frac{1}{2}$	$-\frac{2}{5}$; $-\frac{3}{10}$	$-\frac{3}{5}$; $\frac{1}{5}$	$-\frac{1}{5}$; $-\frac{1}{10}$	$+\frac{1}{5}$; $\frac{1}{10}$	$\frac{2}{5}$; $-\frac{1}{5}$	$-\frac{2}{5}$; $+\frac{1}{5}$

n;m where n refers to a_{En} (activity of enstatite) and m to P_{O2}

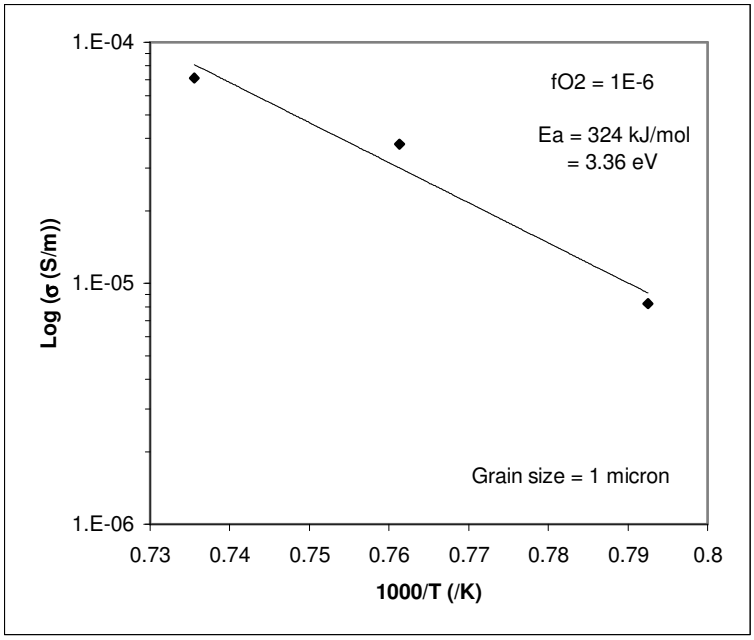

Figure 33. Arrhenius plot for the grain boundaries of Fe01. As the slope indicates, the activation energy in the grain boundaries, for the charge carriers, is much higher than in the grain interior. Temperature range is at 1000°C to 1050°C to 1100°C.

Roberts and Tyburczy (1993) also cited research by Fujkama (1988) where the diffusion of iron on grain boundaries was measured at $D \approx 10^{-11}$ cm^2/s at 1200°C. This happened to be at least one order of magnitude to slow compared to data by Roberts and Tyburczy (1993). However, current data for grain boundaries, as seen in Figure 34, might satisfy that. Iron interstitials do appear to contribute a -1/6 fO_2 dependence as seen in Table 8. Whether these calculated concentrations of different charge species are the same for grain boundaries is unknown. Magnesium interstitials also contribute a -1/6 fO_2 dependence which are have been computed to be 2 orders of magnitude higher in concentration than iron interstitials for the grain interiors (Hirsch and Shankland,1993), which seems logical since olivine looked at only has 10% Fe.

To summarise, the dominant charge carriers contributing to the conductivity obtained in the grain boundaries are most likely iron and magnesium interstitials because they exist in much higher concentration than oxygen vacancies (10 orders of magnitude (Hirsch and Shankland,1993)). In addition, one might think of grain interior Mg vacancy diffusion to be linked to grain boundary Mg interstitial diffusion. If an improved model or future experiments show that oxygen vacancies can exist in high concentrations and diffuse relatively fast in the grain boundaries then they are the most likely candidates. The reason being is because of the decrease in conductivity with an increase in fO_2, the high activation energy and the -1/6 dependence on fO_2 for the grain boundaries. The exact reason why iron and magnesium interstitials could be the dominant charge carriers also relates to high activation energies obtained as observed in e.g. creep experiments. The higher apparent activation energy (324 kJ/mol) in Figure 33 certainly corresponds well to activation energies obtained in other creep experiments and high temperature (1200°C - 1400°C) electrical conduction experiments (315 +/- 35 kJ/mol (Hirth and Kohlstedt 1995), 315 +/- 39 kJ/mol, 321+/- 8 kJ/mol and 323 +/- 15 kJ/mol (ten

Grotenhuis et al 2004), 343 +/- 27 and 376 +/- 47 kJ/mol (Farver et al 1994) (grain boundaries)). Nonetheless, in a study oxygen self-diffusion in forsterite did yield an apparent activation energy of 320 +/- 40 kJ/mol (Jaoul *et al.*, 1980) but in a computational study the activation energy is predicted to be between 94 and 178 kJ/mol (Walker *et al.*, 2003). There was no relationship found between oxygen fugacity and oxygen self-diffusion in forsterite (Jaoul *et al.*, 1980) but there is for iron-bearing olivine with $(fO_2/p_0)^m$, where m is between -0.17 and -0.3 (Gerand and Jaoul, 1989; Ryerson et al., 1989) and p_0 is the atmospheric pressure.

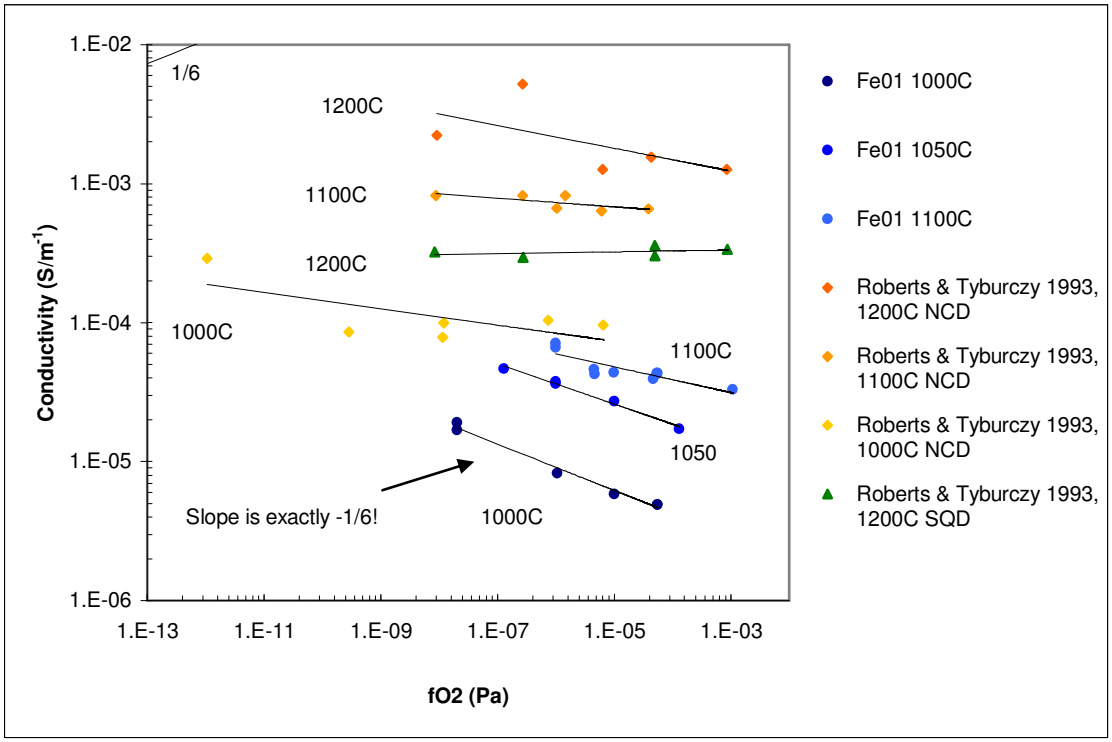

Figure 34. Conductivity data from the second arc in the impedance plot (i.e. grain boundaries) at different temperatures. Note that the synthetic olivine (Fe01) from this study is much more resistant than data from Roberts and Tyburczy, 1993. Also note that natural material is not consistent. The San Carlos Dunite does not give the same result at 1200°C compared to the North Carolina dunite. All slopes are negative except the one of SQD and deviate greatly from the 1/6 slope. Clearly other dominant charge carriers are involved in conduction.

4.3.4. Oxidation of Fe01 (to Fe01-oxi)

Having established which dominant charge carriers are present under stable conditions for (synthetic) olivine (Fo_{90}), namely electrons and magnesium vacancies, it is interesting to see what would happen if we were to oxidise one of the samples. This was done to Fe01-oxi. Figure 25 shows the conductivity of olivine outside its stability field. It can immediately be seen that there is a significant increase in conductivity and that the slope from that point on approaches 1/6. It is speculated that this is what many authors see for natural olivine. This means that natural olivine already contains a concentration of oxidised iron in the olivine crystal lattice. Hence one sees the contribution of small

polarons $Fe_{Mg}^{\bullet}$ which dominate and which also give a slope of 1/6 (see Table 8 again). What is more, is that oxidising Fe01 and bringing it back to the original reducing conditions showed that a change has taken place. In fact, this would make sense because once the iron is oxidised it will not become reducing again unless the sample is taken to near melting temperatures. However, it may be that the excess electrons are taken out by oxidised atmosphere eventually and that the conductivity of oxidised olivine will return to its previous magnitude. This has regrettably not been tested due to time constrains. But theory predicts that, since oxygen fugacity is a state function, one would assume that it does not matter how the system got to an oxidised state and back again. fO_2 is a property of the system that only depends on the current state of the system. Figure 41 in the appendix shows the oxidised sample along with the original samples. It clearly has turned brownish red.

Other research has been carried out to see what happens to olivine under highly reducing conditions (1E-6 Pa to 1E-23 Pa) using San Carlos olivine. A fast (»1±2 min) increase of electrical conductivity is first observed, followed by a slower decrease (1± 10 h, depending on the crystal orientation). The fast conductivity increase in the first transient regime is ascribed to an increase in the population of electrons at the olivine surface. Two effects: (1) equilibration of surface defects with the bulk of the crystal, and (2) iron loss from the olivine due to metal precipitation, could explain the subsequent decrease of electrical conductivity (Lemelle *et al.*, 1998).

4.3.5. Calculating the diffusivity

The diffusivity of magnesium vacancies can be calculated from the Nernst-Einstein relationship:

$$D = \frac{\mu kT}{q}$$

Where μ is the mobility of the species and q its charge. For this study the mobility of magnesium vacancies at 1200°C is 5.14E-10 $m^2V^{-1}s^{-1}$. So the diffusivity of magnesium vacancies at 1200°C is approximately 3.27E-11 m^2s^{-1}. This compares well with other estimates at this temperature by Mackwell *et al.*, (1988) (3.5-9.8E-11 m^2s^{-1}), Nakamura and Schmalzreid (1984) (1.9E-11 m^2s^{-1}), Wanamaker (1986) (4.8E-11 m^2s^{-1}), Duba and Constable (1993) (7E-11 m^2s^{-1}) and Constable and Roberts (1997) (3.2E-11 m^2s^{-1}). Experiments on Fe-Mg interdiffusion in olivine up to 9 GPa and extrapolated to T = 1200°C yields a diffusivity value of only 5.2E-18 m^2s^{-1} (Jaoul *et al.*, 1995). Apparently interdiffusion of magnesium and iron is much slower and thus has no consequence.

4.4. Previous work

4.4.1. Comparison of data

The following figures show the data of several authors compared to the data obtained in this study. It can be seen in Figure 35 that there is an enormous scatter, which

presumably primarily results from the use of natural material. Also note how the data from synthetic olivine samples from this study falls more or less in the middle with the same slope as the data from synthetic forsterite from ten Grotenhuis *et al.*, 2004. The absolute conductivity for similar grain sizes is not the same. It can be said that generally it shows that synthetic forsterite containing 10% fayalite is slightly more conductive than pure forsterite. But when observing natural materials this cannot be said with conviction. Also note that polycrystalline and single crystal data is mixed in this graph. The sample used is a single crystal where stated otherwise it is polycrystalline. The position of the transition from electronic to ionic conduction is unclear as can be seen by the many locations where a line has a distinct bend. The oxygen fugacity is variable. The data of Fe01 and Fe03 are at fO_2 = 1E-5 Pa, for Fe02 at 5.5E-5 Pa. For the other data from the various authors no oxygen fugacity was kept constant, which is very strange as it is yet another variable which can, in reality, be controlled. The activity of silica, being another variable, is on the other hand, is very difficult to control.

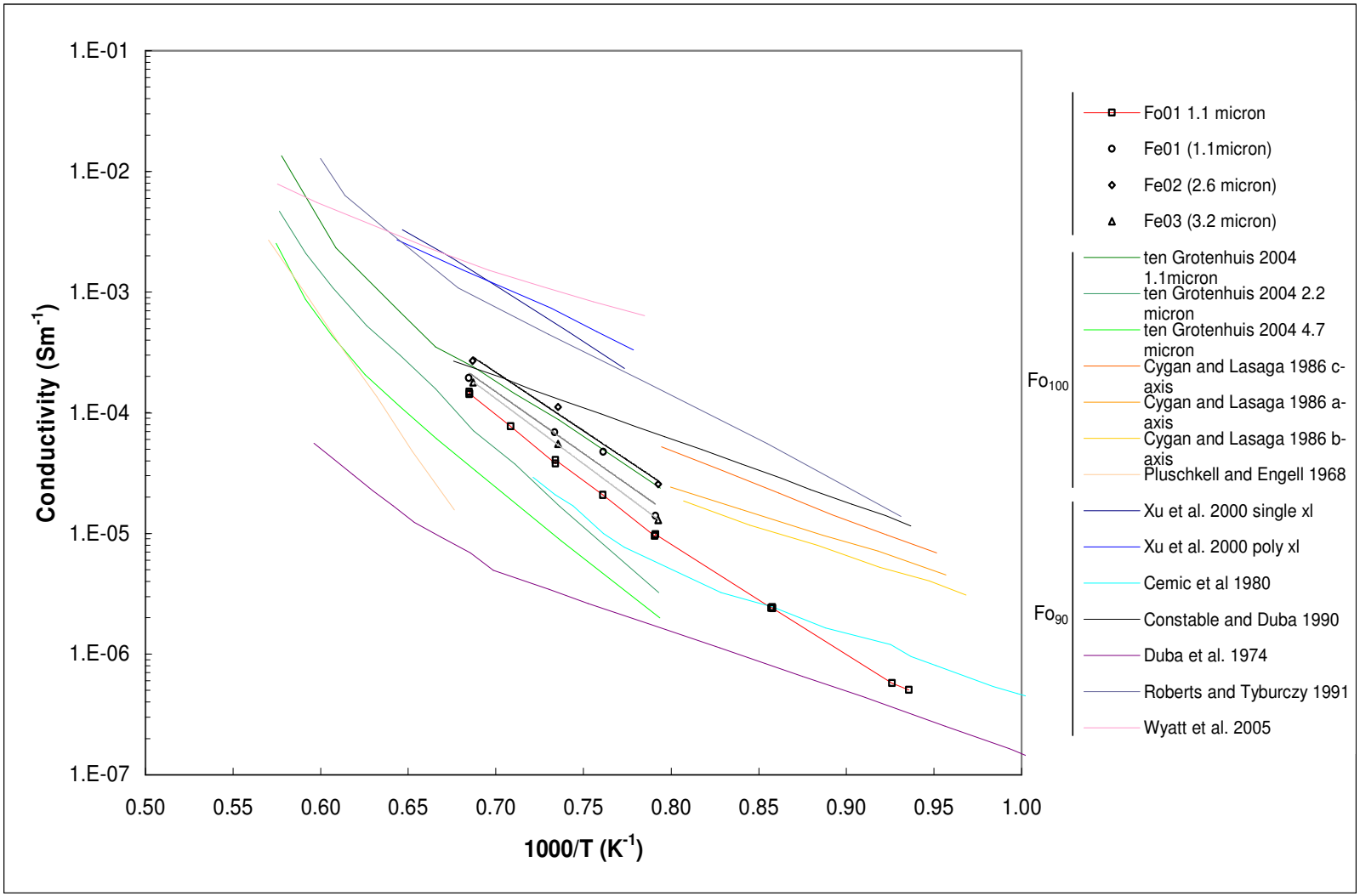

Figure 35. Compilation graph of the data from many authors and this study. In the legend is shown the distinction between forsterite and forsterite with 10% fayalite.

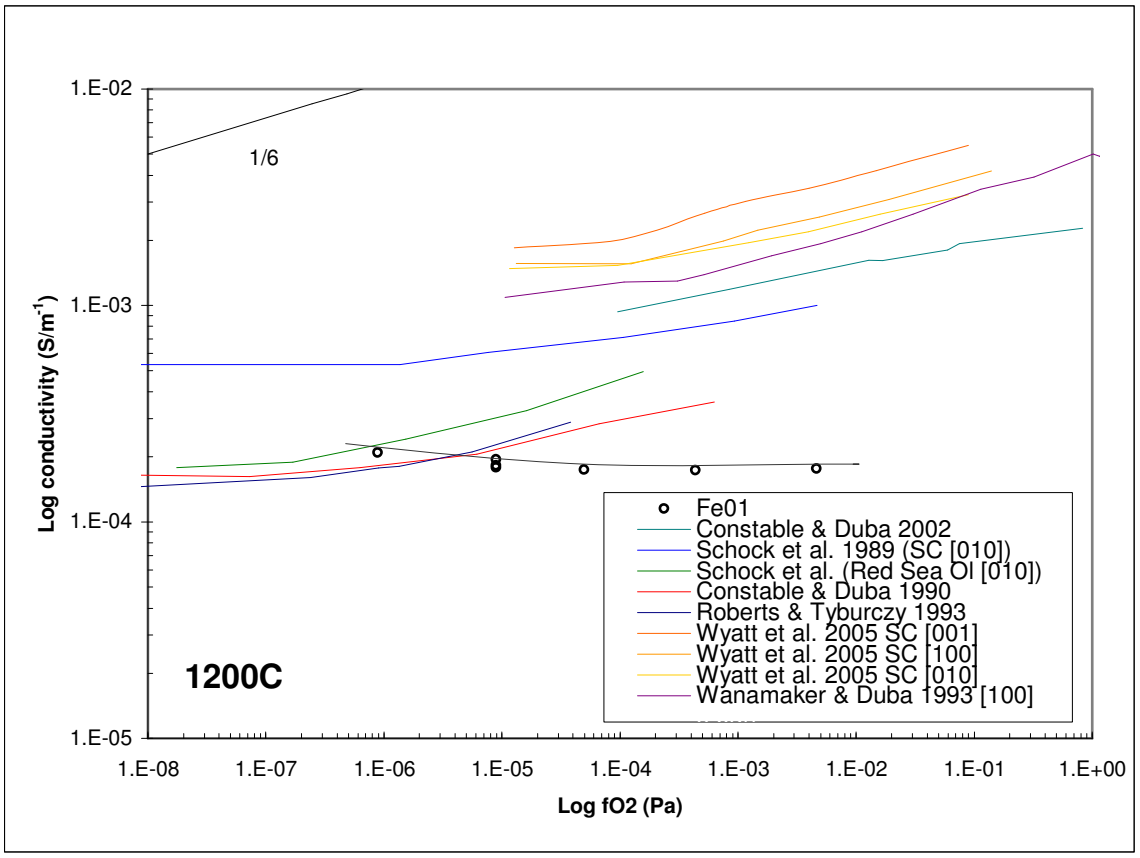

Figure 36. Another compilation graph showing the experimental results obtained by various authors. This graph displays the conductivity data versus the oxygen fugacity. Except for Fe01 from this study, San Carlos olivine (Fo90) was used unless otherwise stated. Note the slope of most data from natural material is around 1/6 as shown in the upper left hand corner. Synthetic Fo90 does not show this relationship.

Figure 36 is a compilation graph of the electrical conductivity versus the oxygen fugacity. This important graph shows several data from different natural olivine (Fo90) material and data from Fe01 at 1200˚C. It is most apparent that all data, except for the synthetic olivine, plots at or near a slope of +1/6. Referring back to previous discussions in sections modelled data and oxidation, this is what one expects if there is already oxidised iron present in abundance yielding therefore high concentrations of small polarons. This is clearly not the correct approach if one wishes to examine the electrical properties of olivine under upper mantle conditions where olivine most likely has not undergone oxidation.

Parkin (1972), as cited by Shankland (1975) and Schock *et al.*, (1989), has conducted experiments on synthetic forsterite with very small amounts of FeO. Figure 37 below shows the results. Even though he only had very small amounts of fayalite it most certainly does not contain oxidised iron. The results with higher amounts of fayalite look remarkably like the results from this study (although note that the experiments were done at 1422°C). While it is apparent that between 0.2% Fa and 0.33% Fa there is a sharp decrease in absolute conductivity, both curve at around the point where data from this study curves from a negative slope to a positive one. Namely between an fO_2 of 1E-5 Pa

and 1E-1 Pa. Authors using natural Fo_{90} clearly have a slope of 1/6 in this region (see Figure 36).

What has not been mentioned so far is that the majority of electrical impedance experiments performed on olivine by the various authors have been carried out under normal atmospheric pressures. This is justified because the electrical conduction in olivine has been tested to be largely independent of pressure (Xu *et al.*, 2000).

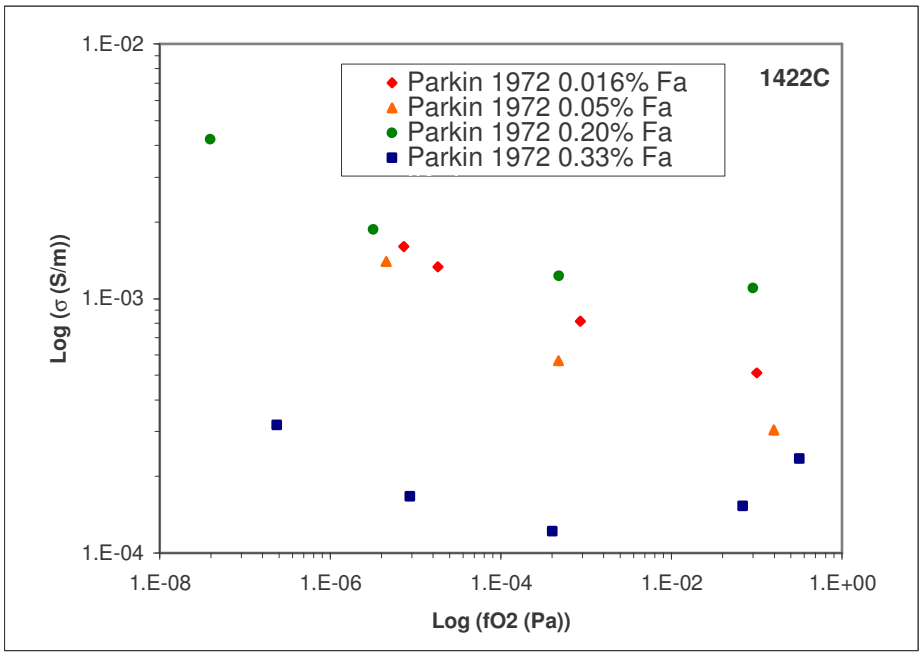

Figure 37. Log-log plot of the conductivity versus the oxygen fugacity for synthetic forsterite containing small amounts of fayalite. Note that the temperature at which the experiments were taken is 1422°C, way higher than the conductivity experiments of this study. This might explain the order of magnitude higher conductivity obtained. The relatively iron-rich samples behave differently at higher fO_2 than the low-iron samples. The fO_2 range is the same as in Figure 36 for comparison.

4.4.1.1. Is there a dependence on grain size?

In previous research on forsterite there was a clear dependence on grain size found and that with increasing grain size, a decrease in conductivity was noted (ten Grotenhuis, *et al.*, 2004). This was obtained from the grain interior conductivity of the samples.

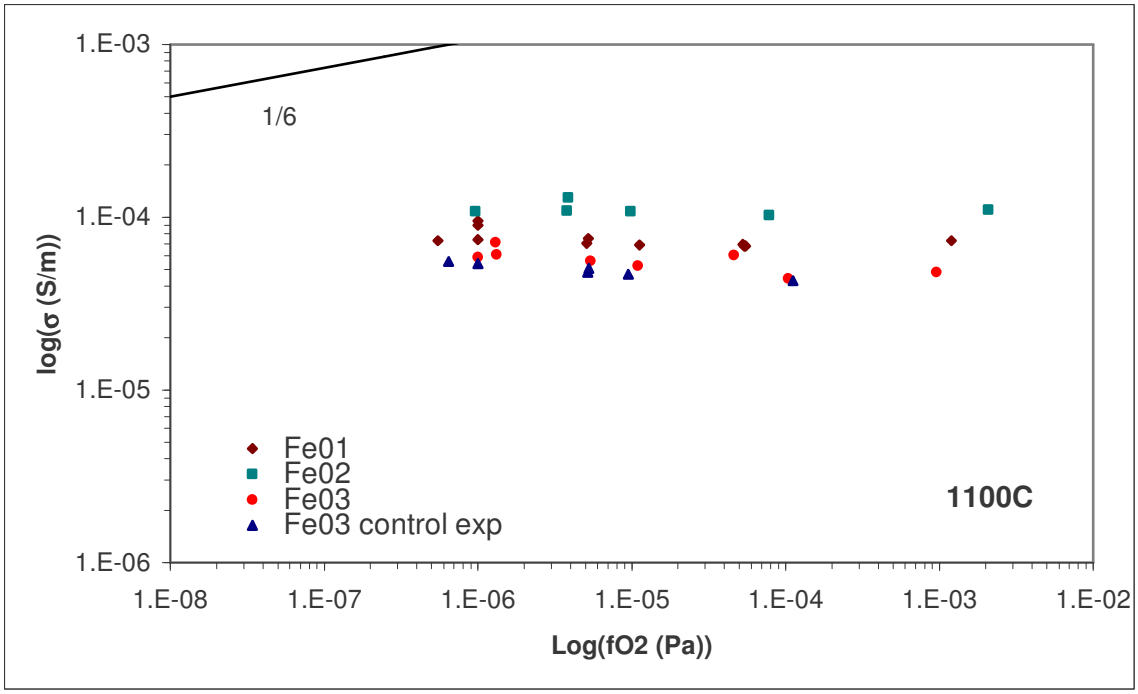

Figure 38. This plot shows the conductivity data for the original sample Fe01, the data obtained from Fe03 before re-sintering and data of Fe03 after re-sintering at 1350°C for 16 hours. Fe03 does not show a distinct change in grain interior conductivity due to a larger grain size. All data show a slightly negative slope curving upwards at higher fO_2.

Figure 38 shows the grain interior conductivity of the samples used in this study, in particular Fe03 (which has sintered for 16 hours at 1350°C). What is shown is virtually no change in conductivity before re-sintering and after and that the absolute values lie very close (approximately within the error range) of Fe01 which was not re-sintered and has a grain size of 1 micron. This indicates that most conduction goes through the grain interiors and is not affected by a change in grain size from a large grain boundary area per unit volume to a smaller grain boundary area per unit volume. Figure 39 shows a log-log plot of the grain size versus the grain interior conductivity where it is clearly seen that if there is a relation between the conductivity of iron bearing olivine and grain size, it is a very poor one to say the least. Most conduction therefore appears to go through the bulk material. In an effort to try explaining the apparent increase and decrease with increasing grain size, it is useful to observe the SEM micrographs of the samples. One is shown in Figure 40. Others can be seen in the appendix. Very large grains can be seen in Fe03 whereas they have not been found in Fe02. Despite the occasional presence of these large grains, it may have been enough to have an impact on the bulk conductivity. In addition, it may help to explain why the average grain size for Fe03 has not increased more than twice the size of Fe02, as Fe02 has compared to Fe01. It would appear that eventually it became more energetically favourable to grow localised larger grains than having a global increase in grain size. No melt was observed, which would contribute to an increase in conductivity (Roberts and Tyburczy, 1999; ten Grotenhuis *et al.*, 2005).

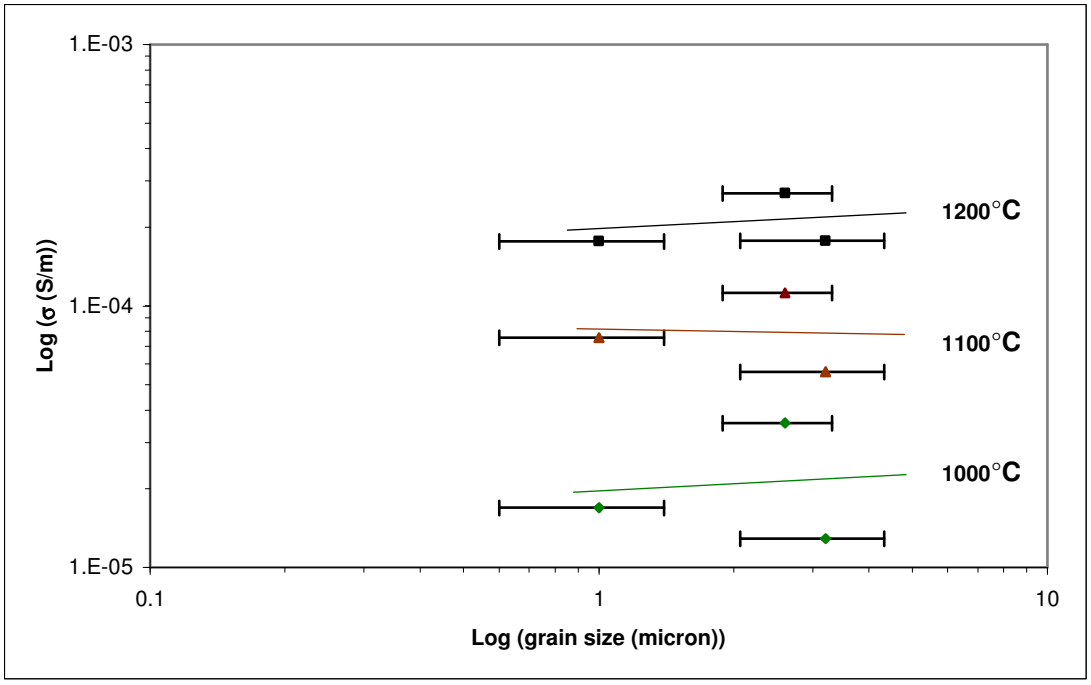

Figure 39. Log – log plot of the grain interior conductivity versus grain size at various temperatures. Fits are best logarithmic fits.

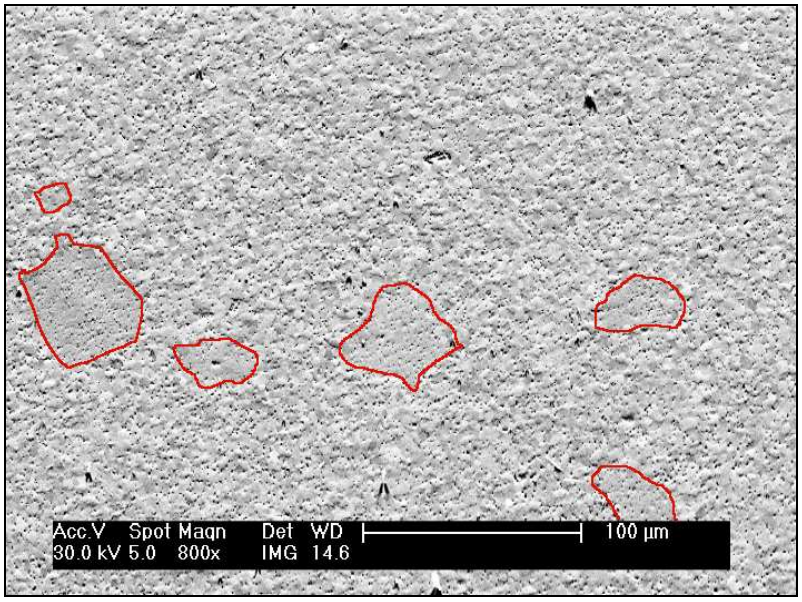

Figure 40. SEM image of Fe03. Note the large grains that have developed. Upon closer inspection these grains average at around 40 micron in size and have grown by means of assimilating the grain boundaries of neighbouring grains. They still contain substantial porosity. Overall porosity has, however, been reduced to 4.8%. These large grains are not present in SEM images from Fe02. For more, see the appendix.

4.5. Geophysical applications

Conductivity data obtained in this study can be used for geophysical applications such as magneto-telluric methods (MT). The region of interest is the upper mantle where olivine is by far the most abundant mineral. MT methods work by measuring the conductivity in the Earth and sometimes certain features are looked at such as the Moho, where a dramatic increase in compressional seismic velocity is observed. The conductivity data can consequently be compared to laboratory data to determine whether there is, for example, an extra conducting phase present under upper mantle conditions if the conductivity data from the field is more conductive. If the lab data compares to the field data, then the temperature distribution in the upper mantle can be computed. One study where MT methods were used was for the slave craton in Canada Measured conductivities in the upper mantle region appeared to be up to two orders of magnitude higher than lab data would suggest, hence it was inferred that "there must be a connected conducting phase" (Jones and Ferguson, 2001).

The nature of a highly conducting phase can be many things. The most popular one is of course the presence of partially molten rocks (Pous *et al.*, 1995; Ichiki *et al.*, 2001; Wenbo Wei *et al.*, 2001) However, the formation and presence of grain boundary carbon films is another widely investigated option (Frost *et al.*, 1989; Jones, 1992; Nover *et al.*, 2005; Glover, 2006). Carbon is of course a good conductor. Other possibilities are the presence of saline fluids (Jones, 1992; Chen *et al.*, 1996; Mai *et al.*, 2004) and/or metastable defect populations (Freund, 2003) and not to forget water: H_2 or OH^- diffusion in olivine (Sweeney, 1997; Demouchy and Mackwell, 2003 and 2006).

However, in a recent study it is argued that a conducting phase does not need to be present as long as there are deep shear zones detected in the middle and lower crust where, as is common in shear zones, grain size is much reduced (Rutter and Brodie, 1991). On experiments on synthetic forsterite it was found that with increasing grain size, the bulk conductivity decreases (ten Grotenhuis *et al.*, 2004). Thus when grain size is very small (at around 1-1000 micron in a mylonite) the conductivity will be higher than when the grain size is larger (1000 -10000 micron in a protomylonite). In this study on synthetic forsterite with 10% fayalite such a relationship with the bulk electrical conductivity versus the grain size is not reproduced or is poorly defined (see Figure 39). Whether this is related to iron and magnesium interstitial diffusion in the grain boundaries is unknown. In another study, the relationship with the grain boundary conductivity versus the grain size for San Carlos olivine compacts appeared equally independent or poorly defined (Roberts and Tyburczy, 1993). They suggested that further experimentation is needed to address this issue. More studies have been focussed on determining a grain boundary relationship with conductivity. In the Y_2O_3 ZrO_2 system a linear dependence of conductivity is seen for grain sizes up to 3 micron (Verkerk *et al.*, 1982b) but no grain size dependence beyond 3 micron. In samples such as high purity polycrystalline alumina, the grain boundary effects are only seen at grain sizes below 0.1 micron or there is a formation of a separate phase at the grain boundaries (Kingery *et al.*, 1976). A more recent study on Ceria also seems to indicate that near a small grain size of 5 micron (and higher) the conductivity becomes independent of the grain size while at lower grain sizes (0.1 micron to 1 micron) there is a strong relationship with increasing grain size and decreasing conductivity (Zhou *et al.*, 2002). In a study of the water content in the transition zone from electrical conductivity of wadsleyite and ringwoodite, it was

assumed that "previous studies on Fe-bearing olivine showed no appreciable effect of grain size" (Huang *et al.*, 2005) and therefore they did not incorporate it into their model. Which studies they referred to was not mentioned, however, which is peculiar because this article made it into Nature.

It thus remains questionable if a high conductivity zone in the lower crust and upper mantle would indicate a small grain size in localised shear zones and not a connected highly conducting phase. Nevertheless, from new experimental data of synthetic forsterite with 10% fayalite and 5% pyroxene in this study, the temperature distribution in MT models can be computed to a higher degree of confidence than from natural olivine for lower crust and upper mantle conditions.

Electrical conductivity measurements are not only relevant to the Earth's upper mantle but also to other planetary bodies such as the moon. However, because the exact composition of the moon's interior is unknown, no definite limits can be placed on temperatures in the lunar interior assuming a model composition of olivine (Housley and Morin, 1972). With future space exploration these models will most likely be refined to give us a better understanding of the temperature distribution in the moon and / or other planets such as Mars and Venus once we know an approximate composition of the interiors of these bodies.

5. Conclusion

So what does this all mean? One thing is certain. Any Earth scientist studying the electrical properties of olivine should be aware that natural olivine is unsuitable as it does not reflect olivine that has never left its stability field. It is strongly unlikely that in the upper mantle, olivine has the potential to become oxidised. Synthetic olivine (Fo_{90}) is therefore the most suitable material to use, which is also free of impurity atoms, other phases such as spinel and altered grain boundaries after crushing and re-sintering natural samples. The results from this study reinforce that statement because:

- Electrical conductivity data of dry synthetic iron-bearing olivine show no +1/6 slope dependence at different fO_2.
- Quantitative modelling, using the same approach as Constable and Roberts (1997) yields a different result, namely that magnesium vacancies and electrons are the major charge carriers within the olivine stability field.
- Synthetic material yields more consistent and reproducible conductivities than the various natural olivines, e.g. San Carlos olivine, Red Sea dunite, North Carolina dunite.
- Oxidation of iron-bearing olivine beyond its stability field does yield a +1/6 slope indicating that the major charge carrier has become the small polaron.

Other results show:

- Three impedance arcs can be produced where the first one is the grain interiors, the second, grain boundaries, and the third, an electrode effect.
- A general apparent activation energy for grain interiors for mixed conduction is at around 200 kJ/mol for all samples.
- An apparent activation energy for grain boundaries for iron-bearing olivine is much higher at around 320 kJ/mol. This may reflect iron and magnesium interstitial diffusion or, but very unlikely, oxygen vacancy diffusion in the grain boundaries / electrons which contribute a -1/6 dependence to fO_2.
- No evident dependence of conductivity on grain size. The path of least resistance is therefore likely to mostly go through the grain interiors.
- Between 5 hours and 16 hours of re-sintering at 1350°C, localised large (~40 micron) grains start to grow at the expense of a general increase of grain growth.
- For this study the mobility of magnesium vacancies at 1200°C is 5.14E-10 $m^2V^{-1}s^{-1}$. The diffusivity of magnesium vacancies at 1200°C is approximately 3.27E-11 m^2s^{-1}. This compares well with other results.
- The conductivity of forsterite is independent of the oxygen fugacity.

This study would benefit from more experiments at different temperatures, better defined parameters for the quantitative model and more samples with different uniform grain sizes.

This study can be continued by doing electrical impedance measurements on dry synthetic fayalite, determining the thermopower of synthetic olivine, applying the four point electrode approach to aid in the interpretation of the last arc, and determining the influence of water in (synthetic) olivine by e.g. carrying out hydrogen diffusion experiments in ‘wet’ (synthetic) olivine.

6. Acknowledgements

I firstly would like to thank C.J. Peach and S.M. ten Grotenhuis immensely for their support and helpful assistance. And of course the technical support, P. van Krieken, G. Kastelein and E. de Graaff, are thanked greatly for preparing my samples and helping to repair broken equipment. The Netherlands Research Centre for Integrated Solid Earth Science (ISES) financially supported this work.

7. References

Brodhold J (1997) Ab Initio Calculations on Point Defects in Forsterite (Mg2sio4) and Implications for Diffusion and Creep. *American Mineralogist* 82: 1049-53.

Cemic L, Will G, Hinze E (1980) Electrical Conductivity Measurements on Olivines Mg2sio4 - Fe2sio4 Under Defined Thermodynamic Conditions. *Phys Chem Minerals* 6: 95-107.

Chen L, Booker J, Jones A, Wu N, Unsworth M, Wei W, Tan H (1996) Electrically Conductive Crust in Southern Tibet From Indepth Magnetotelluric Surveying. *Science* 274: 1694-96.

Constable S, Duba A (1990) Electrical Conductivity of Olivine, a Dunite, and the Mantle. *Journal of Geophysical Research* 95, no. B5: 6967-78.

Constable S, Duba A (2002) Diffusion and Mobility of Electrically Conducting Defects in Olivine. *Phys Chem Minerals* 29: 446-54.

Constable S, Roberts J (1997) Simultaneous Modeling of Thermopower and Electrical Conduction in Olivine. *Phys Chem Minerals* 24: 319-25.

Constable, S. "Internal Constitiution of Earth Electrical Structure." Paper presented at the *SIO 224* 2005.

Demouchy S, Mackwell S (2003) Water Diffusion in Synthetic Iron-Free Forsterite. *Phys Chem Minerals* 30: 486-94.

Demouchy S, Mackwell S (2006) Mechanisms of Hydrogen Incorporation and Diffusion in Iron-Bearing Olivine. *Phys Chem Minerals*.

Duba A (1972) Electrical Conductivity of Olivine. *Journal of Geophysical Research* 77, no. 14: 2438-94.

Duba A, Heard H, Schock R (1974) Electrical Conductivity of Olivine at High Pressure and Under Controlled Oxygen Fugacity. *Journal of Geophysical Research* 79, no. 11: 1667-73.

Farver J, Yund R, Rubie D (1994) Magnesium Grain Boundary Diffusion in Forsterite Aggregates at 1000c - 1300c and 0.1 Mpa to 10 Gpa. *J. Geophys. Res.* 99, no. B10: 19809-19.

Frane WD, Roberts J, Toffelmier D, Tyburczy J (2005) Anisotropy of Electrical Conductivity in Dry Olivine. *Geophysical Research Letters* 32, no. L24315.

Freund F (2003) On the Electrical Conductivity Structure of the Stable Continental Crust. *Journal of Geodynamics* 35: 353-88.

Frost B, Fyfe W, Tazaki K, CHan T (1989) Grain-Boundary Graphite in Rocks and Implications for High Electrical Conductivity in the Lower Crust. *Nature* 340: 134-36.

Gerard O, Jaoul O (1989) Oxygen Diffusion in San Carlos Olivine. *J. Geophys. Res.* 94: 4119-28.

Glover P, Adam A, Zsiros T (2006) Correlation Between Crustal High Conductivity Zones and Seismic Activity and the Role of Carbon During Shear. *Geophysical Research Abstracts* 8.

Hinze E, Will G, Cemic L (1981) Electrical Conductivity Measurements on Synthetic Olivines and on Olivine, Enstatite and Diopsite From Dreiser Weiher, Eifel (Germany) Under Defined Thermodynamic Activities As a Function of Temperature and Pressure. *Physics of the Earth and Planetary Interiors* 25: 245-54.

Hirsch L, Shankland T (1993) Quantitative Olivine-Defect Chemical Model: Insights on Electrical Conduction, Diffusion, and the Role of Fe Content. *Geophys. J. Int.* 114: 21-35.

Hirsch L, Shankland T, Duba A (1993) Electrical Conduction and Polaron Mobility in Fe-Bearing Olivine. *Geophys. J. Int.* 114: 36-44.

Hirth G, Kohlstedt D (1995) Experimental Constraints on the Dynamics of the Partially Molten Upper Mantle: Deformation in the Diffusion Creep Regime. *J. Geophys. Res.* 100, no. B2: 1981-2001.

Houlier B, Jaoul O, Abel F, Liebermann R (1988) Oxygen and Silicon Self Diffusion in Natural Olivine. *Phys. Earth Planet. Inter.* 50: 240-50.

Housley, RM, and FJ Morin. "Electrical Condictivity of Olivine and the Lunar Temperature Profile." Paper presented at the *Lunar Geophysics Conference*, Lunar Science Institute in Houston, Texas, U.S.A. 1971.

Ichiki M, Sumitomo N, Kagiyama T (2000) Resistivity Structure of High-Angle Subduction Zone in the Southern Kyushu District, Southwestern Japan. *Earth Planets Space* 52: 539-48.

Jaoul O, Bertran-Alvarez Y, Liebermann R, Price G (1995) Fe-Mg Interdiffusion in Olivine Up to 9 Gpa at T = 600 - 900c; Experimental Data and Comparison With Defect Calculations. *Physics of the Earth and Planetary Interiors* 89: 199-218.

Jaoul O, Froidevaux C, Durham W, Michaut M (1980) Oxygen Self-Diffusion in Forsterite: Implications for the High-Temperature Creep Mechanism. *Earth and Planetary Science Letters* 47: 391-97.

Jaoul O, Houlier B (1983) Study of 18o Diffusion in Magnesium Orthosilicate By Nuclear Microanalysis. *Journal of Geophysical Research* 88: 613-24.

Jones, A. G. (1992), Electrical conductivity of the continental lower crust, in Continental Lower Crust, edited by D. M. Fountain, R. Arculus, and R. W. Kay, pp. 81– 143, Elsevier Sci., New York.

Jones A, Ferguson I (2001) The Electric Moho. *Nature* 409: 331-33.

Jorcin J, Orazem M, Pebere N, Tribollet B (2006) Cpe Analysis By Local Electrochemical Impedance Spectroscopy. *Electrochimica Acta* 51: 1473-79.

Kingery, WD, HK Bowen, and DR Uhlmann. *Introduction to Ceramics*. 2nd ed. New York: John Wiley, 1976.

Kitaura M, Nakagawa H, Ohnishi A (2001) Reflection Spectra and Electronic Structure of Forsterite (Mg2sio4) Single Crystals. , no. BL-1B.

Lemelle L, Duba A, Guyot F (1998) The Electrical Conductivity of Olivine Under Highly Reducing Conditions. *Phys Chem Minerals* 26: 164-70.

Machwell S, Dimos D, Kohlstedt D (1988) Transient Creep of Olivine: Point Defect Relaxation Times. *Philos. Mag.* 57A: 779-89.

Mai K, Haak V, Schilling F, Brasse H (2004) the Altiplano (Central Andes) High Conductivity Zone: Interpretation and Modelling. *American geophysical union*.

McDonnell R, Spiers C, Peach C (2002) Fabrication of Dense Forsterite-Enstatite Polycrystals for Experimental Studies. *Phys Chem Minerals* 29: 19-31.

Mihály, László, and Martin, Michael. *Solid State Physics : Problems and Solutions*: Wiley-Interscience, 1996.

Mulder W, Sluyters J, Pajkossy T, Nyikos L (1990) Tafel Current at Fractal Electrodes. Connection With Admittance Data. *Journal of Electroanalytical Chemistry* 285: 103-15.

Nakamura A, Schmalzried H (1983) On the Nonstoichiometry and Point Defects in Olivine. *Phys. Chem. Miner.* 10: 27-37.

Nover G, Stoll J, Gonna Jv (2005) Promotion of Graphite Formation By Tectonic Stress - a Laboratory Experiment. *Geophys. J. Int.* 160: 1059-67.

Orazem M, Agarwal P, Garcia-Rubio L (1994) Critical Issues With Interpretation of Impedance Spectra. *Journal of Electroanalytical Chemistry* 378: 51-62.

Parkin, T. "The Electrical Conductivity of Synthetic Forsterite and Periclase.", University of Newcastle upon Tyne, England, 1972.

Pous J, Munoz J, Ledo J, Liesa M (1995) Partial Melting of Subducted Continental Lower Crust in the Pyrenees. *Journal of the Geological Society* 152: 217-20.

Reddy K, Oh S, Major L, Cooper A (1980) Oxygen Diffusion in Forsterite. *J. Geophys. Res.* 85: 322-26.

Roberts J, Tyburczy J (1991) Frequency Dependent Electrical Properties of Polycrystalline Olivine Compacts. *Jounal of Geophysical Research* 96, no. B10: 16205-22.

Roberts J, Tyburczy J (1993) Frequency Dependent Electrical Properties of Dunite As Functions of Temperature and Oxygen Fugacity. *Phys Chem Minerals* 19: 545-61.

Roberts J, Tyburczy J (1993) Impedance Spectroscopy of Single and Polycrystalline Olivine: Evidence for Grain Boundary Transport. *Phys Chem Minerals* 20: 19-26.

Roberts J, Tyburczy J (1999) Partial Melt Electrical Conductivity: Influence of Melt Composition. *Journal of Geophysical Research* 104: 7055-65.

Ryerson F, Durham W, Cherniak D, Lanford W (1989) Oxygen Diffusion in Olivine: Effect of Oxygen Fugacity and Implications for Creep. *J. Geophys. Res.* 94: 4105-18.

Schock R, Duba A, Shankland T (1989) Electrical Conduction in Olivine. *Journal of Geophysical Research* 94, no. B5: 5829-39.

Shankland T (1968) Band Gap of Forsterite. *Science* 161, no. 3836: 51-53.

Shankland T (1975) Electrical Conduction in Rocks and Minerals: Parameters for Interpretation. *Phys. Earth Planet. Inter.* 10: 183-92.

Simpson, Robert E., Introductory Electronics for Scientists and Engineers, 2nd Ed., Allyn and Bacon, 1987

Slotemaker A. and de Bresser, H., work in progress.

Smyth D, Stocker R (1975) Point Defects and Non-Stoichiometry in Forsterite. *Physics of the Earth and Planetary Interiors* 10: 183-92.

Smyth D, Stocker R (1975) Point Defects and Non-Stoichiometry in Olivine. *Physics of the Earth and Planetary Interiors* 10: 183-92.

Stocker R (1978) Influence of Oxygen Pressure on Defect Concentrations in Olivine With a Fixed Cationic Ratio. *Physics of the Earth and Planetary Interiors* 17: 118-29.

Stocker R (1978) Point-Defect Formation Parameters in Olivine. *Physics of the Earth and Planetary Interiors* 17: 108-17.

Sweeney R (1997) The Role of Hydrogen in Geological Processes in the Earth's Interior. *Solid State Ionics* 97: 393-97.

tenGrotenhuis S, Drury M, Peach C, Spiers C (2004) Electrical Properties of Fine-Grained Olivine; Evidence for Grain Boundary Transport. *Journal of Geophysical Research* 109, no. B06203.

tenGrotenhuis S, Drury M, Spiers C, Peach C (2005) Melt Distribution in Olivine Rocks Based on Electrical Conductivity Measurements. *Journal of Geophysical Research* 110, no. B12201.

Verkerk M, Middelhuis B, Burggraaf A (1982) Effect of Grain Boundaries Os the Conductivity of High-Purity Zro2-Y2o3 Ceramics. *Solid State Ion* 6: 159-70.

Walker A, Wright K, Slater B (2003) A Computational Study of Oxygen Diffusion in Olivine. *Phys Chem Minerals* 30: 536-45.

Wanamaker, BJ. "The Kinetics of Crack Healing and the Chemical and Mechanical Reequilibrium of Fluid Inclusions in San Carlos Olivine." PhD, Princeton University, 1986.

Watson E (1991) Diffusion in Fluid-Bearing and Slightly-Melted Rocks: Experimental and Numerical Approaches Illustrated By Iron Transport in Dunite. *Contrib. Miner. Petrol.* 107: 417-34.

Wei W, Unsworth M, Jones A, Booker J, Tan H, Nelson D, Chen L, Li S, Solon K, Bedrosian P, Jin S, Deng M, Ledo J, kay D, Roberts B (2001) Detection of Widespread Fluids in the Tibetan Crust By Magnetotelluric Studies. *Science* 292: 716-18.

Xu Y, Shankland T, Duba A (2000) Pressure Effect on Electrical Conductivity of Mantle Olivine. *Physics of the Earth and Planetary Interiors* 118: 149-61.

Zhou X-D, Anderson H, Huebner W (2002) Grain Size and Chemical Composition Effects on the Grain Boundary Resistance of Ceria. *Mat. Res. Soc. Symp. Proc.* 730.

http://webmineral.com/data/Olivine.shtml

http://www.consultrsr.com/resources/eis/cpe1.htm

http://www.ioffe.rssi.ru/SVA/NSM/Semicond/Si/electric.html

http://www.ioffe.rssi.ru/SVA/NSM/Semicond/Si/bandstr.html

MS Excel thermovader plugin by Stuart Scott and Paul Fennell (2004) from the NASA Glenn thermodynamic database (http://cea.grc.nasa.gov/about).

8. Appendix

8.1. Samples compared

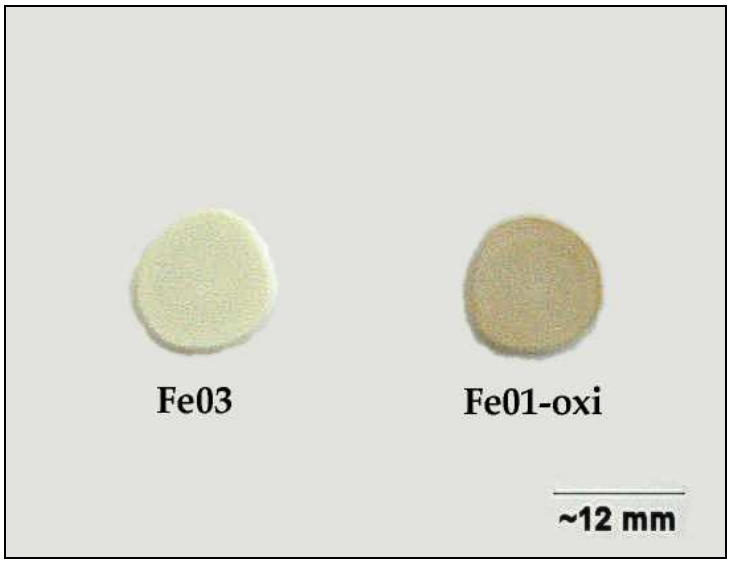

Figure 41. Sample comparison Fe03 and Fe01-oxi. Note the brown colour of the oxidised sample. A lighter brown circle can be seen which indicates the position of the Pt guard ring. Nevertheless, oxygen easily diffused between the sample and the electrode or else only the edges of the sample would be brown coloured.

8.2. SEM images of the various samples

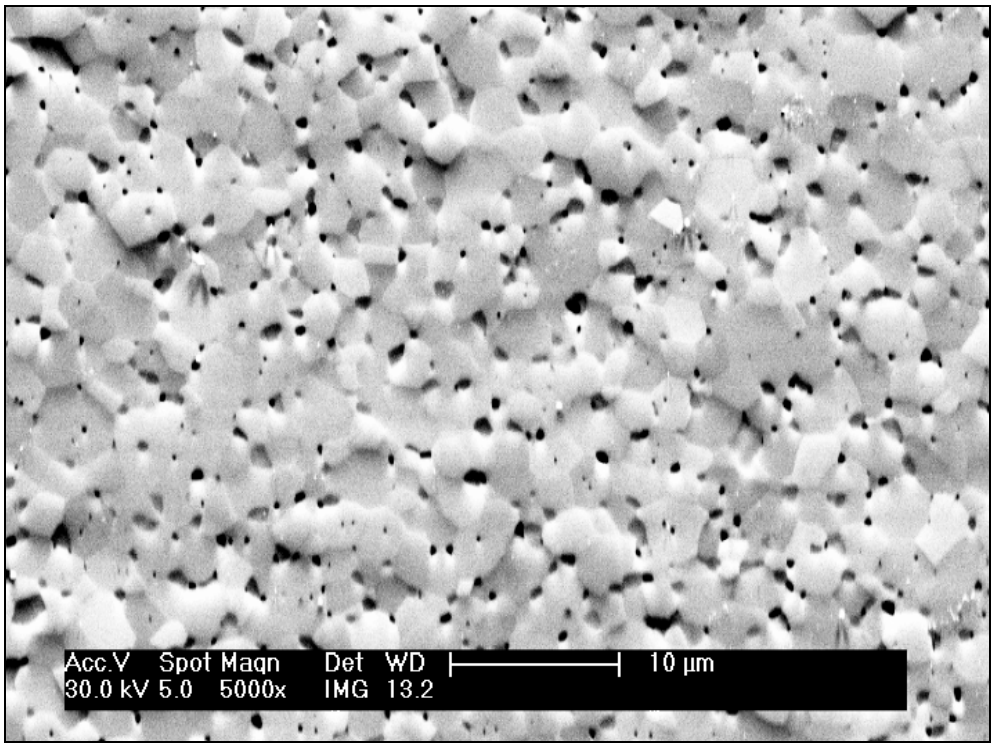

Figure 42. SEM image from Fe02. Grains appear larger than 1 micron but foam texture is preserved. Porosity has been reduced somewhat.

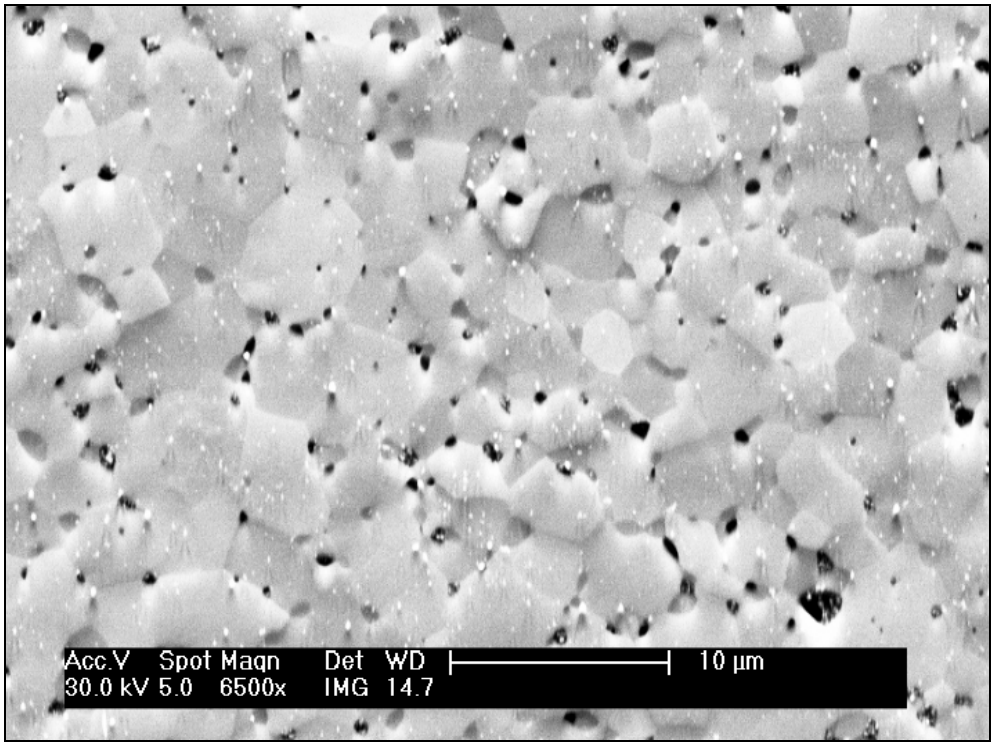

Figure 43. SEM image from Fe03. A beautiful foam texture can be seen. Many grains have increased in size at the expense of porosity.

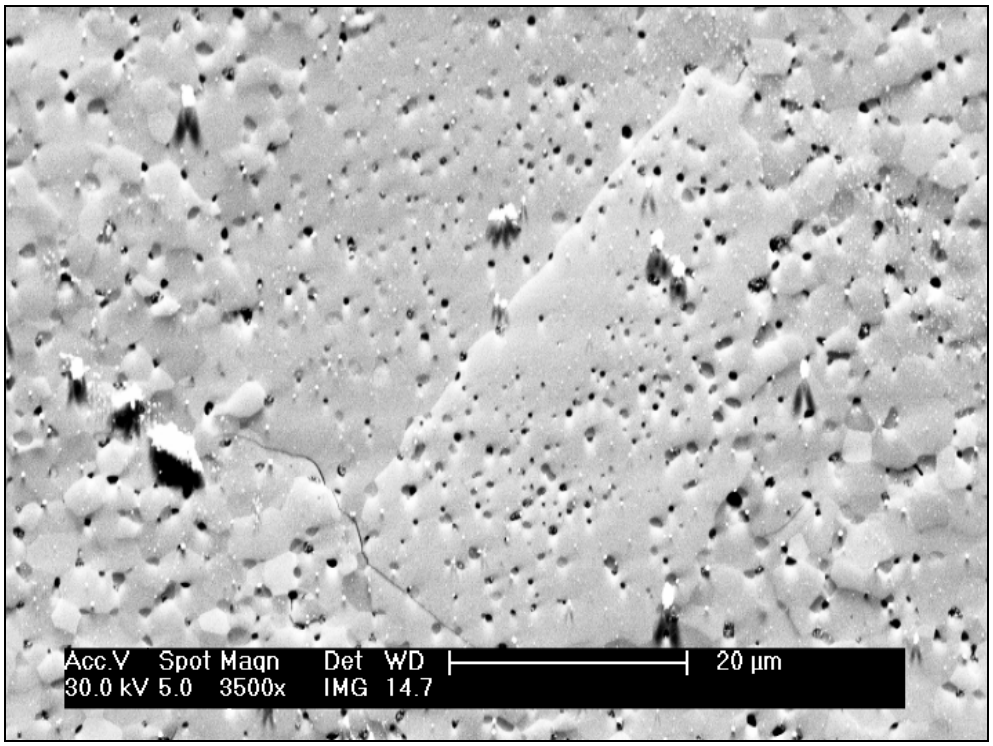

Figure 44. SEM image of Fe03. Notice the two large grains in the centre surrounded by smaller grains. The white 'clouds' are remains from sample preparation. Also notice that the porosity appears to have remained relatively unaffected while the grain boundaries have been destroyed in the large grains.

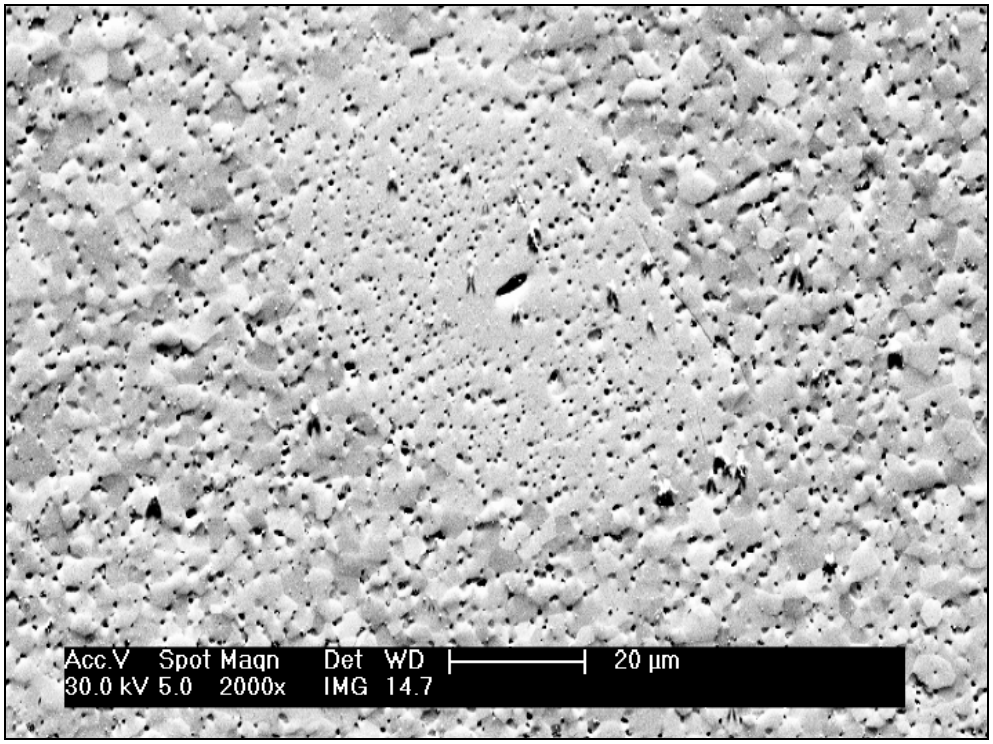

Figure 45. Another SEM image from Fe03 showing a large grain.

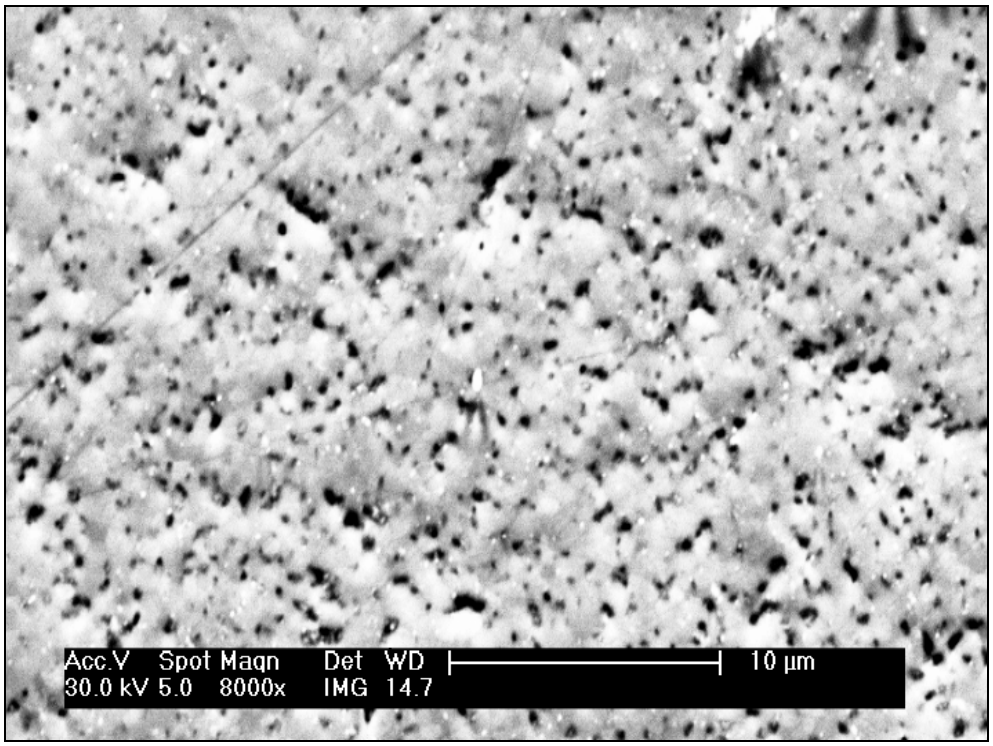

Figure 46. SEM image of Fe01-oxi. At this scale the grains are hardly visible. Porosity is abundant.

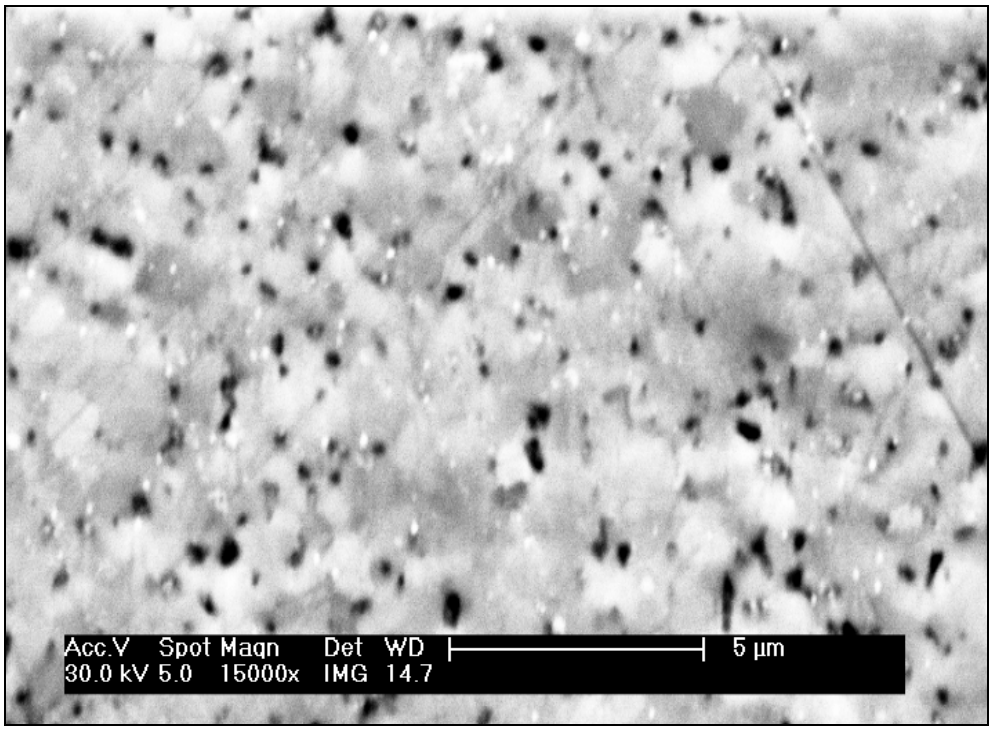

Figure 47. Another SEM image from Fe01-oxi. This is at smaller scale. Despite the unclear image, the grains appear have remained at around 1 micron in size. This sample has not been re-sintered so no grain growth was expected, but apparently the oxidation of Fe in the sample blurred the grain boundaries.

8.3. Overview experiments forsterite (Fo01)

Day 1 to 3 (morning): Only increase in resistance is noted
-At 800C, 50 MOhm increase is seen between day 1 and 2.
-At 900C, 5 MOhm increase in resistance is noted between the heating and cooling stages on day 1. On day 2, 25MOhm increase is seen between the heating and cooling cycle. On day 3, another 5MOhm increase in resistance is seen.
-At 1000C, 1.25 MOhm increase in resistance followed by just less than 1 MOhm increase in resistance upon cooling on day 2. Day 3 shows a slight further increase in resistance.
-At 1100C, day 1, the resistance increased by 250kOhm upon cooling. On day 2 a slight increase is in resistance is noted upon heating. On day 3 a 20 kOhm increase in resistance is seen upon heating.
-At 1200C, 50 kOhm increase in resistance followed by another 25 kOhm increase.

Day 3, afternoon
Big Change 1 : The temperature was brought to 1400C for < 15 minutes. Significant decrease in resistance is noted.

-At 1000C a 1 MOhm decrease in resistance is noted.
-At 1200C, as a result, the resistance was lowered to almost 25 kOhm again.

Day 4
-At 900C the resistance dropped by 7.5 MOhm as compared to day 3, morning.
-At 1000C the resistance remains the same compared to the previous day.

Day 5
-At 800C 25 MOhm decrease in resistance is seen as compared to day 2. Upon cooling another 7 MOhm decrease is seen.
-At 900C no change from day 4.
-At 1100C the resistance has dropped by 13 kOhm compared to day 3 morning.
-At 1200C the resistance remained roughly same.

Day 6 before gas
-At 1100C the resistance has dropped further by 6 kOhm upon heating.

Day 6 after gas
Big Change 2: Whole afternoon at 1100C with introduction of CO/CO2 gas mixture. Another significant decrease in resistance is noted.

-At 1100C upon cooling at 1100C the resistance has dropped another 25 kOhm.

Day 7 after gas
-At 800C a significant decrease of 25MOhm is seen as compared to day 5 (cooling).
-At 1100C resistance changed little from day 6 after gas. Upon cooling resistance decreased slightly.

Day 8
-At 1100C resistance equals that of day 7. Gas mixture does no longer seem to affect the conductivity measurements.

8.3.1. Possible scenario

Day 1 to 3 (morning)

Pt paint is sintering and gradually losing contact with sample surface upon several heating and cooling cycles thus decreasing surface area contact and thus resistance increases. It is important to note that resistance changes only occurred at peak temperatures because a cooling measurement roughly compares in all cases to a heating measurement of the next day. So the Pt paint only evolved at higher temperatures, which is what one would expect.

Flakes of Pt paint loosening from surface due heating and cooling cycles.

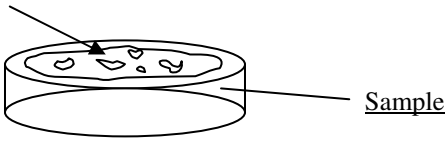

The big change on day 3 (afternoon)

Based on the observation that at each successive peak temperature the surface contact area changed, leading to an increase in resistance across the sample, the furnace temperature was briefly (~15 minutes) raised to 1400C to allow the Pt paint to sinter properly. With the assumption that grain growth was insignificant for this short time, the temperature was subsequently lowered back to 1200C and 1100C. New conductivity measurements showed that the resistance decreased as a result. Research by ten Grotenhuis *et al.* (2004) has shown an increase in conductivity correlates with a decrease in grain size, hence it is safe to assume that no grain growth has occurred during this brief exposure at 1400C. Therefore the change in resistance in the subsequent measurements must be due to the reconfiguring of the Pt paint coverage. Subsequent days show no serious change in the measurements.

The big change (part 2) on day 6 (afternoon)

With the CO/CO_2 gas bottles connected to a gas flow device, exact gas mixtures can be regulated to 0.1% precision for 10ml/s and 100ml/s gas flow. The furnace was heated up to 1100C as usual and this time gas mixtures of CO/CO_2 were injected into the furnace around the sample. After the first test run whereby a target oxygen fugacity of around 2.5E-6 Pa was chosen, the resistance at that temperature significantly decreased again. It is unknown how this is caused. Maybe a similar reconfiguration occurred of the Pt paint due to a prolonged stay at 1100C. Or some way or another the sudden depletion in oxygen in the atmosphere triggered a reaction on the sample surface or within the sample. Possibly oxygen was scavenged from between and below the Pt and the paint formed a better contact to the sample. Or perhaps more oxygen ions became more mobile in the forsterite sample with an exposure to a reduced atmosphere leading to an increase in conductivity. At any rate, conductivity measurements performed under normal atmospheric conditions during subsequent days showed no further serious change, making it, like the big change before, a permanent change. After the sample was taken out of the furnace, the percentage coverage of the Pt paint was calculated and the correction applied to the data in the plots.

8.4. Overview experiments $Fe_{10\%}Mg_{90\%}$ olivine (Fe01)

Day 1, 1100C

Experiments show good closure (i.e. repeatability) going from 5.2E-6 Pa to 1.1E-5 Pa and back to 5.2E-6 Pa especially because all resistance measurements of the first arc for all oxygen fugacity's show a maximum variation of only 4 kOhm compared to variations obtained for forsterite (at 1100C) of 25 – 250 kOhm. A second arc is seen developing at higher $f(O_2)$ and resistance of this arc also increases with

increasing f(O2). For a f(O2) change from 5.3E-5 Pa to 1.2E-3 Pa the resistance increase is roughly 13 kOhm.

Day 2, 1200C

Electrical conductivity measurements at 1200C showed even less variation in resistance (2 kOhm) from f(O2) 1E-6 Pa to 5E-3 Pa as compared to 1100C. Reproducibility at f(O2) of 1E-5 Pa is okay but there is some variation. First return to that oxygen fugacity gave a decrease in resistance but for the second return the resistance had increased again approaching the initial value. A second arc is poorly visible and very stretched at higher oxygen fugacity. Further experimentation in the following days showed equally good repeatability. The decision to stop using the Pt paint paid off.